U.PORTO

MESTRADO

ONCOLOGIA

A New Approach for Cancer Therapy Based on Marine Chemiluminescence

Carla Marisa Pacheco Magalhães

M

2018

A New Approach for Cancer Therapy Based on Marine Chemiluminescence

Carla Marisa Pacheco Magalhães

INSTITUTO DE CIÊNCIAS BIOMÉDICAS ABEL SALAZAR

Carla Marisa Pacheco Magalhães

A New Approach for Cancer Therapy Based on Marine Chemiluminescence

Dissertação de Candidatura ao grau de Mestre em Oncologia – Especialização em Oncologia Molecular, submetida ao Instituto de Ciências Biomédicas Abel Salazar da Universidade do Porto

Orientador – Doutor Luís Pinto da Silva
Categoria – Bolseiro de Pós-Doutoramento
Afiliação – Faculdade de Ciências da Universidade do Porto
Co-orientador – Joaquim C.G. Esteves da Silva
Categoria – Professor Catedrático
Afiliação – Faculdade de Ciências da Universidade do Porto

Agradecimentos

Ao Prof. Dr. JCG Esteves da Silva, pela oportunidade de integrar uma equipa prestigiada de trabalho, na qual pude fortalecer as minhas capacidades de trabalho e desenvolver o meu conhecimento científico. Desta forma, sinto-me preparada para o mundo do trabalho, sendo capaz de responder positivamente a qualquer desafio que o futuro me proporcionará.

Ao meu orientador, Luís Pinto da Silva, por todos os conhecimentos transmitidos, pela paciência e disponibilidade em ensinar-me e corrigir todos os meus erros. Pela dedicação ao projeto e todas as ideias incríveis que só uma mente brilhante poderia ter. Por desenvolver a minha capacidade cognitiva e fazer-me pensar mais além. E por último, pela paciência com os meus problemas pessoais e conselhos valiosos, considero-o não só um colega de trabalho, mas também um amigo que levo comigo para a vida.

À Prof. Dr. Cármen Jerónimo pela possibilidade de integrar o Mestrado em Oncologia, permitindo desenvolver as minhas capacidades na área, assim como integrar uma equipa de renome com alguns dos melhores profissionais. Agradeço também a disponibilidade para resolver problemas que foram surgindo ao longo deste percurso.

Ao ICBAS, por toda a disponibilidade e vontade de auxiliar os seus alunos em todas as questões.

Aos restantes colegas de trabalho, à Diana, ao Paulo, à Ara, ao Ricardo, ao Guilherme, ao Abdo, ao El Hadi, ao José, ao Luís e ao André por toda ajuda e disponibilidade que sempre demonstram. Pela boa disposição e por me proporcionarem bom ambiente de trabalho. Por todas as piadas e momentos musicais. Por todos os conselhos e ajuda pessoal com que pude sempre contar, levo-os a todos no meu coração.

Aos meus pais, por toda a paciência comigo e por todo o apoio que me proporcionaram durante deste período.

Ao João por me acompanhar em todas as fases da minha vida e apoiar todas as minhas decisões. Por ouvir sempre as minhas preocupações e acreditar sempre em mim. Por tornar tudo mais fácil.

Ao Centro de Investigação em Química da Universidade do Porto (CIQUP), onde este trabalho foi realizado, pelas condições realizadas. Este trabalho foi feito no âmbito dos projetos NORTE-01-00145-FEDER-000028, POCI-01-0145-FEDER-006980 e PTDC/QEQ-QFI/0289/2014, financiados por fundos nacionais (FCT) e comunitários (FEDER).

Abreviations

ABDA- 9,10-anthracenediyl-bis(methylene)dimalonic acid

Act- Activator

AMP- Adenosine monophosphate

ATP- Adenosine triphosphate

BET- Back electron transfer

BL- Bioluminescence

BRET- Bioluminescent resonance energy transfer

BS- Broken-symmetry

CASPT2- Complete-active-space second-order perturbation theory

CIEEL- Chemically induced electron-exchange

CL- Chemiluminescence

CO_2- Carbone dioxide

CRET- Chemiluminescent resonance energy transfer

CT- Charge transfe

DMSO- Dimethyl sulfoxide

ET- Electron transfer

FRET- Fluorescence resonance energy transfer

HPLC- High Performance Liquid cromatrography

ICIC- Interstate crossing-induced chemiexcitation

IEFPCM- Integral equation formalism polarizable continuum model

I**RC-** Intrinsic reaction coordinates

LDH- Lactate desidrogenase

MS- Multistate

m-THPC- Meta-tetra-hydroxyphenyl-chlorine

MTT- 3-(4,5-dimethylthiazol-2-yl)-2,5-diphenyltetrazolium bromide

NIR- Near infra-red

PDT- Photodynamic therapy

PS- Photosensitizer

RLU- Relative light units

ROS- Reactive oxygen species

SA- State-average

TD- Time-dependent

TS- Transition states

Abstract

Photodynamic therapy (PDT) is a procedure with the potential for superseding common cancer treatments, due to its minimally invasive character. It consists on the destruction of target tumor cells mainly by singlet oxygen, which is produced by light-induced activation of a photosensitizer. However, due to problems in light-penetration through tissues, this treatment is only applied to small tumors and/or the skin (or just under), as well on the surface of organs/cavities. PDT is unable to deal with metastasized cancer due to its localized nature. Thus, the goal of this work is to use new compounds as the basis for self-activating photosensitizers, which would be able to overcome the current limitations of PDT.

To this end, the novel photosensitizers will be based on marine Coelenterazine, that is able to emit chemiluminescence in the absence of a catalyst. More specifically, excited states are produced in the absence of an external light source. Thus, the problems typically associated with light-penetration into tissues are eliminated. The absence of a catalyst also facilitates the use of Coelenterazine chemiluminescence on PDT, as only the Coelenterazine should be administered to the patient, eliminating the difficulty of delivering several reaction components to the same cellular compartment without reacting during delivery.

Besides, Coelenterazine is not only an excitation source (through chemiluminescence), but also acts as a photosensitizer by itself. That is, the proposed chemiluminescence substrate produces chemiexcited triplet excited states able to produce singlet oxygen by interaction with molecular O_2.

While Coelenterazine presents some advantages to development of self-activated PSs, there are some problems that must be overcome before that. Namely, chemiluminescence reactions have low quantum yields and the Coelenterazine system is known for producing chemiexcited singlet excited states instead of triplet ones (the desired ones for producing singlet oxygen). These problems are difficult to be solved due to lack of knowledge and mechanistic insight into Coelenterazine. To address this, the present project pursued two different avenues of research (which can be considered also as the two main objectives of this thesis):

- Use of a combined spectroscopic, chromatographic and theoretical approach to obtain mechanistic insight into the chemiluminescence of Coelenterazine and related molecules, with emphasis on the chemiexcitation process, in different environments.
- Synthesis of novel Coelenterazine-based photosensitizers, their characterization (with focus on their ability of producing singlet oxygen), and the evaluation of their

in vitro cytotoxicity towards tumor cells. This study can be considered as a proof-of-concept phase.

The chemiexcitation step of Coelenterazine and *Cypridina* luciferin were studied by using a combined spectroscopic and computational approach in model DMSO solutions. It was found that the chemiluminescence of these molecules is pH-dependent: the total light output decreases with increasing pH, while the reaction rate has an opposite behavior. Further studies attributed these differences in the chemical equilibria of the dioxetanone intermediate. The thermolysis of neutral dioxetanone leads to a more efficient chemiexcitation efficiency. This results from neutral dioxetanone having access during its thermolysis to a degeneracy region, in which singlet ground and excited states are degenerated. Anionic dioxetanone does not appear to have access to this region.

While previous studies of the chemiluminescence of Coelenterazine has explored extensively the substitution of the imidazopyrazinone core at difference positions, the effect exerted by the solvent has been relatively unexplored. To bridge this gap in knowledge, it was studied comparatively the chemiluminescence of Coelenterazine and two derivatives in different aprotic solvents, by using a combined spectroscopic, chromatographic and theoretical approach. It was found that only DMSO and DMF allow for significant chemiluminescence at acidic pH. This was explained by the inability of most solvents to deprotonate the imidazopyrazinone core, preventing the oxygenation step of the chemiluminescent reaction.

So far, different researchers have tried to explain the chemiexcitation mechanism based on either electron transfer or charge transfer steps, which resulted in chemiexcitation by charge annihilation. However, recent evidence has discredited these hypotheses. Here was pursued an alternative explanation for the efficient chemiexcitation of dioxetanone molecules. The new mechanism is based on the degree of interaction between the keto and CO_2 moieties of dioxetanone. If favorable, the detachment of CO_2 to produce the light emitter is delayed, and the reacting molecules have access to a zone of degeneracy between ground and excited states, which favors chemiexcitation.

Six novel Coelenterazines were synthesized with the goal that they can act both as a self-activation molecule and as photosensitizer. To this end, the derivatives were characterized spectroscopically in terms of chemiluminescence and the ability to produce singlet oxygen. Proof-of-concept was provided by performing *in vitro* toxicity assays in tumor cell lines. In conclusion, novel photosensitizers were produced with the ability of self-activation, without the need for either photoexcitation or energy transfer steps. This opens the door for using PDT for treating tumors irrespective of their size and localization in the body.

Resumo

A terapia fotodinâmica (TFD) é uma potencial terapia no tratamento do cancro devido ao seu caracter minimamente invasivo. Este tratamento consiste na destruição de células tumorais alvo através de oxigénio singleto, que é produzido pela ativação do fotossensibilizador (FS), na presença de luz. No entanto, devido a problemas de penetração da luz nos tecidos, este tratamento apenas é aplicado a pequenos tumores e/ou na pele, bem como na superfície de órgãos/cavidades. A TFD é então incapaz de tratar cancros metastizados devido à natureza da sua localização. Posto isto, o objetivo deste trabalho é utilizar novos compostos como base para fotossensibilizadores auto-ativáveis, que serão capazes de superar as limitações correntes da TFD.

Para tal, o novo FS será baseado na Coelenterazina marinha que é capaz de emitir quimioluminescência (QL) na ausência de um catalisador. Mais concretamente, estados excitados são produzidos na ausência de uma fonte de luz externa. Logo, os problemas associados com a penetração de luz nos tecidos são eliminados. A ausência de catalisador também facilita o uso da QL da Coelenterazina na TFD, uma vez que apenas a Coelenterazina seria administrada ao paciente, eliminando as dificuldades associadas à libertação de todos os componentes reacionais no mesmo compartimento celular sem reagir durante a libertação.

Além disso, a Coelenterazina não é apenas a fonte de excitação (através da QL), mas também atua como FS. Isto é, o substrato QL proposto produz estados tripleto excitados capazes de produzir oxigénio singleto através de interação com O_2.

Apesar da Coelenterazina apresentar algumas vantagens para o desenvolvimento de FS auto-ativáveis, há alguns problemas que têm ainda que ser ultrapassados. Nomeadamente, as reações QL têm baixo rendimento quântico e o sistema da Coelenterazina é conhecido pela produção de estados singleto excitados em vez de estados tripleto (os necessários para a produção de oxigénio singleto). Estes problemas são difíceis de resolver devido à falta de conhecimento e informação mecanística sobre a Coelenterazina. Para abordar este problema, o projeto presente segue duas vias de investigação (que podem ser considerados os dois objetivos principais desta tese):

- Uso de uma abordagem espetroscópica, cromatográfica e teórica combinada para obter informação mecanística sobre a QL da Coelenterazina e moléculas relacionadas, com ênfase no processo de quimioexcitação (QE), em diferentes meios. Este estudo foi feito através da compreensão dos mecanismos básicos da QL da Coelenterazina.

- Síntese de novos FS baseados na Coelenterazina, a sua caracterização (com foco na sua capacidade de produzir oxigénio singleto) e a avaliação da sua citotoxicidade in vitro em células tumorais. Este estudo pode ser considerado como uma fase de prova de conceito.

O passo de QE da Coelenterazina e *Cypridina* luciferina foi estudado através de uma abordagem espetroscópica e computacional combinada em soluções modelo de DMSO. Foi descoberto que a QL destas moléculas é dependente do pH: o output total de luz diminuí com o aumento de pH, enquanto que a velocidade da reação apresenta o comportamento oposto. Estas diferenças foram atribuídas ao equilíbrio químico do intermediário dioxetanona. Mais especificamente, a termólise da dioxetanona neutra leva a uma QE mais eficiente. Isto resulta da dioxetanona neutra ter acesso a uma região de degeneração, na qual o estado fundamental singleto e estados excitados estão degenerados. A espécie aniónica não tem acesso a esta região.

Enquanto estudos prévios da QL da Coelenterazina exploraram extensivamente a substituição do core imidazopirazinona em diferentes posições, o efeito exercido pelo solvente não tem sido explorado. Para colmatar esta falta de conhecimento, foi feito um estudo comparativo da QL da Coelenterazina e dois derivados em diferentes solventes apróticos, através de uma abordagem espetroscópica, cromatográfica e teórica combinada. Foi descoberto que apenas o DMSO e o DMF permitem uma QL significativa a pH ácido. Isto foi explicado pela incapacidade da maioria dos solventes de desprotonar o core imidazopirazinona, o que previne a oxigenação da reação QL.

Até agora, diferentes investigadores têm tentado explicar os mecanismos de QE baseando-se em transferência eletrónica ou transferência de carga, o que resulta em QE por aniquilação de carga. No entanto, evidências recentes desacreditaram estas hipóteses. Neste trabalho propusemos uma explicação alternativa para a QE eficiente das moléculas de dioxetanona baseado no grau de interação entre os fragmentos ceto e CO_2 da dioxetanona. Quando favorável, a separação do CO_2 para produzir a molécula emissora de luz é retardada e as moléculas reagentes têm acesso a uma zona de degeneração entre o estado fundamental e os estados excitados, o que favorece a QE.

Seis novas Coelenterazinas foram sintetizadas com o objetivo de atuarem como molécula auto-ativável e como FS. Os derivados foram caracterizados espetroscopicamente e foi avaliada a capacidade de produção de oxigénio singleto. Prova de conceito foi adquirida pela realização de ensaios *in vitro* de toxicidade em linhas celulares tumorais. Para concluir, novos FS foram produzidos com capacidade de auto-ativação, sem a necessidade de fotoexcitação ou passos de transferência de energia. As descobertas abrem então uma porta para o uso TFD no tratamento de tumores independentemente do seu tamanho e localização no corpo.

Index

1. Introduction 1
1.1. Photodynamic therapy 1
1.2. General Mechanisms of Chemi- and Bioluminescence 3
1.3. Chemiexcitation Mechanisms Responsible for CL/BL Emission 5
1.4. Mechanisms of the Systems Already Studied for Photodynamic Therapy 7
1.4.1. Luminol reaction 7
1.4.2. Firefly luciferin reaction 8
1.4.3. Coelenterazine reaction 8
1.5. Application of Chemi- and Bioluminescence to Photodynamic Therapy 11
1.5.1. Firefly Luciferin-Mediated Photodynamic Therapy 11
1.5.2. Coelenterazine-Mediated Photodynamic Therapy 11
1.5.3. Luminol-Mediated Photodynamic Therapy 12
1.6. Pitfalls of Chemi-/Bioluminescence-Mediated Photodynamic Therapy 14
1.7. Other Strategies for Deep Photodynamic Therapy 15
1.8. Objectives of this work 17
1.9. Structure of this work 19
2. Mechanistic insight *Cypridina* luciferin and Coelenterazine chemiexcitation . 21
2.2.1. Kinetic chemiluminescent assay 21
2.2.2. Measurement of chemiluminescence and fluorescence spectra 22
2.2.3. Measurement of UV-visible spectrum 22
2.2.4. Theoretical investigation of *Cypridina* Dioxetanone 22
2.3.1. Chemiluminescence of *Cypridina* Luciferin in DMSO 23
2.3.2. Theoretical Investigation of *Cypridina* Dioxetanone 26
2.3.3. Chemiluminescence of Coelenterazine in DMSO 30
2.3.4. Theoretical Investigation of Coelenterazine Dioxetanone 36
2.3.5. UV-Vis spectrum of Coelenterazine 37
3. Comparative Study of the Chemiluminescence of Coelenterazine, Coelenterazine-e and Cypridina Luciferin 40
3.2. Materials and methods 40
3.2.1. Kinetic chemiluminescent assays for Cypridina luciferin, Coelenterazine, Coelenterazine-e and Coelenteramide 40
3.2.2. Measurement of fluorescence spectra for *Cypridina* luciferin, Coelenterazine, Coelenterazine-e and Coelenteramide 41
3.2.3. Chromatographic assays 41
3.2.4. Theoretical study of chemiexcitation mechanism of model dioxetanones in different solvents 41

3.2. Results and discussion 42
4. Theoretical study of chemiexcitation mechanism of model dioxetanones from TD-DFT and Multi-Reference Calculations 58
4.2. Materials and methods 58
4.3. Results and Discussion 60
5. Synthesis and evaluation of self-illuminating photosensitizers 69
5.2. Materials and methods 69
5.2.1. Synthesis Methodology 69
5.2.2. Kinetic chemiluminescent assay 69
5.2.3. Measurement of chemiluminescence and fluorescence spectra 70
5.2.4. Fluorescent assay for detection of singlet oxygen 70
5.2.5. *In vitro* assays for the cellular viability 70
5.3. Results and discussion 70
5.3.1. Chemiluminescence and fluorescence of Compounds 3, 4 and 5 in DMSO . 70
5.3.2. Fluorescent assay for detection of singlet oxygen 72
5.3.3. *In vitro* toxicity assays 73
6. Conclusions and future work 78
7. References 81

Index of figures

Figure 1- Rate constants (k, in s^{-1}) at acidic and basic pH in DMSO solutions (a). Plateau of light intensity (normalized values) at and basic pH (b). Chemiluminescence spectra in DMSO (c). 24
Figure 2- Potential energy curves of S_0 and S_1 states, as a function of intrinsic reaction coordinates, of model (Scheme 9, R_2=R_3=CH_3) neutral (a) and anionic (b) dioxetanone. 27
Figure 3- Electron spin density of the dioxetanone and imidazopyrazinone moieties of anionic (a) and neutral (b) model Cypridina dioxetanone (Scheme 9, R_2=R_3=CH_3), as a function of intrinsic reaction coordinates. 28
Figure 4- Atomic Mulliken charge of the CO_2 and oxyluciferin moieties of anionic (a) and neutral (b) model Cypridina dioxetanone (Scheme 9, R_2=R_3=CH_3), as a function of intrinsic reaction coordinates. 30
Figure 5- Calculated area (in RLU) of the CL profile of Coelenterazine, between 0 and 85 seconds, with increasing concentrations. Values were obtained at acidic (by addition of acetate buffer pH 5.12), neutral (phosphate buffer pH 7.4) and basic pH (by addition of NaOH). 32
Figure 6 - CL spectra (normalized values) of the light-emitting reaction of Coelenterazine (3 µM) in DMSO (A). UV-Vis spectra (normalized values) obtained in DMSO (in the presence of acetate buffer pH 5.12, 0.68%), with increasing concentrations of Coelenterazine (B). 34
Figure 7- Atomic Mulliken charge of the CO_2 and Coelenteramide moieties of an anionic and neutral model Coelenterazine dioxetanone (a phenol and methyl groups at the C6 and C2, respectively), as a function of intrinsic reaction coordinates. Calculations were made at ωB97XD/6-31G(d,p) level of theory in implicit diethyl ether, as described in reference [45] 37
Figure 8- CL profile (light emission as a function of time) for Coelenterazine in DMSO/DMF (A) and acetonitrile/pyridine (B), with addition of acetate buffer pH 5.12. These profiles are also representative for the other imidazopyrazinones here studied (Cypridina luciferin and Coelenterazine-e). Fluorescence spectra (normalized) for Coelenteramide in DMF and acetonitrile (C), with addition of acetate buffer pH 5.12.. 44
Figure 9- Chromatograms obtained for the reaction mixtures of Coelenterazine CL in DMF (A), acetonitrile (B) and diethyl ether (C), all with addition of acetate buffer pH 5.12 (0.68%). The mobile phase was composed of water (70%) and acetonitrile (30%) for reaction mixtures in acetonitrile and diethyl ether. For reaction mixtures in DMF the percentage of acetonitrile was increased to 40%. The flux was of 0.35 mL per minute. 47
Figure 10- Chromatograms obtained for the reaction mixtures of Coelenterazine CL in DMF (A), acetonitrile (B) and diethyl ether (C), all with addition of NaOH 0.1M. The experimental conditions were the same as the ones indicated in Figure 9. 48
Figure 11- Potential energy curves for S_0 and S_1 states, as a function of intrinsic reaction coordinates, of model neutral dioxetanone (Scheme 9; R_1 = indole, R_2 = R_3 = CH_3). The calculations were made at the TD UωB97XD/6-31+G(d,p) level of theory, in implicit DMF (A), acetonitrile (B) and diethyl ether (C). 50
Figure 12- Potential energy curves for S_0 and S_1 states, as a function of intrinsic reaction coordinates, of model anionic dioxetanone (Scheme 9; R_1 = indole, R_2 = R_3 = CH_3). The calculations were made at the TD UωB97XD/6-31+G(d,p) level of theory, in implicit DMF (A), acetonitrile (B) and diethyl ether (C). 51

Figure 13- Calculated area of the CL profile (up to 85 seconds) obtained in the chemiluminescent reaction of Coelenterazine (1µM), in either DMF, DMSO and acetonitrile (A). Fluorescence intensity of Coelenteramide (1 µM), in either DMF, DMSO and acetonitrile (B). To the mixtures were added either acetate buffer pH 5.12 (0.68%), NaOH 0.1M or NaOH 0.3 M. 54
Figure 14- Hole-electron distribution for the $S_0 \rightarrow S_1$ chemiexcitation at the TS structure for the thermolysis reaction of a neutral dioxetanone model (Scheme 10, R_1 = phenol, R_2 = R_3 = CH_3), at the TD UωB97XD/6-31+G(d,p) level of theory in implicit DMF (A) or diethyl ether (B). 55
Figure 15- Transition dipole moment for the $S_0 \rightarrow S_1$ chemiexcitation at the TS structure for the thermolysis reaction of a neutral dioxetanone model (Scheme 10, R_1 = phenol, R_2 = R_3 = CH_3), at the TD UωB97XD/6-31+G(d,p) level of theory in implicit DMF (A) or diethyl ether (B). 56
Figure 16- Active orbitals included in the MS-CASPT2 calculations for the thermolysis of -CH_2CH_3 dioxetanone..... 59
Figure 17- Active orbitals included in the MS-CASPT2 calculations for the thermolysis of -CH_2CF_3 dioxetanone. 59
Figure 18- Potential energy curves of S_0 and S_1 states, as a function of intrinsic reaction coordinates, of model dioxetanones (Scheme 11). The curves were calculated at the ωB97XD/6-31+G(d,p) level of theory. Dioxetanone species: -CH_3 (A), -OH (B), -CH_2CH_3 (C) and -CH_2CF_3 (D). 62
Figure 19- Potential energy curves of the S_0, S_1 and S_2 states as a function of intrinsic reaction coordinates of model dioxetanones (Scheme 11). The calculations were made at the MS-CASPT2/ANO-RCC-VDZ, on top of geometries obtained in ωB97XD/6-31+G(d,p) optimizations. Dioxetanones species: -CH_2CH_3 (A) and -CH_2CF_3 (B). 63
Figure 20- ESP atomic charges, as a function of intrinsic reaction coordinates, of model dioxetanones. The charge densities were calculated at the ωB97XD/6-31+G(d,p) level of theory. Dioxetanone species: -CH_3 (A), -OH (B), -CH_2CH_3 (C) and -CH_2CF_3 (D)..... 64
Figure 21- E(ζ), ΔΔE(ζ)strain and ΔΔE(ζ)int values plotted as a function of intrinsic reaction coordinates, during the thermolysis of model dioxetanones (Scheme 11). They were calculated at the ωB97XD/6-31+G(d,p) level of theory. Dioxetanone species: -CH_3 (A), -OH (B), -CH_2CH_3 (C) and -CH_2CF_3 (D). 65
Figure 22- Variation of the O-C-O angle (in Å), as a function of intrinsic reaction coordinates, of the CO_2 moieties of model dioxetanones during their thermolysis reactions. Dioxetanone species: -CH_3 (A) and -CH_2CH_3 (B). 67
Figure 23- CL profile (light emission as a function of time) for Compounds 3, 4 and 5 and respective area of chemiluminescence profile. 71
Figure 24- Fluorescence spectra (normalized) for light emitter species of the Compounds 3, 4 and 4. 72
Figure 25- CL spectra of the light-emitting reaction of Compounds 3 and 5. 72
Figure 26- Analysis of the fluorescence of an oxygen singlet probe (ABDA), with increasing concentrations of the studied compounds. Values were obtained at neutral (phosphate buffer pH 7.4). 73
Figure 27- Percent viability measured by MTT reduction assays for Compounds 1 (24 and 48h) and 2 (24H), at increasing concentrations. The percentage values above some bars refer to toxicity measured with the LDH assay, when statistically significative. Percent viability was obtained by comparing with control cell viability, considered as 100%. Data represents the mean ± SD of measurements of three independent experiments. Results of the one-way ANOVA factorial analysis. 74
Figure 28- Percent of cytotoxicity measured by MTT assay (bars) and percentage of total LDH of compounds 3-5 (24 and 48h), at increasing concentrations of both

compounds. Percent viability was obtained by comparing with control cell viability, considered as 100%. Data represent the mean ± SD of measurements of three independent experiments. Results of the one-way ANOVA factorial analysis..... 75

Index of schemes

Scheme 1 - The Type I and II mechanisms of action of PDT. 1
Scheme 2- Representation of the three sub-groups of peroxide-containing CL/BL substrates. 3
Scheme 3- Reaction mechanisms for the thermal decomposition of dioxetanones..... 4
Scheme 4- Representation of the intermolecular CIEEL (a) and revised CIEEL mechanisms (b) for dioxetanones CL. 5
Scheme 5 - Schematic representation of the chemi- and bioluminescent reactions studied as excitation sources in PDT. 7
Scheme 6- General structure of imidazopyrazinones, and structures for relevant examples of natural imidazopyrazinones. 9
Scheme 7- General mechanism for the CL reaction of Coelenterazine. 10
Scheme 8- Comparison between the conventional CL-mediated PDT and the approach proposed in this dissertation..... 17
Scheme 9- Reaction mechanism of Cypridina CL. 25
Scheme 10- Schematic representation of Coelenterazine and solvent molecules and its respective state of protonation. 52
Scheme 11- Representation of known cyclic peroxides involved on chemi- and bioluminescence and the model dioxetanone species here studied. 60

Index of tables

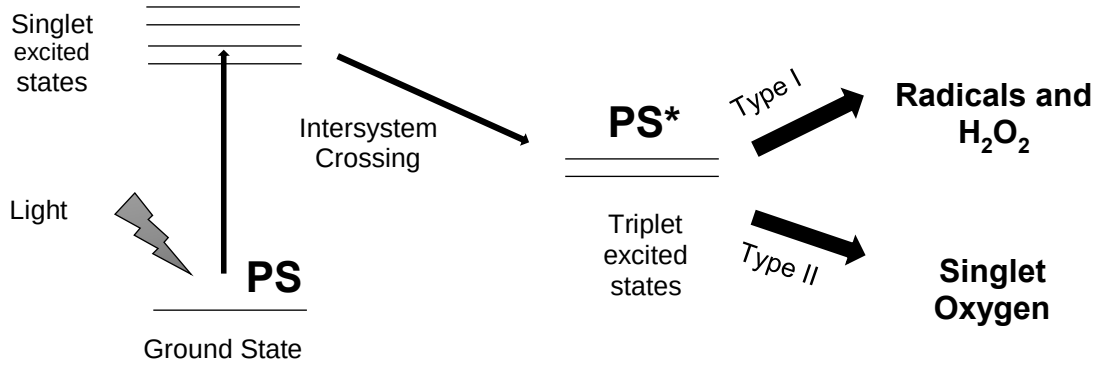
Table 1- Rate constants (k, in s^{-1}) and plateau of light intensity (normalized values) of Cypridina CL in DMSO, with addition of phosphate buffer pH 7.4 or NaOH (0.1M). 23
Table 2- Activation energies, with thermal corrections, (in kcal mol^{-1}) for the thermolysis reaction of neutral and anionic model Cypridina dioxetanones (Scheme 9), at the ωB97XD/6-31+G(d,p) level of theory in DMSO. The R_1 substituent is an indole moiety in all models (Scheme 9). 26
Table 3- Rate Constants (k, in s^{-1}) and Plateau of Light Intensity (in Relative Light Units, RLU) of Coelenterazine Chemiluminescence in DMSO, with Addition of Acetate Buffer pH 5.12, Phosphate Buffer pH 7.4 or NaOH (0.1 M). 31
Table 4- Ratios between Coelenterazine, Coelenteramide and the proposed dimer, in DMSO solutions with increasing concentrations of Coelenterazine (in the presence of acetate buffer pH 5.12, 0.68%). The ratios were calculated by measuring the UV-Vis spectra of these solutions (Figure 7.B), and by considering the absorbance of the peaks attributed to each species, based on previous findings by us and other authors. [84–87] 38
Table 5- Calculated area (in RLU) of the CL profile of different imidazopyrazinones, between 0 and 85 s, with addition of acetate buffer pH 5.12. 42
Table 6- Light intensity maxima (in RLU) of the CL profile of different imidazopyrazinones, between 0 and 85 s, with addition of acetate buffer pH 5.12. 43
Table 7- Initial velocities (in RLU s^{-1}) under steady-state conditions for the CL reaction of different imidazopyrazinones, with addition of acetate buffer pH 5.12. 43
Table 8- Activation energies (Eact, in kcal mol^{-1}) for the thermolysis reaction of four model dioxetanone species (Scheme 11), at the ωB97XD/6-31+G(d,p). 60

1. Introduction

1.1. Photodynamic therapy

Photodynamic therapy (PDT) is a therapeutic approach used for treating esophageal, skin, non-small cell lung cancers [1,2]. To induce cytotoxicity, this therapy induces the synthesis of reactive oxygen species (ROS). ROS can destroy cancer cells by inducing immunostimulation, apoptosis, vessels shutdown and necrosis [2]. A non-toxic photosensitizer (PS), presence of molecular oxygen and light (of specific wavelength) are three fundamental requirements of PDT [1–3]. The excitation of PS induces the cytotoxic effects, once light is irradiated in the target site. More specifically, photo-excitation occurs from the singlet ground state to an excited singlet state. Then, that excited state, via intersystem crossing, crosses to long-lived triplet states, inducing ROS production [3,4].

There are two pathways to form ROS (Scheme 1) [3,4]: the Type I and II reaction. On the first one, the triplet state of the PS transfers an electron or a hydrogen-atom to biological molecular oxygen or substrates, resulting in the formation of radical species. The latter one is the most prevalent one in PDT, in which the triplet state of the PS transfer its energy to molecular O_2, leading to the formation of singlet O_2.



Scheme 1 - The Type I and II mechanisms of action of PDT.

PDT has some advantages over other cancer treatments (such as surgery, radiotherapy and chemotherapy), as the PS only undergoes activation under light excitation under specific wavelengths. This feature of PDT allows for reduced side-effects. However, the depth of light penetration into biologic tissues is smaller than 1 cm, [1–4]. Therefore, PDT can only be used on tumors located on the lining of internal organs/cavities and under the skin. Given all this, PDT is a localized therapy, being unsuccessful against metastatic tumors [1].

Consequently, it is essential to design PSs that can be activated intracellularly without the need for external light sources. This achievement can increase the potential of PDT in successful cancer therapy. Several researchers have been trying to accomplish this goal through the creation of “self-illuminating” PDT systems based on either chemiluminescent resonance energy transfer (CRET) or bioluminescent RET (BRET) [1–6]. Such processes consist on non-radiative energy from chemi- or bioluminescent donors to an appropriate acceptor molecule.

Bioluminescence (BL) is defined as the light emission in enzyme-catalyzed reactions in living organisms [7–10]. This phenomenon is observed in fireflies, worms, insects and bacteria. BL is originated from the oxidation of a molecule termed luciferin, in a reaction catalyzed by an enzyme, luciferase. BL can be considered a sub-type of chemiluminescence (CL), consisting in the production of light as a result of chemical reactions [8]. Many BL/CL systems have been studied [8,9,11–15] and both have numerous advantages as high quantum yields, specificity and speed of reaction. Consequently, these systems have been useful in microbial detection, bioimaging, analytical determination, and gene reporter [16,17].

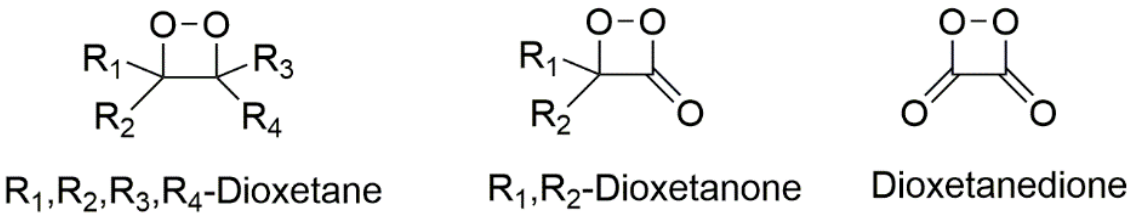
1.2. General Mechanisms of Chemi- and Bioluminescence

Light emission from CL/BL systems results from enzyme-catalyzed reactions that are divided into two classes: luciferase-luciferin reactions [8,9,18,19] and photoprotein systems [19,20]. In luciferase-luciferin reactions (the most prevalent in bioluminescent systems), the luciferase enzyme catalyzes the oxidation of luciferin, generating an electronically excited singlet state product. This product, oxyluciferin, relaxes to the S_0 state by photon emission. The luciferin, luciferase and oxyluciferin show differences between bioluminescent species [8,9,21].

Photoprotein systems are present only in marine organisms. In these systems occurs the formation of a stable enzyme-substrate [8,9,18,19] , which is formed between the apoprotein and an oxygenated marine luciferin (2-hydroxyperoxycoelenterazine). The light emission is due to the decomposition of the stable complex, which occurs when calcium ions bind to the photoprotein [22].

The efficiency of light emission of CL/BL reactions is described as quantum yield, which is determined by three different factors [8,9]: yield of the S_0 conversion of luciferin into oxyluciferin; chemiexcitation yield of singlet luminophores; fluorescent quantum yield of the emitter. Commonly, BL reactions have higher quantum yields, with some reactions reaching yields of 45-61% [23]. Given the efficient conversion of chemical energy into light emission, the relative non-toxicity of luciferin molecules and relatively simple chemistry of these systems (among other characteristics), several CL/BL systems gained several biomedical, pharmaceutical and bioanalytical applications (besides PDT) [16,23].

Most of CL substrates possess a peroxide bond (-O-O-), which provides a pathway for the production of excited state products [14,24,25]. These peroxide substrates are sub-divided into three groups, as seen in Scheme 2 [8,9,11,26].

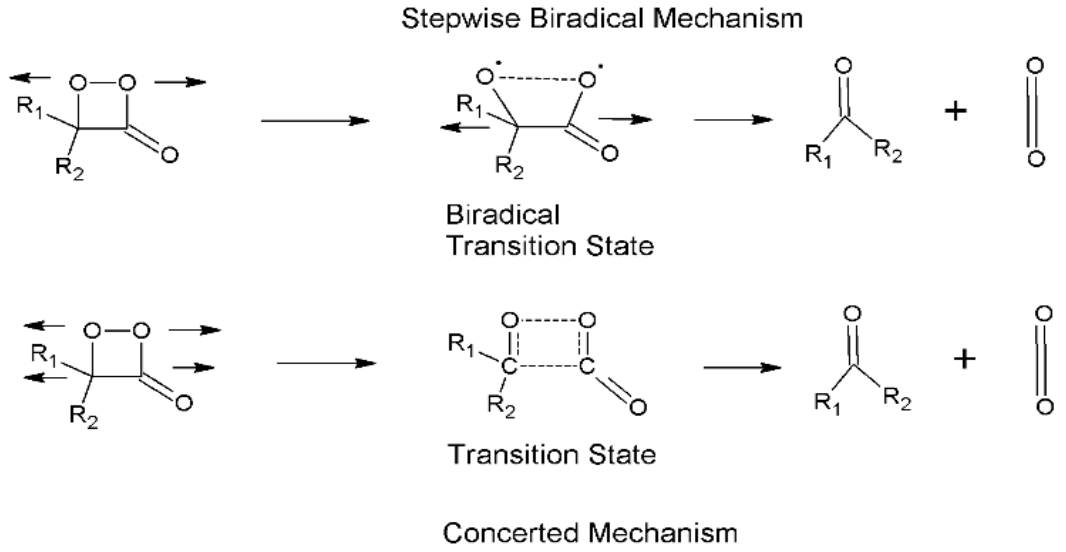


Scheme 2- Representation of the three sub-groups of peroxide-containing CL/BL substrates.

Dioxetanes and dioxetanones decompose thermally into an optically-active excited state, which is the most important feature for a CL molecule. This was verified

by thermochemical calculations (heats of reaction and activation energies varying between 70-90 and 20-30 kcal mol^{-1}, respectively).

There are two reaction mechanisms proposed for the ground state decomposition of these peroxides [9,11,27]: the stepwise-biradical mechanism and the concerted mechanism (Scheme 3). In the first one, the reaction is initiated by homolytic cleavage of the peroxide bond, producing a biradical transition state. The C-C bond breaking occurs only after the formation of the transition state; the one based on a concerted thermolysis, in which both O–O and C–C bond breaking occurs simultaneously.

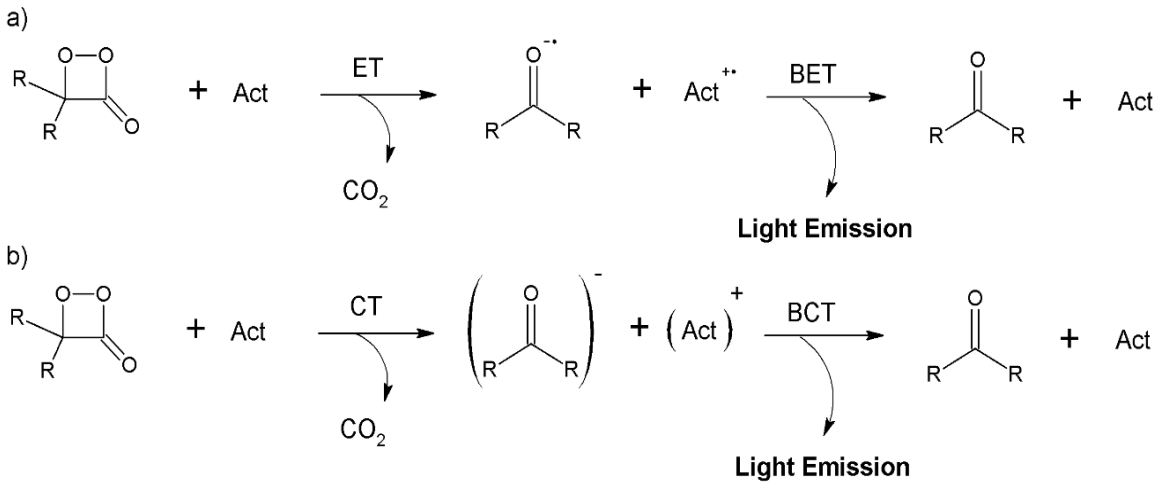


Scheme 3- Reaction mechanisms for the thermal decomposition of dioxetanones.

1.3. Chemiexcitation Mechanisms Responsible for CL/BL Emission

The Chemically Induced Electron-Exchange Luminescence (CIEEL, Scheme 4) explains the efficient generation of singlet excited states by CL/BL [28,29]. Namely, a radical ion pair is generated by an electron transfer (ET) from an oxidazable electron-rich moiety (or activator, Act) to the peroxide. This ion pair then suffers back electron transfer (BET) from the carbonyl radical anion to the radical cation, forming excited states with high efficiency. This mechanism can be called intramolecular or intermolecular CIEEL. The first, when the Act is part of the organic peroxide and the latter if the Act is another molecule.

Nevertheless, the validity of the CIEEL theory has been questioned since the CL of main examples of CIEEL (diphenoyl peroxide and dimethyldioxetanone) was re-examined [30,31]. The studies revealed these peroxides presented relatively low CL quantum yields, despite undergoing a CIEEL decay. Given the failure of this mechanism, different authors have suggested different mechanisms in which the formation of excited states is explained by charge (CT) and back charge transfer (BCT), instead of full electron transfer (Scheme 4). Such mechanisms are generally termed Charge Transfer Induced Luminescence (CTIL) [30,32,33]. Nevertheless, these new formulations of CIEEL still clash with the known data. Theoretical calculations showed that CT/BCT also occurred when no Act moiety was found [9,11]. Additionally, the presence of Act moieties does not guarantee the efficient generation of singlet excited states [24,30].



Scheme 4- Representation of the intermolecular CIEEL (a) and revised CIEEL mechanisms (b) for dioxetanones CL.

Taking these finding into account, our group have developed the Interstate Crossing-Induced Chemiexcitation (ICIC) mechanism [11,34,35]. While ET/CT steps appear to have an important and beneficial effect on the activation barrier for the

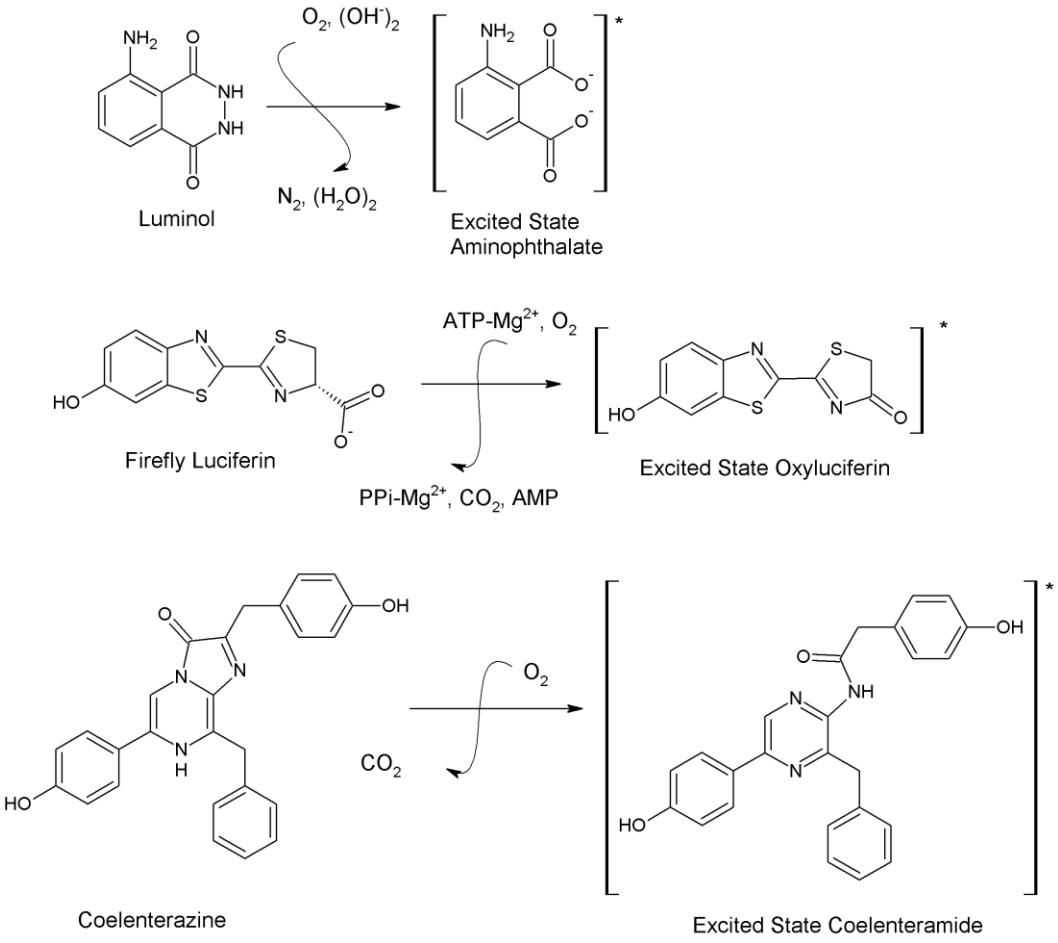
thermolysis, these processes seem to have an opposite effect on the chemiexcitation step. Theoretical calculations have showed that a more efficient chemiexcitation is achieved when the reacting molecules can access a region of the PES, where the ground and excited states are degenerated/near-degenerated [11,32,34–36].

Despite the ongoing discussion regarding the mechanism responsible for efficient chemiexcitation, three key structural moieties were identified for the different CL/BL substrates (Scheme 3) [8,34]. The first is the peroxide bond that initiates the thermally-activated singlet chemiexcitation. Despite some differences, this type of bond is a constant in this type of process. The second moiety is an electron-rich moiety, responsible for tuning the activation energy of the thermolysis [11,34,35]. This is also a ubiquitous moiety, except for *Latia* luciferin in which is thought that the enzyme provides the moiety in the form an amino-acid. [16] Finally, the last moiety is an ionizable group, that finely tunes the activation energy for the thermolysis [11,32,34–36].

1.4. Mechanisms of the Systems Already Studied for Photodynamic Therapy

1.4.1. Luminol reaction

The oxidation of luminol in basic solutions is the most efficient CL reaction (Scheme 5) [37–39]. It is observed with the addition of hydrogen peroxide and oxidant catalysts (such as Cu (II), Fe (II), periodate ions, Co (II), or hydrogen peroxidase). The CL reaction is triggered by the interaction of luminol with hydroxide anions, leading to the formation of a dianion [37–39]. The dianion reacts with oxygen to yield the aminophthalate ion in an emissive state, which is responsible for the emission of bright blue light (with a maximum of 425 nm) [37–39].



Scheme 5 - Schematic representation of the chemi- and bioluminescent reactions studied as excitation sources in PDT.

1.4.2. Firefly luciferin reaction

While luminol oxidation is the most well-described CL reaction, the luciferase-catalyzed oxidation of firefly luciferin is the most studied BL system (Scheme 5). The luciferase enzyme catalyzes the adenylation between luciferin and adenosine triphosphate (ATP), leading to the formation of an adenylyl intermediate. Then, this intermediate is oxidized by O_2, leading to the formation of the chemiexcited luminophore (oxyluciferin), and to the release of adenosine monophosphate (AMP) and carbon dioxide (CO_2).

One of the interesting features of this BL system is its pH-sensitive light emission [8,9,40]. While at basic pH the emission peaks at ~560 nm, it shifts to a maximum of ~620 nm at acidic pH. This phenomenon occurs due to pH-induced changes on the active site microenvironment, which leads to changes in the intermolecular interactions formed between oxyluciferin and active site molecules [7,41,42]. Another relevant feature for the application of this system to photodynamic therapy is its flash pattern of light emission [21,43,44]. The *in vitro* emission, at relatively high substrate concentration, commences with a brief flash that quickly decays to negligible levels. This pattern is caused by the production of inhibitory products, with one of them being the light emitter itself: oxyluciferin (Ki = 0.50 ± 0.03 µM) [21,43,44]. However, the most important inhibitor is dehydroluciferyl-adenylate (Ki = 3.8 ± 0.7 nM), an oxidation by-product of the bioluminescent reaction [21,43,44].

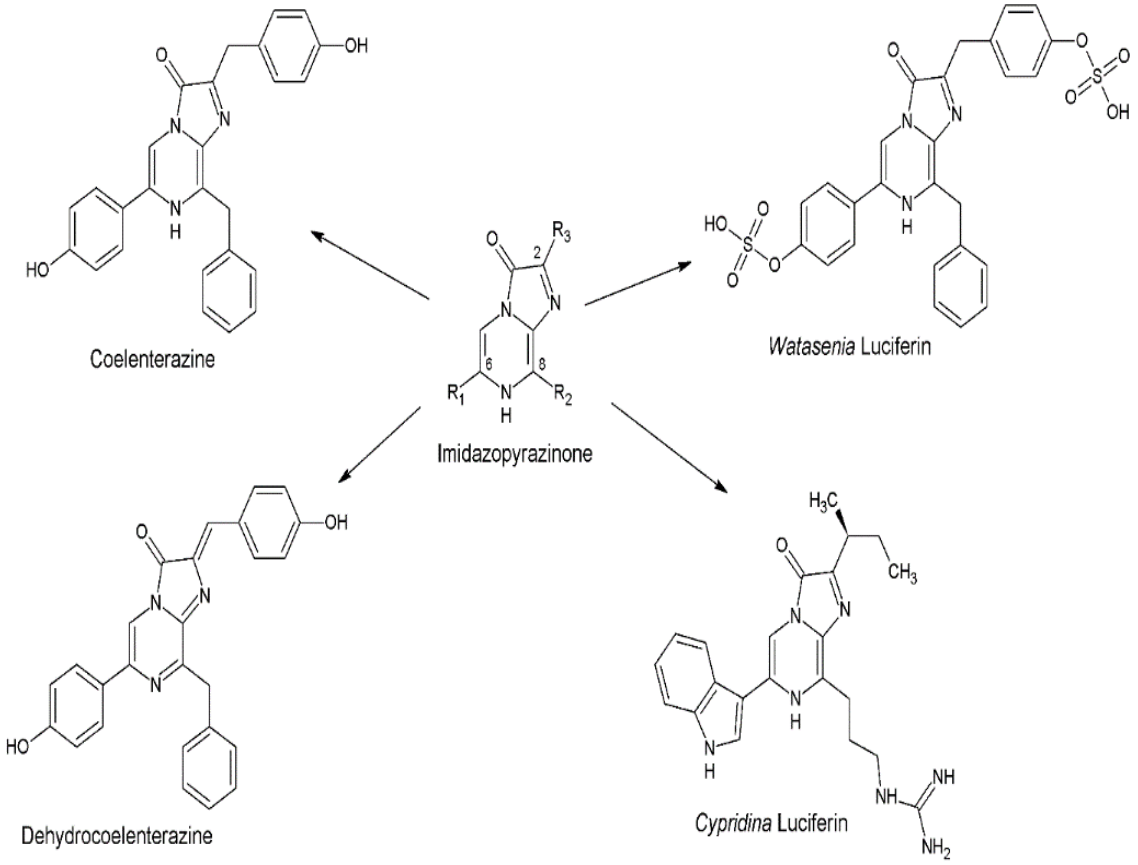
1.4.3. Coelenterazine reaction

Coelenterazine is a common marine luciferin, which is used by most BL marine organisms as a substrate for luciferase-luciferin and photoprotein-based reactions [22]. Several luciferases from natural sources have demonstrated activity by using Coelenterazine as a substrate [22]. However, *Renilla reniformis*, *Gaussia* and *Metridia longa* luciferases are the ones which have been used in practical applications of luciferase-Coelenterazine reactions.

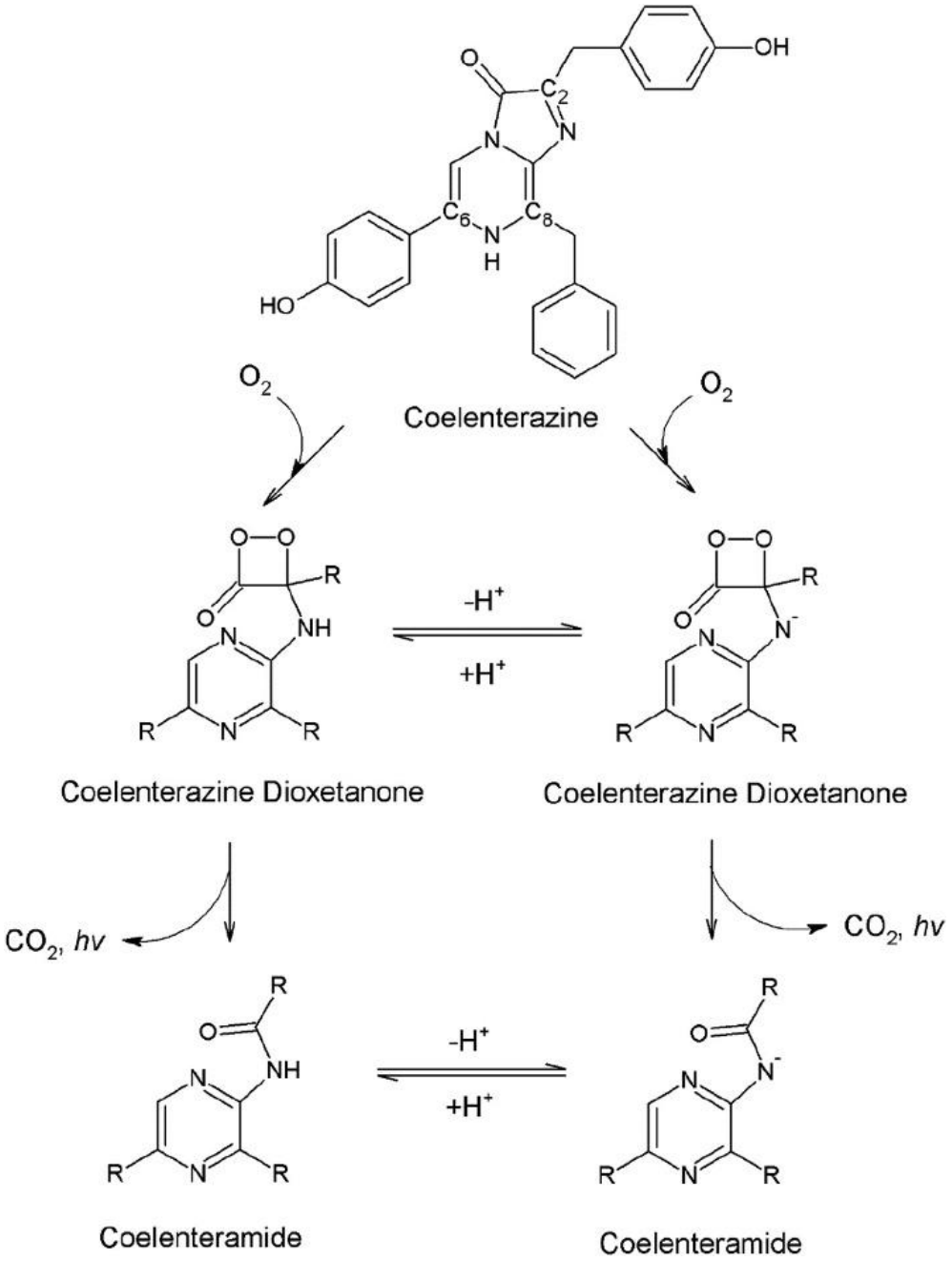
Coelenterazine is part of the imidazopyrazinone class of CL/BL molecules, in which also are included *Cypridina* and *Watasenia* luciferins (Scheme 6). This class connects many luminescent substrates found in marine organisms [23,45]. The luminescent reactions of imidazopyrazinone-based compounds have been described as follows (Scheme 7) [13,22,46,47]: the imidazopyrazinone scaffold reacts with O_2, which quickly leads to the generation of a dioxetanone intermediate. Upon decomposition of this latter species into chemiexcited oxyluciferin, visible light is emitted due to radiative decay of the chemiluminophore to the ground state. Besides O_2, the imidazopyrazinone scaffold can also react with other oxidizing species (as reactive oxygen species) to

generate visible light. In this way, these species have also been used as CL probes for reactive oxygen species [47].

In the specific case of Coelenterazine, the oxyluciferin species is called Coelenteramide (Scheme 7). Upon chemiexcitation, this luminophore is responsible for emission of blue-green light with a spectral peak at 480 nm.



Scheme 6- General structure of imidazopyrazinones, and structures for relevant examples of natural imidazopyrazinones.



Scheme 7- General mechanism for the CL reaction of Coelenterazine.

1.5. Application of Chemi- and Bioluminescence to Photodynamic Therapy

1.5.1. Firefly Luciferin-Mediated Photodynamic Therapy

Theodossiou and co-workers tested the potential application of BL to PDT by using the firefly luciferase-luciferin system as an intracellular excitation source for Rose Bengal [6]. They transfected cell lines with a Fluc gene, adding latter both luciferin and the PS to the cell cultures. These tested system led to a 90% toxicity, thus supporting the use of firefly BL as an excitation source [6].

Later, Schipper and colleagues have re-assessed the use of the firefly system in PDT [48], affirming that it was not clear if the photon output of Fluc transfected cells could cause similar photodynamic effects to those induced by light doses typically administrated in PDT (around 50 mW/cm^2, and above 1 J/cm^2) [48]. Contrary to the previous study, the photon output obtained was only $1.2x10^{-9}$ mW/cm^2 [6]. Thus, according to this study, two different PS (hypericin and Rose Bengal) were not capable to produce a cytotoxic effect [48]. However, while Theodossiou and co-workers used luciferin concentrations of 500 *μM* [6], Schipper and colleagues used significantly lower concentrations (as high as 20 *μM*) [48]. Thus, the different results obtained in these studies are not unexpected.

1.5.2. Coelenterazine-Mediated Photodynamic Therapy

The Renilla reniformis luciferase-Coelenterazine BL system was also tested as an intracellular excitation source in PDT. Lai and co-workers [49] were the first group that have studied this system in the context of PDT. To absorb the photons emitted by Coelenterazine BL via BRET, they have conjugated luciferase with quantum dots. This approach allows the use of the BRET reaction with a higher number of PS, as the emission wavelength of the quantum dots is more easily tunable than that of BL.

These BL-quantum dots conjugates were used to excited the marketed PS meta-tetra-hydroxyphenyl-chlorine (m-THPC, Foscan®), in mice treated with human lung adenocarcinoma epithelial A549 cells [49]. The results were promising since in the mice treated with the conjugates, the tumor growth was significantly reduced. Besides that, when compared to treated with m-THPC/Coelenterazine (4.2% inhibition) or luciferase/Coelenterazine/quantum dot (23.3% inhibition) the isolated tumor sizes of PDT-treated groups (luciferase/quantum dots/m-THPC/Coelenterazine) was meaningfully lower. However, this study also showed that the luciferase-quantum dot conjugates can be cytotoxicity by themselves, reducing its clinical applicability. The conjugates were demonstrated to decrease the degree of vascularization, leading to suppression of tumor growth.

The authors had also aimed towards the evaluation of the efficiency of bioluminescence-mediated PDT compared with conventional external light irradiation [49]. They have observed, at the same concentration of PS, that the BRET-induced PDT yielded an irradiation of 0.6-0.8 J/cm^2. This was enough to produce a significant photodynamic effect *in vivo*, despite being lower than the light doses used in clinical PDT (above 1 J/cm^2). Additionally, the photon output measured (0.6-0.8 J/cm^2) is significantly higher than the measured values by Schipper et al. in the study of firefly luciferin-mediated PDT (1.03 x 10-4 mJ/cm^2) [48,49].

In conclusion, the work of Lai and co-workers supported the use of Coelenterazine BL, when coupled to quantum dots, being an alternative for excitation source for PDT [49]. As the induced cytotoxicity was not significant, further optimization of the system will be needed. The decrease of efficiency of the system can be due to a great number of energy transfer steps, as there are two energy transfer steps: the BRET step, in which the energy is transferred from the BL reaction to the nanoparticles; the second step is a FRET process from the quantum dots to the PS.

Recently it was reported a *Renilla* reniformis luciferase-Coelenterazine BL-mediated PDT [50]. Given the lower energy output obtained when compared to the required for conventional PDT, Kim and co-workers wanted to assess if BL is a good excitation source to be used in PDT [48–50]. Thus, they developed luciferase-quantum dot conjugates to excite intracellularly chlorine e6 (Ce6). Mice's were treated with three tumor cell lines: colorectal (CT26), melanoma (B16F10) and lung cancer cells (LLC). The authors began with the calculation of the efficiency of BRET from Coelenterazine to the quantum dots (60-65%). It is interesting to note that while Ce6 molecules (concentration of 100 µM) are activated 4 x 10^7 times per minute by a flux from a 660 nm laser light with 2.2 mW, the same PS is activated 3 x 10^8 per minute by the luciferase/Coelenterazine/quantum dot conjugates [50]. Hence, BRET energies in the order of 100 µJ can generate a more efficient activation in the cellular membrane than a laser energy.

1.5.3. Luminol-Mediated Photodynamic Therapy

The well-known luminol system was first studied by Firer and co-workers, towards its use in PDT [1]. They added luminol, hydrogen peroxide and a catalyst (ferrous sulphate) to murine hybridoma cells. The aim was to evaluate the efficiency of luminol for the activation of the PS haematoporphyrin (Hp) [1]. The results showed potential, as the activation of Hp by luminol resulted in an approximate 100% cytotoxicity [1]. However, the system revealed some biocompatibility issues, as luminol induced by itself about 15% cytotoxicity [1].

Besides that, a similar luminol system (containing hydrogen peroxide and horseradish peroxidase) was assessed by Wang *et al.* These researchers analyzed the potential of luminol to activate the PS oligo (*p*-phenylene vinylene) (OPV) [51]. Less than 10% *in vitro* cellular viability was observed with increasing OPV concentration [51]. Still, the CL system was also toxic to normal human cells, induced 30% toxicity by itself towards HeLa cells [51]. Similarly to other studies, [1,51] this system has some biocompatibility issues. Furthermore, the results indicated that this system has no specificity for tumor cells. The therapeutic efficacy of luminol was also evaluated by Wang and co-workers in HeLa cell tumor-bearing nude mice [51]. They observed ~ 30% of tumor inhibition ratio by the CL-mediated PDT group in comparison with the CL system alone.

The most recent report involving luminol [52] consisted on the construction of a nanoconjugate. In it, semiconducting polymer dots (Pdots) incorporating the PS m-THPC and amphiphilic Janus dendrimers were used to conjugate horseradish peroxidase and aminated folic acid onto the surface of the Pdots [52]. The potential for PDT was assessed *in vitro* by incubating the Pdots nanoconjugates with C6 glioma, MCF-7 breast cancer and NIH 3T3 fibroblasts cells. [52]. When the concentration of the nanoconjugates was 10μg/mL, 72%, 32%, and 17% cell viabilities were observed for the NIH 3T3, C6, and MCF-7 cells, respectively. It should be noted that the difference in cell viabilities between non-cancerous (NIH 3T3) and cancerous (C6 and MCF-7) cells can be attributed to aminated folic acid present in the surface of Pdots, given the overexpression of folate receptors in tumor cells [52].

1.6. Pitfalls of Chemi-/Bioluminescence-Mediated Photodynamic Therapy

The studies previous discussed showed the potential of CL/BL systems for acting as intracellular excitation sources in PDT, opening the way for addressing the current limitations of clinical PDT. However, the cytotoxicity induced by the studied CL/BL systems is not high enough for their use in clinical PDT and require further optimization. This insufficient cytotoxicity can be attributed to their mechanism of use. It is required that the CL/BL substrate and the catalyst are in the same microenvironment, to generate the required photon output. Nevertheless, it is not easy that all components are delivered to the same cellular compartment without reacting during delivery. Additionally, CRET and BRET require donor-acceptor proximity, so the chosen PS should be in that same cellular compartment as the luminophore.

The effectiveness of CL/BL-mediated PDT is dependent on four sequential steps: CL/BL → CRET/BRET to the PS → intersystem crossing → ROS production. These steps can lead to a decrease in the overall yield of PDT. Also, of note is that PDT has high selectivity, as the photodynamic effect affect only tissue containing the PS and irradiated by light. As these systems have no tumor-specificity, substituting laser photo-excitation by CL/BL activation will result in the loss of this advantage. This is especially of concern once some of the studied systems (as that of luminol) presented significant cytotoxicity by themselves. So, the use of these systems in PDT will require the development of new strategies for providing tumor-selectivity.

1.7. Other Strategies for Deep Photodynamic Therapy

Besides CL/BL, some authors have been testing other types of excitation sources for deep PDT. These strategies generally consist on an indirect excitation of the chosen PS by FRET via photo-conversion nanoparticles. Thus, different nanoparticles have been developed for deep PDT with indirect excitation of the PS by near infra-red (NIR) light and X-ray, based on physical absorption, covalent conjugation and surface coating.

NIR light (from 650 to 1350 nm) is more suitable for deep PDT than UV and visible light, as it provides a higher penetration depth in biological tissues. Organic dyes and upconversion nanoparticles have been used to convert one- and two-photon NIR light into UV/visible light to excite PS in deep PDT [53–55]. Lanthanide-doped upconversion nanoparticles have better optical properties than other fluorescent compounds (such as organic dyes). First, they present high photostability, large anti-Stokes shift, sharp multi-wavelength emission bandwidth, weak auto-fluorescence and deep tissue penetration [53]. Second, they can convert low-energy NIR (generally at 980 nm) light into high energy UV-Vis light [56],[58]. Thus, their use allows the excitation of PS in deeper locations in the body than conventional light sources, once NIR light has a higher depth of penetration. Despite these beneficial properties, upconversion nanoparticles present only relatively low quantum yields [53]. Besides that, the use of NIR light may lead to heat damage to the tissues. The conservative limit for skin exposure to 980 nm laser is 726 mW/cm^2, however this power density is too low to provide the photodynamic effect needed [53]. In this wise, the use of upconversion nanoparticles does not resolves all the problems of conventional PDT.

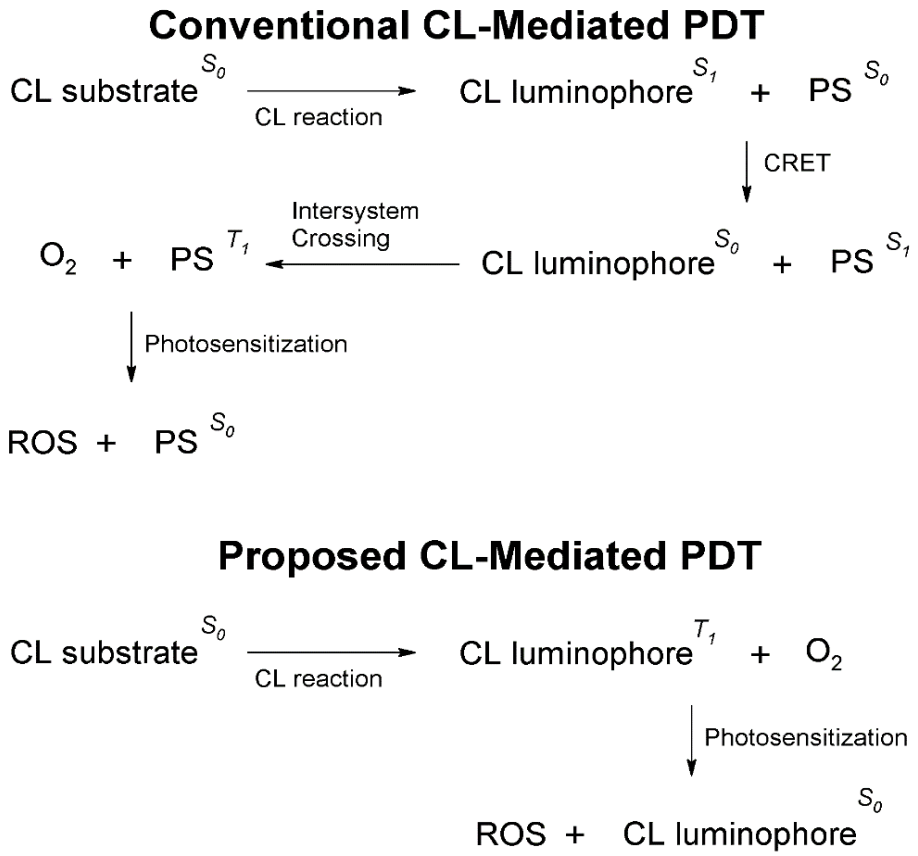
Another attempt to overcome the issues of conventional PDT has been the use of X-rays, ionizing radiation with photon energy between keV to MeV. Contrary to UV-Vis and NIR light, X-rays have an unlimited depth of penetration into the body, thus have been widely used in CT imaging and radiotherapy. Based on this, X-ray-mediated PDT has the potential to be used to excite a PS inside tumors, irrespective of their localization in the body. Moreover, a single X-ray treatment is able to induce a synergistic PDT and radiotherapeutic effect [57]. On the other hand, X-rays are not able to activate the PS directly due to the energy difference between X-ray (photon energy of keV-MeV) and the energy required to excited different PS (in the order of eV). Therefore, scintillating nanoparticles [53,58] and X-ray excited persistent luminescence nanoparticles [53,58] have been explored to convert high energy ionizing radiation into photons of the appropriated energy to excite PS. The use of such nanoparticles did show potential for X-ray-mediated PDT in tumors localized deeper in the body. However, the photo-conversion of these nanoparticles is still low [53]. Once the energy of this type of radiation is high, this approach can cause considerable damage to surrounding normal tissues,

leading to serious side-effects. It is also difficult to develop scintillating-PS conjugates with good stability, enhanced tumor retention and optimal FRET efficiency.

In summary, while alternative approaches to CL/BL-mediated PDT have been proposed, they do not provide better results. The “PS-excitation” output is still too low for use in clinical PDT, these systems do not present any specific tumor-selectivity, and these chosen excitation sources (NIR light and X-ray radiation) may lead to damage to normal tissues and cause serious side-effects. Moreover, the use of these systems requires external excitation equipment that CL/BL do not. Thus, CL/BL -mediated PDT is still one of the alternatives with the highest potential for generalizable antineoplastic PDT in a clinical environment, without limitations regarding tumor-localization.

1.8. Objectives of this work

The main goal of this work is to develop self-illuminating PS based on CL, so to be no need for external light sources: the PS can convert thermal energy into excitation energy via a chemical reaction. Thus, the problems typically associated with light-penetration into tissues is eliminated. The choice for a CL system instead of BL (which are known for higher quantum yield) is to eliminate the need for a luciferase or a photoprotein to catalyze the reaction. Namely, only the CL substrate must be administered to the patient, eliminating the difficulty of delivering several reaction components to the same cellular compartment without reacting during delivery. To ensure that losses during energy transfer steps are minimized, our objective is that the CL is not only the excitation source, but also acts as the PS by itself. That is, instead of ROS production being triggered by the chemiexcited production of singlet excited states (during CL) that transfer their energy to the PS towards its activation (Scheme 8), the proposed CL substrate produces chemiexcited triplet excited states during the CL reaction, able to produce ROS by interaction with molecular O_2 (Scheme 8). The proposed scheme is significantly simplified, which is expected to minimize efficiency losses.



Scheme 8- Comparison between the conventional CL-mediated PDT and the approach proposed in this dissertation.

The new PS will be based on marine Coelenterazine (described in section 1.4.3.), which besides being a BL substrate in the presence of luciferase/photoprotein, is also able be used in CL reactions without a catalyst. Namely, it reacts with superoxide anion to rapidly form a dioxetanone intermediate, with then decomposes in a chemiexcited luminophore [47,59]. That is, superoxide anion activates the CL reaction of Coelenterazine, with no need for other co-factors or catalysts. This gives a two-fold advantage for Coelenterazine to act as a self-activated PS in PDT:

1. Tumor cells are under significant oxidative stress, one of the reasons for this being the over-expression of superoxide anion [60,61]. Thus, the need of the Coelenterazine CL reaction for superoxide can be used as a tumor-selective factor.
2. As superoxide anion is already over-expressed in tumor cells, it is already present in the cells of the patient. Therefore, only the Coelenterazine-based PS needs to be administered to the patient, which significantly simplifies the procedure.

While Coelenterazine presents some advantages to development of self-activated PSs, there are some problems that must be overcome before that. Namely, CL reactions have low quantum yields (especially when compared with BL reactions) [24]. Furthermore, the Coelenterazine CL system is known for producing chemiexcited singlet excited states [23] instead of triplet ones (the desired ones for producing ROS species by interacting with O_2). In short, the major challenges for achieving the proposed goals are to increase the efficiency of chemiluminescence and modulate the chemiexcited triplet to singlet product ratio. These problems are difficult be solved, however, due to lack of knowledge and mechanistic insight into Coelenterazine and related imidazopyrazinones. To address this, the present project pursued two different avenues of research (which can be considered also as the two main objectives of this thesis):

- Use of a combined spectroscopic, chromatographic and theoretical approach to obtain mechanistic insight into the CL of Coelenterazine and related imidazopyrazinones, with emphasis on the chemiexcitation process, in different environments. Such study was made towards the understanding of the basic mechanics of Coelenterazine CL.
- Synthesis of novel Coelenterazine-based PSs, their characterization (with focus on their ability of producing ROS), and the evaluation of their *in vitro* cytotoxicity towards tumor cells. This study can be considered as a proof-of-concept phase.

1.9. Structure of this work

The remainder of this Thesis is divided into two sections: the presentation and discussion of results; the conclusions and future perspectives. Each section is composed of chapters, corresponding to scientific outputs produced during this work, in the form of published and submitted papers in specialized peer-review international journals, patents, book chapters, oral communications and scientific posters:

Papers Published and Submitted:

1. C.M. Magalhães, J.C.G. Esteves da Silva, L. Pinto da Silva, Comparative Study of the Chemiluminescence of Coelenterazine, Coelenterazine-e and *Cypridina* Luciferin with an Experimental and Theoretical Approach. *J. Photochem. Photobiol. B* **2018**, *Submitted.*
2. L. Pinto da Silva, C.M. Magalhães, Mechanistic Insights into the Efficient Intramolecular Chemiexcitation of Dioxetanones from TD-DFT and Multi-Reference Calculations. *Int. J. Quantum Chem.* **2018**, *Submitted.*
3. C.M. Magalhães, J.C.G. Esteves da Silva, L. Pinto da Silva, Study of Coelenterazine luminescence: electrostatic interactions as the controlling factor for efficient chemiexcitation. *J. Lumin.* **2018**, *199*, 339-347.
4. L. Pinto da Silva, R.F.J. Pereira, C.M. Magalhães, J.C.G. Esteves da Silva, Mechanistic Insight into *Cypridina* Bioluminescence with a Combined Experimental and Theoretical Chemiluminescent Approach. *J. Phys. Chem. B* **2017**, *121*, 7862-7871.

Patents:

1. Patent PPP59213 (Pending): Chemiluminescent Imidazopyrazinones-based photosensitizers with available singlet and triplet excited states.

Book Chapters:

1. L. Pinto da Silva, C.M. Magalhães, P.J.O. Ferreira, D.M.A. Crista, Chemi- and Bioluminescence in Self-Illuminating Photodynamic Therapy, *In* Photodynamic Therapy (PDT): Principles, Mechanisms and Applications. Nova Science Publishers, Inc., 2017. ISBN: 978-1-53611-912-1.

Oral Communications:

1. “Study of the Chemiexcitation Step of Coelenterazine Luminescence”. Oral presentation at IJUP, February 2018, Faculdade de Medicina da Universidade do Porto, Porto, Portugal.

2. “A New Approach for Cancer Therapy Based on Marine Chemiluminescence”. Oral presentation at 2nd SYMPOSIUM OF THE MSc IN ONCOLOGY, May 2018, Instituto Português de Oncologia (IPO), Porto, Portugal.

Poster:

1. “Development of Self-Excitable Photosensitizers for Photodynamic Therapy of Cancer”. C. Magalhães, P. Ferreira, A. Montenegro, E. Borges, L. Pinto da Silva, J. Esteves da Silva. Poster presentation at VIII Meeting of the Paul Ehrlich Euro-PhD Network, July 2018, Faculdade de Ciências da Universidade do Porto, Porto, Portugal.

The Results and Discussion section encompasses four chapters corresponding to the characterization of the chemiexcitation mechanism of Coelenterazine and *Cypridina* luciferin (section 2.), the study of the solvent effect on the CL reaction of Coelenterazine, Coelenterazine-e and *Cypridina* luciferin (section 3.), elucidation of a general mechanism for the chemiexcitation of dioxetanone molecules (section 4.), and the synthesis and characterization of novel PSs (section 5.).

The last section presents the main conclusions of the work performed, as well as perspectives of future research.

2. Mechanistic insight *Cypridina* luciferin and Coelenterazine chemiexcitation

2.1. Aim

The chemiexcitation step of Coelenterazine and related imidazopyrazinones during the CL reaction is still far from understood. This can be explained by the instability of the dioxetanone intermediate, which thermolysis leads to chemiexcitation, which impairs its experimental characterization. Theoretical modelling can circumvent this limitation by providing reliable and accurate insight into the thermolysis of this peroxide. However, the lack of experimental data that can be used as reference makes the interpretation of theoretical data rather difficult.

Herein, the chemiexcitation step of Coelenterazine and *Cypridina* luciferin (Scheme 6 and 7) CL was studied by using a combined spectroscopic and computational approach. The energy and kinetic CL profiles of these reactions were obtained with luminometric and fluorescence methods. These experiments were made in model dimethyl sulfoxide (DMSO) solutions, as imidazopyrazinones have been found to chemiluminesce readily in aprotic solvents by interacting with O_2 [13]. Thus, DMSO and other aprotic solvents are useful media for studying CL reactions. The thermolysis and chemiexcitation mechanisms of Coelenterazine and *Cypridina* CL were studied with an accurate density functional theory (DFT)-based approach. This combined experimental-computational approach allowed the rationalization of the CL mechanism for these molecules. It should be noted while that the major focus of this Thesis is on Coelenterazine, *Cypridina* luciferin was also studied to ensure that the conclusions here obtained are also valid for other imidazopyrazinone-based CL substrates, which can be found in about eight *phyla* of luminescent organisms.

2.2. Material and Methods

2.2.1. Kinetic chemiluminescent assay

Cypridina luciferin and Coelenterazine were dissolved in methanol. Kinetic chemiluminescent assays were performed in a homemade luminometer using a Hamamatsu HC135-01 photomultiplier tube, at ambient temperature.

To prepare the light reactions was used a solution of DMSO. To this solvent was added either acetate buffer pH 5.12 (0.68%), phosphate buffer pH 7.4 (0.075 M) or NaOH (0.1 M). The injection of the DMSO solution reaction into a tube containing Coelenterazine or *Cypridina* luciferin initiated the reaction. Increasing concentrations of

Coelenterazine was used. The final solution of *Cypridina* luciferin had a concentration of 4.3 μM. To integrate and record the light, it was used 0.1 s intervals. The Graphpad software package (Version 7.03 for Windows) allowed to analyze the resulting data.

2.2.2. Measurement of chemiluminescence and fluorescence spectra

A Horiba Jovin Yvon Fluoromax 4 spectrofluorometer was used to measure the chemiluminescence spectra for Coelenterazine and *Cypridina* luciferin. The integration time was of 0.1s and for the emission monochromators were used slit widths of 29 nm. Quartz cells were used. The spectra were obtained in solutions with a final volume of 500 μL, being the Coelenterazine concentration of 3 μM. The spectra were obtained in solutions with a final volume of 500 μL, being the *Cypridina* luciferin concentration of 12.3 μM. Besides, the fluorescence spectra of Cypridina was obtained, using a slit of 5 nm.

2.2.3. Measurement of UV-visible spectrum

UV spectra were obtained in DMSO solutions with addition acetate buffer pH 5.12 (0.68%), increasing the levels of the target imidazopyrazinone (5, 60 and 150 μM).

2.2.4. Theoretical investigation of *Cypridina* Dioxetanone

S_0 geometry optimizations and frequency calculations were performed at the ωB97XD/6-31G(d,p) level of theory, [62]. The U approach was used with a broken-symmetry (BS) technology, which mixes the HOMO and LUMO, making an initial guess for a biradical [35,36,63–65]. Intrinsic reaction coordinates (IRC) were carried out to assess if the obtained transition state (TS) connect the desired reactants and products. The energies of the S_0 IRC-obtained structures were re-evaluated by single-point calculations at the ωB97XD/6-31+G(d,p) level of theory. The S_1 state was calculated by using the time-dependent (TD) DFT approach, at the TD ωB97XD/6-31+G(d,p) level of theory. ωB97XD is a long-range-corrected hybrid exchange-correlation functional, [35,36,63–65] which provides accurate estimates for π → π*, n → π* local excitation, and CT and Rydberg states.

ωB97XD has already been used in the study of other imidazopyrazinone-based dioxetanones, which facilitates the comparison of results here obtained with previous work.[35,65] Geometry optimizations, frequency and IRC calculations were made in vacuo, while single-point calculations were made in implicit DMSO. This was achieved with the Polarizable Continuum Model using the integral equation formalism variant (IEFPCM) [66]. All calculations were made with the Gaussian 09 program package.

2.3. Results and discussion

2.3.1. Chemiluminescence of *Cypridina* Luciferin in DMSO

We have the measured the direct light-emission intensity at different pH values. By performing the exponential fitting of the kinetic chemiluminescent curves, we were able to obtain the plateau of light intensity (in relative light units, RLU) and the rate constants (k, in s^{-1}) [21,44]. Initially, these values were obtained in basic (with 0.1 M NaOH solution) and neutral (with phosphate buffer pH 7.4) pH. The results can be found in Table 1.

Analyzing the results, we can see that despite the reaction being slower in neutral pH, the light emission is five times higher. Additionally, we have performed assays in acidic and basic media (Figures 1.a and 1.b), that supported the previous results. Also, to achieve an acidic media we added acetate buffer (pH 5.12) to DMSO, in different amounts (0.1%, 0.08% and 0.04%). The basic media was achieved with different concentrations (0.01, 0.05 and 0.1 M) of NaOH. This approach was used to better compare with previous CL studies [67–71]. The plateau at 0.1 M of NaOH is only 5% of the plateau of a DMSO solution with 0.1% acetate buffer. So, the plateau values (light intensity at infinite times) decrease with increasing pH. On the other hand, with increasing pH the reaction rate increases significantly, between 0.65±0.01 s^{-1} and 1.51±0.10 s^{-1}. In conclusion, both the light intensity and the velocity of the CL reaction are pH-dependent.

Table 1- Rate constants (k, in s^{-1}) and plateau of light intensity (normalized values) of *Cypridina* CL in DMSO, with addition of phosphate buffer pH 7.4 or NaOH (0.1M).

	Phosphate buffer pH 7.4	NaOH (0.1 M)
k	0.30±0,06	1.59±0,09
Plateau	1.00±0,16	0.23±0,03

The pH-dependence of *Cypridina* light intensity is not exactly a new finding. Some authors have reported previously that appreciable CL yields (ca. 10% of the BL yield) for Cypridina-related imidazopyrazinones were only found in acidic solutions containing acetate buffer. By its turn, solutions containing NaOH (0.1 M) presented only negligible CL [67,68]. However, it was not clear if this difference in quantum yields was due to the pH, the polarity of the environment, or to a combination of both factors, since these measurements were made in different solvents. Moreover, it is not clear if the pH-dependence of the reaction rate and the plateau is caused by the same mechanism, or any unrelated processes. If the light emitting species is not the same in different pH, the

light intensity could be affected without the reaction rate being necessarily affected [8,9]. The oxyluciferin and dioxetanone species of imidazopyrazinone-based molecules can be found in either a neutral or anionic (amide) forms (Scheme 7) [36].

We have then obtained the CL spectra (Figure 1.c) for *Cypridina* light emission in DMSO solutions at different pH: acetate buffer pH 5.12 (0.68%), phosphate buffer pH 7.4, and NaOH (0.1M). The obtained spectra indicated that it is the same oxyluciferin species (with emission wavelength at ~460 nm) at different pH. The only difference between the spectra is the emission intensity that decreases with increasing pH.

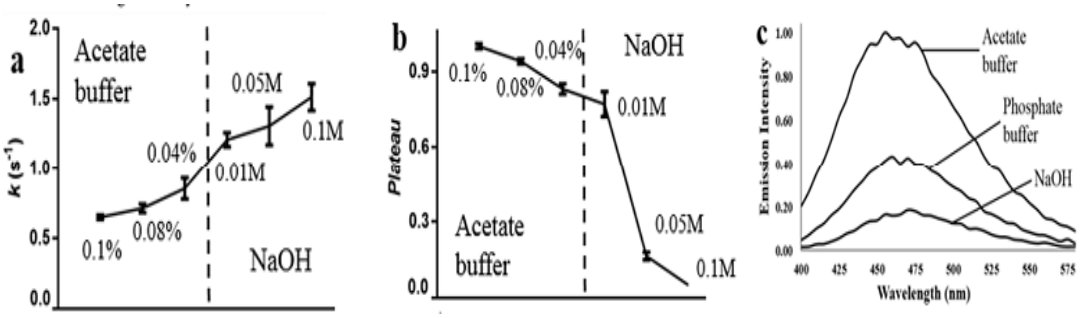


Figure 1- Rate constants (k, in s^{-1}) at acidic and basic pH in DMSO solutions (a). Plateau of light intensity (normalized values) at acidic and basic pH (b). Chemiluminescence spectra in DMSO (c).

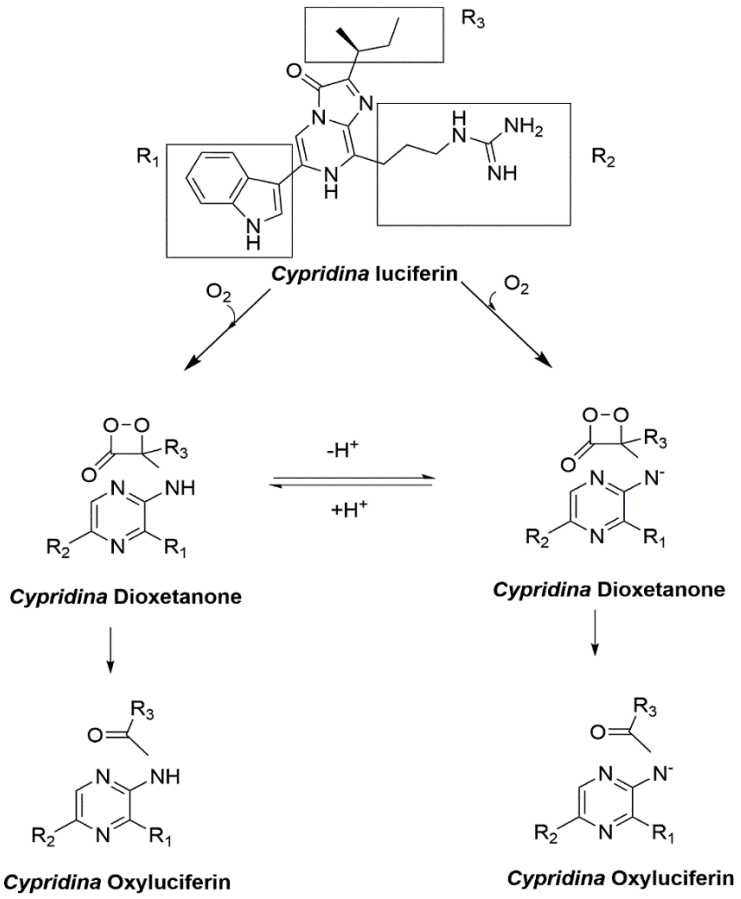
Some authors have stated that CL and fluorescent state are different for imidazopyrazinone-based compounds [72,73]. Nevertheless, following studies indicated that the CL state is a “dark” state that needs to evolve to a bright fluorescent state [45]. Thus, using a state-specific (SS) TD-DFT approach, [74] we analyzed if CL can be attributed to either neutral or amide *Cypridina* oxyluciferin, by calculating the fluorescent emission spectra of the anionic and neutral forms of a Cypridina oxyluciferin derivative. The results showed peaks with identical emission maxima, supporting the previous studies [45]. Our calculations indicate that the CL species is the neutral species, as the theoretical emission energy (2.87 eV) only differs 0.17 eV from the experimental value (2.70 eV), which is well within the type error attributed for TD-DFT calculations (0.20 eV). By its turn, the amide species (2.93 eV) differs from the experimental value by 0.24 eV. Moreover, the oscillator strength of the neutral species is higher than for the amide species (0.29 vs. 0.16). The identification of the neutral species as the chemiluminophore agrees with previous studies [75].

Taking all this into account, we have showed that both the light intensity and the reaction rate *Cypridina* CL are pH-dependent in DMSO. Moreover, these parameters present opposite behavior. Besides, as it is the same species (neutral oxyluciferin) to emit in acidic and basic pH, the effect of pH on the light intensity is not related to ϕF. The

increase of reaction rate with pH indicates that the activation barrier of the CL reaction decreases with increasing pH. As already noted, the global activation barrier of CL is determined by the two major steps of the reaction (oxygenation and thermolysis) [67,68], as seen in Scheme 7.

Oxygenation involves the deprotonation of the imidazopyrazinone scaffold, so it only explain some of the variation of the reaction rate as a function of pH [63,67,68]. It is expected that oxygenation step affects the speed of the reaction, once the deprotonation should be slower in acidic pH. However, slowing the reaction only delay reaching the plateau. Thus, there is no obvious reason for the oxygenation to affect the light intensity at infinite times.

Given that, the answer should be in the thermolysis of dioxetanone, [8,9,32,33,35,36,54,63] which is the one responsible for chemiexcitation. Furthermore the two species of dioxetanone (anionic and neutral) show different activation barriers and chemiexcitation processes [32,33,35,36,54,63]. The pH-dependent reaction rate and light intensity value could be explained if neutral dioxetanone is responsible for chemiexcitation at acidic pH and the anionic species at basic pH.



Scheme 9- Reaction mechanism of Cypridina CL.

2.3.2. Theoretical Investigation of *Cypridina* Dioxetanone

We have characterized the thermolysis and chemiexcitation of both forms of *Cypridina* dioxetanone (neutral and dioxetanone) by performing theoretical calculations at the TD-DFT level of theory. First, we have obtained the activation energies for the two dioxetanone models (Scheme 9; R_2=R_3=CH_3), which can be found in Table 2. The activation energies were also calculated for two more dioxetanone models (Scheme 9; R_2=R_3=H; R_2=H and R_3=CH_3).

Table 2- Activation energies, with thermal corrections, (in kcal mol^{-1}) for the thermolysis reaction of neutral and anionic model Cypridina dioxetanones (Scheme 9), at the ωB97XD/6-31+G(d,p) level of theory in DMSO. The R_1 substituent is an indole moiety in all models (Scheme 9).

Model molecule	Neutral species	Anionic species
R_2=R_3=H	22.0	10.6
R_2=H and R_3=CH_3	22.9	9.6
R_2=R_3=CH_3	21.3	10.4

These results are in line with previous studies [8,9,32,33,35,36,54,63], as the activation energy for the neutral-anionic forms of the dioxetanones is significantly different. Besides that, the anionic form presents the lower activation barrier (~10 kcal mol^{-1}), comparing to neutral dioxetanone (~22 kcal mol^{-1}). This result agrees with the experimental behavior observed for the reaction rate as a function of pH (Figure 1.b and Figure 1.c). Additionally, the activation energies for the neutral species are in line with the activation parameters for other dioxetanones and dioxetanes (~20 kcal mol^{-1}) [76–78].

The S^2 (an expectation value from the calculated wavefunction) value was calculated and it indicated the involvement of a biradical species in the thermolysis reaction of both forms of dioxetanone [8,9,32,33,35,36,54,63]. By analyzing the behavior of O1-O4 and C2-C3 bonds, we have determined that thermolysis occurs in all cases via a stepwise-biradical mechanism, in line with previous reports [8,9,32,33,35,36,54,63]. In Figure 2.a and Figure 2.b are presented the potential energy curves of S_0 and S_1 states, as a function of intrinsic reaction coordinates, of model dioxetanone (Scheme 9, R_2=R_3=CH_3). According to this, the S_1 and S_0 states of the neutral species in the biradical region, generated by O_1-O_4 elongation. Both states become nearly-degenerated, with an energy gap between 10.5 and 12.8 kcal mol-1 during a large portion of the thermolysis reaction (Figure 2.a). Previous studies indicate that multi-reference calculations will surely predict

smaller energy gaps between S_0 and S_1 states [32,33,35,36,54,63,79,80], due to the role of multi-reference correlation in these systems [8,9,32,36,54,79,80]. The energetic error present in the biradical region may come from spin contamination in the reference state, introduced by a BS technology.[36,63] On the other side, multi-reference methods are too computationally difficult to employ on situations where complex system are present . Therefore, we have to employ a long-range-corrected density functional (ωB97XD), which performs well for π → π*, n → π* local excitation, and CT and Rydberg states, [74] providing good qualitative pictures for dioxetanone-based systems [32,33,35,36,54,63,79,80]. As the potential energy curves of S_0 and S_1 states are in line with other studies for imidazopyrazinone-based dioxetanones [35,36,63,65], the applicability of this approach is proved.

The potential energy curves (Figure 2.b) reveal a less effective chemiexcitation process for the anionic species, since the region of degeneracy between S_1 and S_0 is not present. Indeed, there are only two points where the energy gap between states is of 15.2 and 13.9 kcal mol-1. For the contrary, in neutral species is observed a S_1-S_0 energy gap between 10.5 and 12.8 kcal mol-1 during a large region of the thermolysis potential curve (Figure 2.a). This result are in line with other studies of imidazopyrazinone-based dioxetanones [35,36,63,65]. Keeping this in mind, it appears that the thermolysis reaction of *Cypridina* dioxetanone explains the pH-dependence of the chemiluminescent reaction. The experimental results are in line with theoretical results since the neutral dioxetanone presents the more effective chemiexcitation path and the higher activation barrier.

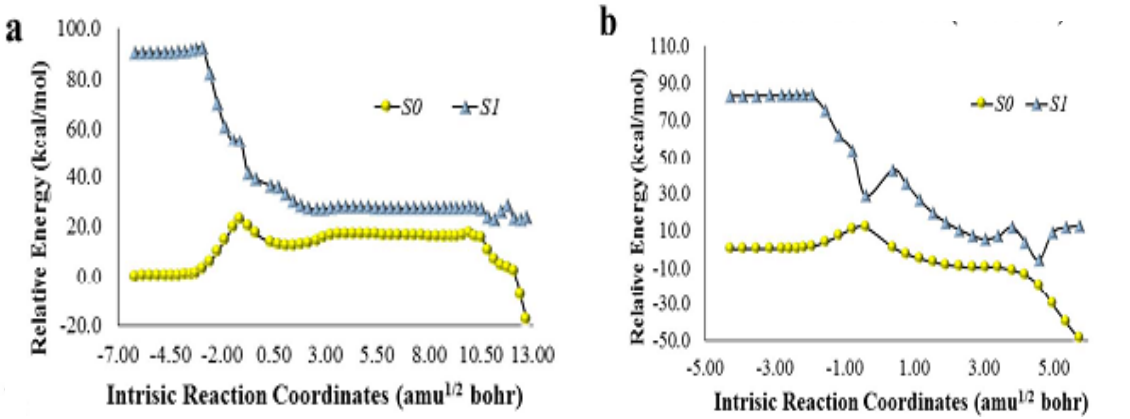


Figure 2- Potential energy curves of S_0 and S_1 states, as a function of intrinsic reaction coordinates, of model (Scheme 9, R_2=R_3=CH_3) neutral (a) and anionic (b) dioxetanone.

The proposed mechanisms for chemiexcitation are based on ET (CIEEL)[28,29]/CT (CTIL) [28,32,33,54,63] from electron-rich moieties to the dioxetanone ring, with chemiexcitation resulting from charge annihilation (caused by

BET/BCT steps) [29,33,36,54,63]. Consequently, to understand the mechanism responsible for the chemiexcitation step of *Cypridina* CL/BL, we have analyzed the charge and electron spin density transfer between the imidazopyrazinone and dioxetanone moieties, for both neutral and anionic dioxetanone (Figure 3; R_2=R_3=CH_3).

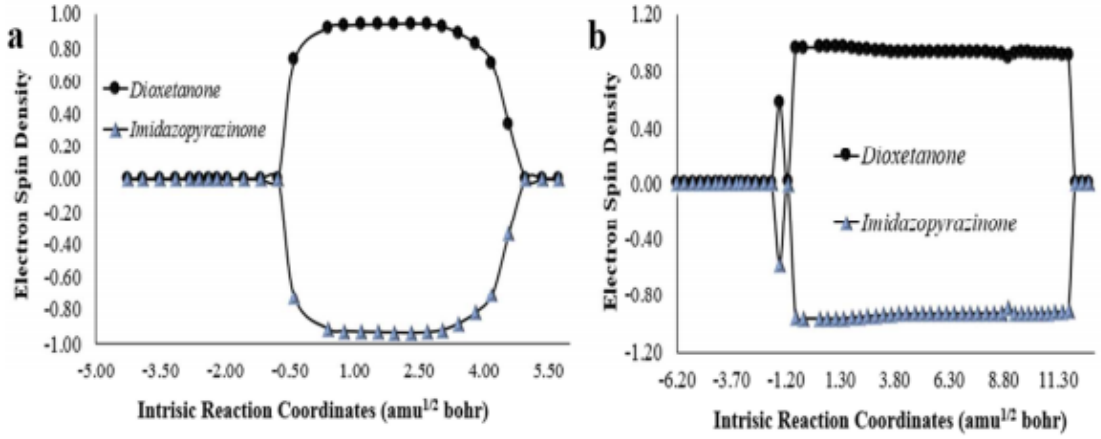


Figure 3- Electron spin density of the dioxetanone and imidazopyrazinone moieties of anionic (a) and neutral (b) model Cypridina dioxetanone (Scheme 9, R_2=R_3=CH_3), as a function of intrinsic reaction coordinates.

The thermolysis reaction of anionic dioxetanone proceeds with significant CT, with the transfer of negative charge (-0.67e) from the imidazopyrazinone to dioxetanone. In the final stages of the reaction, BCT is also observed. The investigation of the electron spin density reveals a separation in the spin density between the two moieties. This indicate that the ET from the imidazopyrazinone moiety to dioxetanone leads to the formation of the biradical species, as in line with the charge density. The return to a non-biradical is caused by BET. Thus, our data indicates that anionic dioxetanone decomposes via a CIEEL/CTIL mechanism, which agrees with previous theoretical work [35,36,63,65].

More interesting is the same analysis, but for the neutral species. CT (-0.85e) was observed from the imidazopyrazinone to the dioxetanone, followed by BCT. Analyzing the electron spin density (Figure 3), we found that the thermolysis of neutral dioxetanone proceeds by ET from the imidazopyrazinone moiety and not by homolytic bond cleavage of O_1-O_4. These findings are not in line with previous theoretical studies of imidazopyrazinone dioxetanones [35,36,63,65], as they indicated that the thermolysis reaction of neutral dioxetanones occurs via the homolytic bond cleavage of O_1-O_4. However, the R_1 substituent was either -H [35,65] or benzyl groups,[36,63]. In this work, the substituent was an indole moiety, which was found to present the higher electron-donating ability among several other electron-rich moieties [13,67]. Thus, the absence

of significant ET/CT in the thermolysis of neutral dioxetanone (as seen in [35,36,63,65]) can be due to the insufficient electron-donating ability of those substituents to trigger these ET/CT processes. Also, it has been hypothesized that the region of PES where S_1 and S_0 are degenerated could only be accessed if the thermolysis reaction proceed by homolytic cleavage of O_1-O_4 with limited CT/ET [35,36,63,65]. However, the present study found that neutral *Cypridina* dioxetanone can access this region, despite undergoing thermolysis with significant CT/ET. Given this, it appears safe to say that this region is not linked to the degree of CT/ET between the imidazopyrazinone moiety and dioxetanone.

With that in mind, we can conclude that the CIEEL and CTIL theories are not supported by the results here presented (and in other studies) [35,36,63,65], at least for imidazopyrazinone-based systems. The chemiexcitation pathway do not have a clear relationship with ET/BET and CT/BCT. Instead, it appears to be explained by the access to a long region of the PES where S_1 and S_0 are nearly-degenerated. Significant ET/CT appears to be only a consequence of the S_0 thermolysis reaction under specific conditions, such as deprotonation of the amide group and the electron-donating ability of the substituents of the imidazopyrazinone scaffold, and not the cause for efficient chemiexcitation.

To this point, it is not yet clear why the neutral dioxetanones can reach these regions of degeneracy. By analyzing the potential energy curves of S_0 and S_1 states (Figure 2) and the behavior of both O_1-O_4 and C_2-C_3 bonds, it is clear that the anionic species does not spend time on the region of degeneracy, releasing the CO_2 molecule sooner than the neutral species. Accordingly, the quicker CO_2 detachment can be the reason why anionic dioxetanones are not able to access the region of nearly-degeneracy. To access the veracity of this statement, we have measured the CT between the CO_2 and oxyluciferin moieties as a function of intrinsic reaction coordinates (Figure 4), for both anionic and neutral dioxetanone. For anionic dioxetanone (Figure 4.a), there is a clear CT (-0.41e) from the oxyluciferin moiety to CO_2 with O_1-O_4 bond elongation. Though, both moieties remain negatively charged, probably due to anionic dioxetanone having a single negative charge. This is expected to create electrostatic repulsion between the moieties and accelerate the detachment of CO_2. In the case of neutral dioxetanone, there is also a clear CT (-0.49e) from the oxyluciferin moiety to CO_2. However, due to the charge neutrality of neutral dioxetanone, this CT step significantly increases the negative charge of CO_2 and the positive charge of oxyluciferin. This should then lead to attractive electrostatic interactions and favorable polarization effects between the two moieties, which should stabilize their interaction and slow down the release of CO_2. Thus, our calculations support neutral dioxetanone having access to a

region of degeneracy (which accounts for efficient chemiexcitation), due to attractive interactions between the CO_2 and oxyluciferin moieties, which slows down the release of CO_2 and allows the reaction to spend time in a long region of S_1-S_0 nearly-degeneracy.

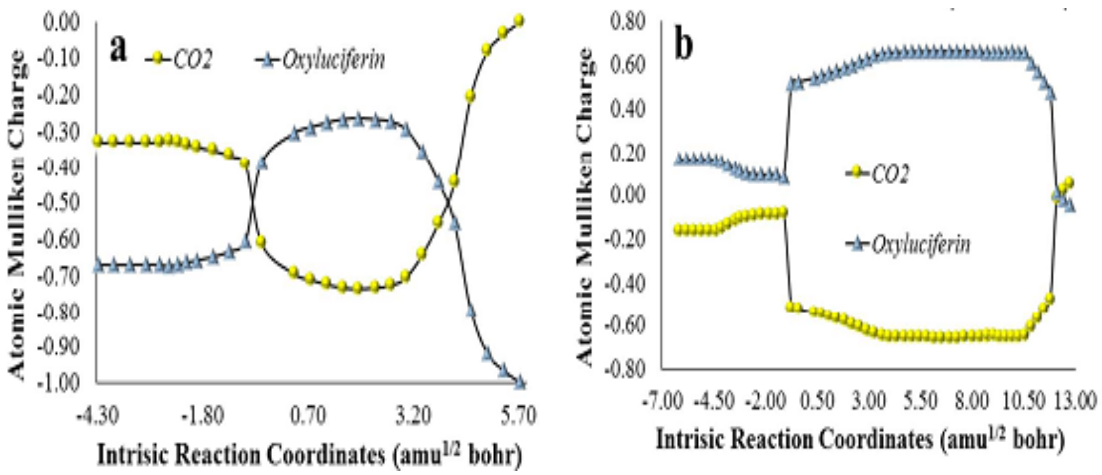


Figure 4- Atomic Mulliken charge of the CO_2 and oxyluciferin moieties of anionic (a) and neutral (b) model Cypridina dioxetanone (Scheme 9, R_2=R_3=CH_3), as a function of intrinsic reaction coordinates.

2.3.3. Chemiluminescence of Coelenterazine in DMSO

The results obtained for *Cypridina* luciferin indicate that both CIEEL and CTIL theories cannot be applied to imidazopyrazinone-based systems, at least as they are now formulated. However, it is valid to question if the same conclusions can be expanded to more imidazopyrazinone-based molecules. Due to this we have studied the chemiexcitation mechanism of Coelenterazine. The kinetic assays for Coelenterazine chemiluminescence were also performed in DMSO, being followed by the measurement of direct light-emission intensity, at different pH values. The kinetics curves gave rise to rate constants (*k*, in s^{-1}) and to the plateau of light intensity (in RLU), corresponding to the value of light intensity at infinite times. These values were obtained by exponential fitting. The plateau and *k* values of the emission phase were obtained in acidic (acetate buffer pH 5.12), neutral (phosphate buffer pH 7.4) and basic pH (NaOH 0.1 M), with increasing concentrations of Coelenterazine, and can be found in Table 3.

Table 3- Rate Constants (*k*, in s^{-1}) and Plateau of Light Intensity (in Relative Light Units, RLU) of Coelenterazine Chemiluminescence in DMSO, with Addition of Acetate Buffer pH 5.12, Phosphate Buffer pH 7.4 or NaOH (0.1 M).

Acetate Buffer pH 5.12					
Concentration (in μM)	0.5	3	4	50	60
Plateau	$6.43 \times 10^5 \pm 5{,}82 \times 10^4$	$2.13 \times 10^6 \pm 9.28 \times 10^4$	$2.06 \times 10^6 \pm 5.25 \times 10^4$	$6.36 \times 10^5 \pm 5.47 \times 10^4$	$7.22 \times 10^5 \pm 8.69 \times 10^4$
k	0.87 ± 0.05	0.62 ± 0.02	0.55 ± 0.02	0.24 ± 0.01	0.23 ± 0.02
Phosphate Buffer pH 7.4					
Concentration (in μM)	1	6	8	100	120
Plateau	$3.05 \times 10^5 \pm 4.12 \times 10^4$	$2.06 \times 10^6 \pm 6.19 \times 10^4$	$2.70 \times 10^6 \pm 5.84 \times 10^4$	$2.58 \times 10^6 \pm 6.41 \times 10^4$	$2.13 \times 10^6 \pm 6.01 \times 10^4$
k	0.63 ± 0.04	0.47 ± 0.01	0.53 ± 0.01	0.68 ± 0.03	0.70 ± 0.03
NaOH					
Concentration (in μM)	5	30	60	100	150
Plateau	$1.30 \times 10^5 \pm 4.29 \times 10^4$	$2.28 \times 10^6 \pm 1.69 \times 10^5$	$2.03 \times 10^6 \pm 5.30 \times 10^3$	$2.40 \times 10^6 \pm 1.09 \times 10^5$	$1.67 \times 10^6 \pm 2.24 \times 10^4$
k	1.85 ± 0.17	0.79 ± 0.07	0.83 ± 0.09	0.80 ± 0.05	1.23 ± 0.07

As we can see, the value of the plateau generally increases with increasing Coelenterazine concentration (Table 3). However, the highest concentrations led to a decrease in the emission maximum in all pH ranges. Therefore, there should be some concentration-dependent factor responsible for quenching the emission at higher concentrations. Additionally, the CL is pH-dependent, as at low concentrations the light output is higher with decreasing pH. For instance, a concentration of 0.5 μM at acetate buffer produces a higher plateau value than a concentration of 1 μM (at phosphate buffer) or 5 μM (with the addition of NaOH). Besides, a concentration of 4 μM (at acetate buffer) or 8 μM (at phosphate buffer) produce similar/higher plateau values than concentration of 30 and 60 μM, in the presence of NaOH (0.1 M). This pH-dependency is analogous to what was found for *Cypridina* system [64].

By analyzing the values used in these kinetic assays we can see some differences between the concentration range used in different pH, and a gap between low and high concentrations, more significant at acidic (between 4 and 50 μM) and neutral (between 8 and 100 μM) pH. This can be due to the fact that the light emission of Coelenterazine CL is pH-dependent, as in line with the Cypridina system [64]. Additionally, the higher concentrations of Coelenterazine led to overflow in our system, so we cannot obtain kinetic curves at those concentrations. More precisely, at acetate

buffer overflow of light is achieved with concentrations as higher than ~4 µM. By its turn, overflow at neutral pH was achieved with concentrations higher than ~8 µM. Interestingly, the quenching effect makes the light output small enough at higher concentrations, which allow us to once again measure kinetic chemiluminescent curves. It should also be noted that quenching of the emission is achieved at lower concentrations at acidic pH, which is starting to be seen with concentrations of ~50 µM. For higher pH values, this decrease is only seen with concentrations higher than ~100 µM (acetate buffer pH 7.4) or ~150 µM (in the presence of NaOH 0.1 M).

While the determination of the values for the plateau does provide a measure of the light, this parameter might not provide a fully accurate picture of the system. Namely, the plateau corresponds to the value of light intensity at infinite times, and so, can be used as a measure of the light emission maximum. However, it does not correlate directly with the total light output. Thus, we have calculated the area of the CL profile (emitted light as a function of time), between times of 0 and 85 seconds, in which most of light is emitted. These values are presented in Figure 5.

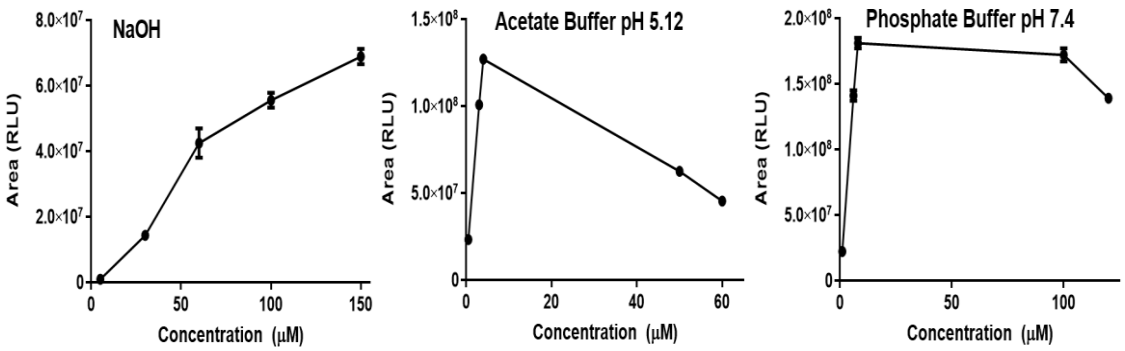


Figure 5- Calculated area (in RLU) of the CL profile of Coelenterazine, between 0 and 85 seconds, with increasing concentrations. Values were obtained at acidic (by addition of acetate buffer pH 5.12), neutral (phosphate buffer pH 7.4) and basic pH (by addition of NaOH).

First, at lower concentrations of Coelenterazine, the light output is similar at acidic and neutral pH at similar concentrations (as 0.5 and 1 µM, and 4 and 6 µM, respectively), being smaller at basic pH. For instance, the calculated area obtained with a concentration of 5 µM at basic pH corresponds only to ~0.67% and ~0.74% of the area obtained with a concentration of 6 µM (at neutral pH) and 4 µM (at acidic pH), respectively. Therefore, these results support our finding regarding the *Cypridina* CL system, [81] in which the light output decreases with increasing pH. Besides, this finding

indicates that our conclusions can be expanded to different imidazopyrazinone-based molecules.

In the same way as for the plateau, the amount of Coelenterazine affect the total light output (Figure 5). However, this effect is not the same in all pH ranges. For example, both at acidic and neutral pH there is an increase of the total output with increasing Coelenterazine levels, up to concentrations of 4 and 8 µM (respectively). On the other hand, with concentrations higher than 40 (at acidic pH) and 100 µM (at neutral pH), there is now a quenching effect that is more pronounced with increasing Coelenterazine levels. The dual effect caused by increasing concentrations of Coelenterazine is consistent to what was found for the plateau levels at acidic and neutral pH (Table 3). At basic pH, the area increases with increasing concentration, without any quenching effect. Thus, while this concentration-linked effect may lead to a decrease of the light emission maximum at high Coelenterazine levels (Table 3), this effect does not appear to be relevant enough to affect the total light output. Interestingly, at neutral pH there is a decrease of ~23% in the total light output between concentrations of 8 and 120 µM, while at acidic pH the decrease is nearly the triple (~64%) between concentrations of 4 and 60 µM. In conclusion, it appears that the concentration-based quenching effect is pH-dependent, and it is more pronounced with decreasing pH.

Coelenteramide can co-exist as several species due to the presence of ionizable amide and phenol groups, [45] which may affect the CL process. Consequently, we have obtained the CL spectra (Figure 6.A) for Coelenterazine in DMSO solutions of different pH: acetate buffer pH 5.12 (0.68%), phosphate buffer pH 7.4, and NaOH (0.1 M). We have found that the spectra obtained at acidic and neutral pH are very similar, with a peak at ~475 nm. At basic pH, there is a shift to ~515 nm, which indicates that the protonation state of the chemiluminophore is different. The peak at acidic/neutral pH is consistent with values previously reported for CL reactions in DMSO at acidic pH (465 nm).[82] Moreover, a previous theoretical study indicated that Coelenteramide is a neutral species at acidic/neutral pH and a phenolate molecule at basic pH [45]. So, we think that it is reasonable to assign the peak in the former conditions to neutral Coelenteramide and the peak in the latter medium to the phenolate species. The fact that the CL spectra is the same at acidic and neutral pH (Figure 6.A) indicates that the differences found for the light output (Table 3 and Figure 5) cannot be explained by the presence of different emitting species. However, the presence of distinct species could potentially explain the different results at basic and acidic/neutral pH, given this red-shift measured in the chemiluminescent spectra obtained at the former pH range (Figure 6.A). Nevertheless, previous computational research did not find significant differences between the oscillator strengths of different Coelenteramide species [45,72]. So, it is not

likely that this is the determining factor. Besides, we have already found a similar pH-dependent effect for the light emitted by *Cypridina* CL, and only one emitting species was found in all pH range [64].

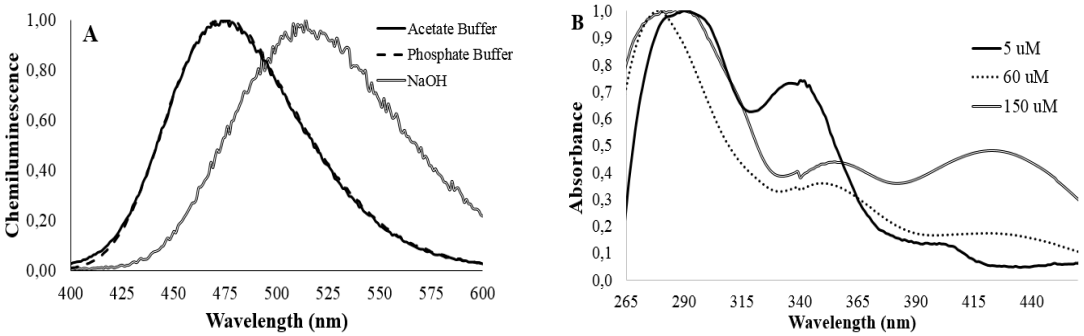


Figure 6 - CL spectra (normalized values) of the light-emitting reaction of Coelenterazine (3 µM) in DMSO (A). UV-Vis spectra (normalized values) obtained in DMSO (in the presence of acetate buffer pH 5.12, 0.68%), with increasing concentrations of Coelenterazine (B).

Considering the *k* values, we can see that the velocity of the CL reaction is also pH-dependent (Table 3). At low Coelenterazine amounts (between 0.5 and 8 µM), the rate constant is similar at acidic and neutral pH. By its turn, the rate constant is generally higher at basic pH. This points to the activation energy for the CL reaction being higher in acidic/neutral pH than in basic medium.

In summary, we can conclude that, in DMSO, the light output and reaction rate of Coelenterazine CL are pH-dependent. Nevertheless, the pH affects these parameters in opposite ways. Taking into account this pH-dependent behavior of the reaction rate, it appears that the activation barrier decreases with increasing pH, in line with what was found for the *Cypridina* system [81]. As already said, the light-emitting reaction of imidazopyrazinones involves two major steps: oxygenation and thermolysis, which determine the global value of the activation energy [67,68,83,84]. However, while the oxygenation step might affect the speed of the reaction, there is no obvious reason for it to induce a higher light output at acidic/neutral pH. So, the answer for this question should be found in the thermolysis reaction of dioxetanone [32,33,35,36,45,63,65,81].

As we have found for *Cypridina* system, different theoretical studies have indicated that neutral species possess a higher activation barrier than their corresponding anionic form (~20 *vs.* ~10 kcal mol^{-1}) [32,33,35,36,45,63,65,81]. Moreover, while neutral dioxetanone presents the higher activation barrier, it also presents the more efficient singlet chemiexcitation pathway [32,33,35,36,45,63,65,81]. This results from the ability of neutral dioxetanone to access a region of the PES where the S_0 and S_1 are

degenerated [33,35,36,45,63,65,81]. Thus, the features associated with both neutral (higher activation barrier and more efficient chemiexcitation) and anionic (lower activation barrier and less efficient chemiexcitation) correlate well with the pH-dependency recorded here for the light output and reaction rate. We then conclude that the experimental results obtained for Coelenterazine can be explained by the thermolysis of neutral dioxetanone at acidic pH and by the thermolysis of the anion at basic pH, which agree with the results obtained before by us for the *Cypridina* system [81]. This agreement provides two considerations: on the one hand, the agreement between the results here obtained and those obtained for *Cypridina* CL reinforces the validity of these findings; for another, this agreement indicates that these conclusions can be expanded to the family of imidazopyrazinone compounds.

2.3.4. Theoretical Investigation of Coelenterazine Dioxetanone

The next step of this work was to understand the mechanism responsible for the chemiexcitation step of Coelenterazine CL/BL. As already referred, proposed mechanisms are based on ET (CIEEL) [28,29]/CT (CTIL)[30,33,36,54,63] from the electron-rich moiety to the peroxide, with chemiexcitation resulting from charge annihilation due to BET/BCT steps. However, as it was already discussed, available data do not support either the CIEEL not the CTIL theories, at least for imidazopyrazinone-based systems [35,45,65,81].

Having said that, it is still needed to discover why neutral dioxetanones have access to the region of S_0-S_1 degeneracy, while the anion forms do not. The analysis of the potential energy curves computed in previous studies [35,45,65,81] indicates as the anionic species does not spend time on the region of degeneracy, and it releases the CO_2 molecule sooner than the neutral species. Thus, it is possible that the quicker CO_2 detachment is the reason why anionic dioxetanones cannot access the region of degeneracy. In fact, the measurement of CT between CO_2 and oxyluciferin moieties of *Cypridina* dioxetanone as a function of intrinsic reaction, showed that for anionic dioxetanone, both moieties remain negatively charged during the thermolysis reaction, probably due to this species possessing a single negative charge. This is expected to create electrostatic repulsion between the moieties and accelerate the release of CO_2. On the other hand, the CO_2 and oxyluciferin moieties of the neutral species possess opposite charges. This should lead to attractive electrostatic interactions between the moieties, slowing down the detachment of CO_2. Consequently, these calculations indicate that neutral dioxetanones have access to the region of degeneracy due to attractive interactions between the CO_2 and oxyluciferin moieties, which slow down the release of CO_2 and allow the reaction to spend time in the region of $S_0 \rightarrow S_1$ chemiexcitation [81]. In order to assess if this conclusion regarding the *Cypridina* system can be applied to Coelenterazine, we have also measured the CT between CO_2 and Coelenteramide moieties (Figure 7) of a Coelenterazine dioxetanone model (a phenol at the C_6 position and a methyl group at the C_2 position) studied previously [45]. The calculations were made at the ωB97XD/6-31G(d,p) level of theory with a broken-symmetry approach in implicit diethyl ether.

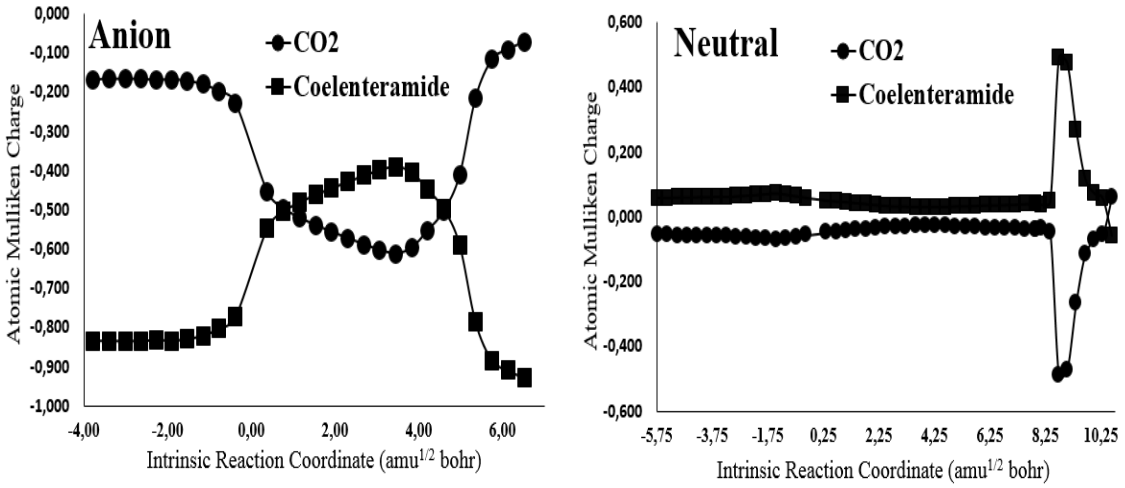


Figure 7- Atomic Mulliken charge of the CO_2 and Coelenteramide moieties of an anionic and neutral model Coelenterazine dioxetanone (a phenol and methyl groups at the C6 and C2, respectively), as a function of intrinsic reaction coordinates. Calculations were made at ωB97XD/6-31G(d,p) level of theory in implicit diethyl ether, as described in reference [45].

The obtained results (Figure 7) agree with what was found for the Cypridina system. For the anion, both the CO_2 and Coelenteramide moieties possess negative charge, which should induce repulsive electrostatic charge. Furthermore, CT is observed upon entering the biradical region of the thermolysis reaction, followed by BCT afterwards. The CT step reduces the charge separation between the moieties, thereby reducing possible favorable polarization effects that could slow down the release of CO_2. For the contrary, the two moieties of neutral dioxetanone possess opposite charges, with CO_2 being negative and Coelenteramide positively charged. So, these results (combined with our previous study of Cypridina luciferin) provide support for the efficient chemiexcitation of imidazopyrazinone-based dioxetanones being controlled by electrostatic interactions between the CO_2 and Coelenteramide/oxyluciferin, which if favorable could provide access to a region of S_0-S_1 degeneracy.

2.3.5. UV-Vis spectrum of Coelenterazine

These conclusions obtained so far for Coelenterazine CL can only be applied directly to results obtained at low concentrations of the substrate. At higher levels of Coelenterazine, there is a concentration-dependent quenching effect more prevalent at acidic pH, which overcomes the chemiexcitation efficiency of individual dioxetanone molecules. Goto and co-workers have provided evidence in 1985 for the formation of a biluciferyl dimer in the *Cypridina* system, which possesses a light absorption band at

longer wavelength than the luciferin molecule [85]. The dimerization was stated to result from the interaction of two luciferyl radicals, which originate from the oxygenation step. Thus, this dimerization might explain the concentration-dependent quenching effect measured more prevalently at acidic pH. If the concentration of Coelenterazine is increased, the probability of Coelenterazine radicals colliding and reacting within their lifetime increases. Besides, if the radicals react to form dimers instead of recombining with superoxide anion to produce Coelenteramide in the S_1 state, less light is emitted due to decreasing levels of produced chemiluminophore.

We have measured the UV-Vis spectrum of Coelenterazine in DMSO at acidic pH with addition acetate buffer pH 5.12 (0.68%), with increasing levels of the imidazopyrazinone (5, 60 and 150 µM). The recorded spectra are present in Figure 6.B, while the ratio between Coelenterazine, Coelenteramide and the dimer are present in Table 4. Three different peaks can be seen: one at ~285 nm, other at ~340 nm and another at ~420 nm. The first peak was attributed to Coelenterazine, the second one to Coelenteramide, and the last one to the dimer structure. Previous studies have already attributed a peak at ~280 nm to Coelenterazine,[84,86] while Shimomura and Teranishi found that Coelenteramide and analogs possess an excitation maximum at ~340 nm in DMSO [87]. The dimer having an absorption band at a higher wavelength than Coelenterazine is in line with the work of Goto and co-workers [85]. Interestingly, while the band attributed to the dimer is almost inexistent at a concentration of 5 µM, the band increases significantly and consistently with increasing concentration of Coelenterazine. For the contrary, there is a decrease of the ratio of Coelenteramide, regarding both Coelenterazine and the dimer, with increasing levels of the chemiluminescent substrate. Thus, this evidence allows us to conclude that the concentration-dependent quenching effect is caused by formation of a dimer structure, composed of two Coelenterazine radicals, a process that is favored in acidic conditions [85].

Table 4– Ratios between Coelenterazine, Coelenteramide and the proposed dimer, in DMSO solutions with increasing concentrations of Coelenterazine (in the presence of acetate buffer pH 5.12, 0.68%). The ratios were calculated by measuring the UV-Vis spectra of these solutions (Figure 6.B), and by considering the absorbance of the peaks attributed to each species, based on previous findings by us and other authors. [84–87]

Concentration	Coelenterazine	Coelenteramide	Dimer
5 µM	0.527 ± 0.006	0.371 ± 0.023	0.120 ± 0.029
60 µM	0.652 ± 0.001	0.237 ± 0.002	0.111 ± 0.001
150 µM	0.523 ± 0.002	0.227 ± 0.001	0.250 ± 0.001

2.4. Conclusion

It was found that Coelenterazine and *Cypridina* CL reactions are pH-dependent: they present a lower reaction rate with lower pH, while the total light output presents the opposite trend. However, none of this pH-dependency can be attributed to the neutral-anionic equilibria of the chemiluminophore. Theoretical calculations at the TD-DFT level showed that this pH-dependency can be explained by the neutral-anionic equilibria of the dioxetanone intermediates: neutral dioxetanone is present at acidic pH, while the anion is present at basic pH.

More specifically, neutral dioxetanone decomposes with a higher activation energy than the anion, which explains the increasing reaction rate with increasing pH. Moreover, the thermolysis of the neutral species leads to a more efficient chemiexcitation pathway than the anion, which explains why the total light output decreases with increasing pH. The higher efficiency of chemiexcitation results from neutral dioxetanone having access (during its thermolysis) to a long region of the PES where S_0 and S_1 degenerated. Further data obtained by performing theoretical calculations showed that neither ET/BET nor CT/BCT between the imidazopyrazinone moiety and dioxetanone have any clear relationship with the efficiency of chemiexcitation. Thus, neither known theories such as CIEEL and CTIL can explain the CL of imidazopyrazinone-based molecules.

Efficient chemiexcitation by neutral dioxetanones was explained by attractive electrostatic interactions between the CO_2 and oxyluciferin moieties, which allow for the reacting molecules to spend time in the region of degeneracy. On the contrary, repulsive electrostatic interactions between the moieties of anionic dioxetanones lead to a quicker CO_2 detachment and prevent access to the region of degeneracy.

3. Comparative Study of the Chemiluminescence of Coelenterazine, Coelenterazine-e and Cypridina Luciferin

3.1. Aim

Previous studies aimed to the understanding of the CL reaction of imidazopyrazinones have been focused on the substitution of the imidazopyrazinone core at the C2, C6 and/or C8 position (with emphasis on the C6 position) studies (Scheme 7) [67,68,70,71,83,85,88]. Nevertheless, while the molecular diversity included in these studies has been increasing, the solvent effect on these reactions has not been particularly well studied. In fact, most of these studies [67,68,70,71,83,85,88] have been performed solely on model solutions of DMSO – base and/or diglyme – acetate buffer. Thus, this field of research may benefit from a more in-depth characterization of the solvent effect for the chemiluminescence of imidazopyrazinones.

Herein, we have studied the CL of three different and commercial imidazopyrazinones in model solutions, which are composed by aprotic solvents at different pH ranges (due to addition of acetate buffer and NaOH). The imidazopyrazinones included in this study were *Cypridina* luciferin, Coelenterazine and Coelenterazine-e, which is a synthetic analogue of native Coelenterazine with an additional ethyl group [20]. To obtain a better understanding of the CL of these molecules in different environments, we have studied mechanistically the different steps of the chemiluminescent reaction with a combined experimental (spectroscopic and chromatographic) and theoretical approach in these model solutions.

3.2. Materials and methods

3.2.1. Kinetic chemiluminescent assays for Cypridina luciferin, Coelenterazine, Coelenterazine-e and Coelenteramide

The light emitting reactions were carried out in different aprotic solvents (DMSO, DMF, acetonitrile, acetone, pyridine, diglyme, toluene, diethyl ether, dichloromethane and ethyl acetate), to which was added either acetate buffer pH 5.12 (0.68%), NaOH 0.1 or NaOH 0.3M. The reaction was initiated by the injection of the aprotic solvent solution into an assay tube containing the imidazopyrazinone, to which resulted a final volume of 500 µL and a concentration of chemiluminescent substrate of 1 µM (Coelenterazine-e

was used in a concentration of 0.5 µM). The light was integrated and recorded in 0.1 s intervals.

3.2.2. Measurement of fluorescence spectra for *Cypridina* luciferin, Coelenterazine, Coelenterazine-e and Coelenteramide

The fluorescence was recorded with a Horiba Jovin Fluoromax 4 spectrofluorometer, with an integration time of 0.1 s. Slit widths of 5 nm were used for both the excitation and emission monochromators. Quartz cells were used.

3.2.3. Chromatographic assays

The RP-HPLC-DAD chromatographic system consisted of a Rheodyne manual injection valve, Thermo Scientific SpectraSystem P1000 pump, a Thermo Finnigan UV6000 LP diode array detector and a Hypersil GOLD (Thermo Scientific) column. Two different mobile phases were used. For the analysis of reaction mixtures in diethyl ether and acetonitrile, it was used a mobile phased composed by water (70%) and acetonitrile (30%), with addition of acetate buffer pH 5.12 (0.68%). For analysis of reaction mixtures in DMF, the percentage of acetonitrile was increased to 40%. The flow was set to 0.35 mL per minute in all cases.

The CL reaction was initiated by addition of an aprotic solvent solution to Coelenterazine, leading to a final solution with a concentration of imidazopyrazinone of 40 µM and a final volume of 500 µL. The mixtures were left to react for 10 minutes, after which 20 µL were injected into the chromatographic system and analyzed.

3.2.4. Theoretical study of chemiexcitation mechanism of model dioxetanones in different solvents

The study of the thermolysis reaction was performed by considering the same computational strategy described in section 2.1.4.

The study of the deprotonation potential of Coelenterazine in different solvents was performed by considering a Coelenterazine derivative (Scheme 10, R_1 = phenol, R_2 = R_3 = CH_3). Geometry optimizations, frequency and single-point calculations were made at M06-2X/6-31+G(d,p) level of theory [89]. This functional was chosen due to good results in applications involving main-group thermochemistry, kinetics and noncovalent interactions [89]. All calculations were made in implicit solvent by using the SMD implicit solvation model, which includes nonelectrostatic terms in the calculations [90]. The computation of hole-electron distribution and transition dipole moment was made by considering a neutral Coelenterazine dioxetanone model derivative (Scheme 9, R_1 = phenol, R_2 = R_3 = CH_3). The S_0 TS for the thermolysis reaction was optimized at the BS-

ωUB97XD/6-31G(d,p) level of theory, in implicit solvent by using the IEFPCM implicit solvation model. The S_1 state was calculated by using the time-dependent (TD) DFT approach, at the ωB97XD/6-31+G(d,p) level of theory. The resulting wavefunctions were used to obtain the hole-electron distribution and transition dipole moment by using the Multiwfn code [91].

All theoretical calculations were performed with the Gaussian 09 program package.

3.2. Results and discussion

The CL of Coelenterazine, Coelenterazine-e and *Cypridina* luciferin was recorded in a homemade luminometer in different model solutions. We have calculated the area of the CL profile, between times of 0 and 85 s [92]. These values are presented in Table 5. The area values can be considered as a measure of total light output, and so, an indicative for chemiluminescence quantum yield (Φ_{CL}). The light-intensity maxima were also obtained and presented in Table 6. Acetate buffer (pH 5.12) was added to all solvents to ensure chemiexcitation from the neutral dioxetanone species, which were found to result in more efficient chemiexcitation [13,24,68–71].

Table 5- Calculated area (in RLU) of the CL profile of different imidazopyrazinones, between 0 and 85 s, with addition of acetate buffer pH 5.12.

Solvents	*Cypridina* luciferin	Coelenterazine	Coelenterazine-e
DMSO	$5.29 \times 10^6 \pm 4.53 \times 10^5$	$5.46 \times 10^7 \pm 4.65 \times 10^6$	$2.30 \times 10^7 \pm 3.58 \times 10^6$
DMF	$1.07 \times 10^7 \pm 2.10 \times 106$	$6.14 \times 10^7 \pm 6.28 \times 10^6$	$4.91 \times 10^7 \pm 4.90 \times 10^6$
Diglyme	$1.29 \times 10^7 \pm 1.85 \times 10^5$	$2.95 \times 10^4 \pm 8.37 \times 10^3$	$2.34 \times 10^5 \pm 4.56 \times 10^4$
Acetonitrile	$6.99 \times 10^5 \pm 5.73 \times 10^4$	$1.56 \times 10^6 \pm 4.80 \times 10^5$	$9.27 \times 10^6 \pm 2.39 \times 10^6$
Pyridine	$1.70 \times 10^5 \pm 3.71 \times 10^4$	$2.77 \times 10^6 \pm 3.08 \times 10^5$	$8.71 \times 10^5 \pm 9.16 \times 10^4$
Acetone	$5.03 \times 10^6 \pm 3.25 \times 10^5$	$2.06 \times 10^5 \pm 6.05 \times 10^4$	$2.81 \times 10^6 \pm 8.86 \times 10^5$
Dichloromethane	$1.24 \times 10^4 \pm 7.98 \times 10^3$	$1.03 \times 10^4 \pm 2.52 \times 10^3$	$1.64 \times 10^5 \pm 2.41 \times 10^4$
Diethyl Ether	$2.59 \times 10^4 \pm 4.47 \times 10^3$	$1.02 \times 10^4 \pm 1.42 \times 10^3$	$3.28 \times 10^3 \pm 3.81 \times 10^2$
Ethyl Acetate	$3.20 \times 10^4 \pm 4.53 \times 10^5$	$1.09 \times 10^4 \pm 1.61 \times 10^3$	$2.60 \times 10^5 \pm 2.92 \times 10^4$
Toluene	$1.06 \times 10^4 \pm 3.28 \times 10^3$	$1.70 \times 10^4 \pm 7.51 \times 10^3$	$4.02 \times 10^4 \pm 8.03 \times 10^3$

DMSO and DMF were the solvents that consistently led to a higher total light output and light-intensity for all imidazopyrazinones. Interestingly, most of the other solvents appear to not be compatible with CL. Dichloromethane, diethyl ether, ethyl acetate and toluene led to negligible light emission. Diglyme lead to equivalent results for Coelenterazine and Coelenterazine-e but allowed surprisingly high efficiency for *Cypridina* luciferin. Acetone, acetonitrile, and pyridine led to somewhat higher light emission, but still significantly lower than for DMF and DMSO. It should be noted that the

results for the three imidazopyrazinones are quite similar, except for the high efficiency in diglyme for *Cypridina* luciferin.

Table 6- Light intensity maxima (in RLU) of the CL profile of different imidazopyrazinones, between 0 and 85 s, with addition of acetate buffer pH 5.12.

Solvents	*Cypridina* luciferin	Coelenterazine	Coelenterazine-e
DMSO	7.24×10^5	2.13×10^6	1.98×10^6
DMF	9.83×10^5	1.73×10^6	2.56×10^6
Diglyme	1.68×10^5	5.42×10^2	3.71×10^3
Acetonitrile	1.17×10^4	3.20×10^4	1.38×10^5
Pyridine	2.83×10^3	3.94×10^4	1.97×10^4
Acetone	7.20×10^4	3.29×10^3	4.59×10^4
Dichloromethane	4.83×10^2	2.18×10^2	2.09×10^3
Diethyl Ether	7.77×10^2	2.38×10^2	7.83×10^1
Ethyl Acetate	5.65×10^2	2.04×10^2	5.67×10^3
Toluene	2.87×10^2	4.49×10^2	7.15×10^2

It should be noted that solutions of diglyme – acetate buffer have been considered as a model environment for the BL reaction of imidazopyrazinones, mainly by the efficient CL of *Cypridina* luciferin and derivatives [13,24,68–71]. However, our results indicate that this only holds true indeed for *Cypridina* luciferin, but not for either Coelenterazine or Coelenterazine-e. Thus, the role of diglyme – acetate buffer as a model environment for BL should be re-thought.

Table 7- Initial velocities (in RLU s^{-1}) under steady-state conditions for the CL reaction of different imidazopyrazinones, with addition of acetate buffer pH 5.12.

Solvents	*Cypridina* luciferin	Coelenterazine	Coelenterazine-e
DMSO	4.05×10^5	2.51×10^6	1.04×10^6
DMF	8.23×10^5	1.74×10^6	3.90×10^6
Acetonitrile	8.13×10^3	1.46×10^4	7.17×10^4
Pyridine	2.09×10^3	2.63×10^4	1.38×10^4
Acetone	2.44×10^4	7.73×10^2	4.44×10^4

In Table 7 are presented the initial velocities for the three imidazopyrazinones under steady-state conditions, obtained in solvents where CL was generally non-negligible (DMSO, DMF, acetone, pyridine and acetonitrile). In Figure 8, are presented

representative CL profiles measured in some solvents. Consistent with the results for light-intensity, the initial velocities are significantly higher in DMSO and DMF than for the other solvents, by about three or four orders of magnitude. This can be explained by differences in the kinetics of the CL reaction, as can be seen in Figure 8.

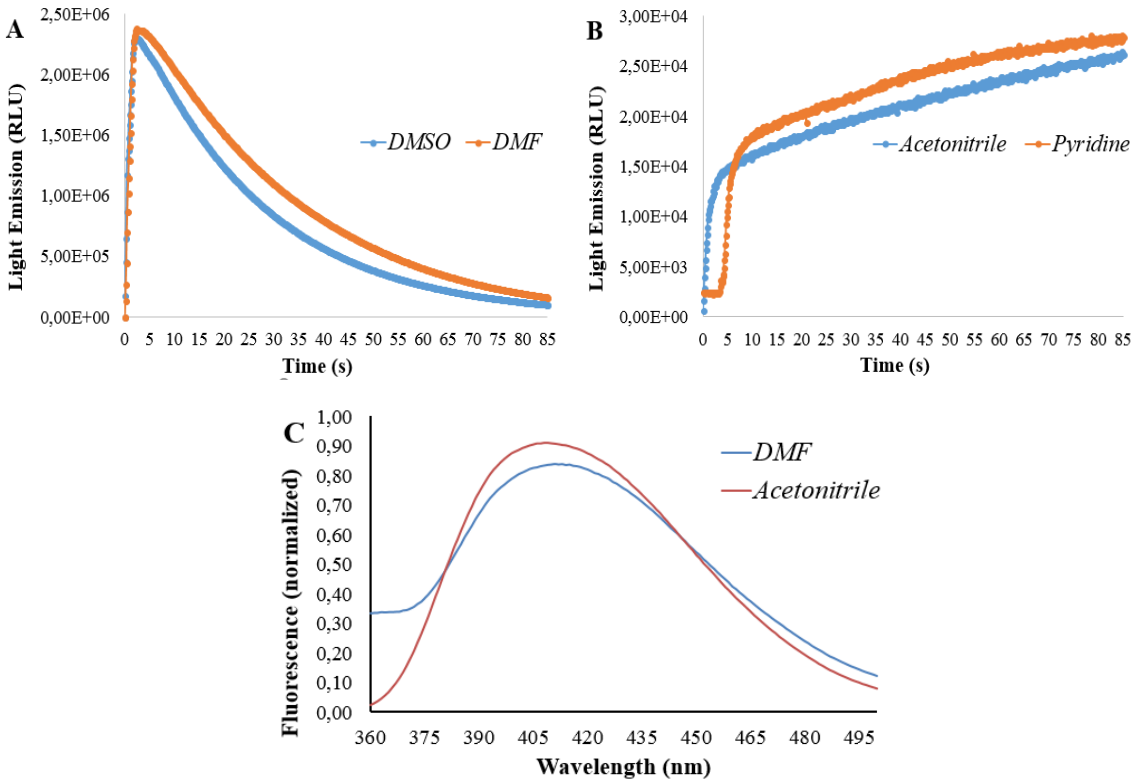


Figure 8- CL profile (light emission as a function of time) for Coelenterazine in DMSO/DMF (A) and acetonitrile/pyridine (B), with addition of acetate buffer pH 5.12. These profiles are also representative for the other imidazopyrazinones here studied (Cypridina luciferin and Coelenterazine-e). Fluorescence spectra (normalized) for Coelenteramide in DMF and acetonitrile (C), with addition of acetate buffer pH 5.12.

In DMSO and DMF, the reaction consists on an initial burst of light, which is responsible for most of emitted light. After the initial maximum, there is a quick decay toward basal levels. That is not the case however for the other solvents. There is quick increase of light, but there is no quick decay to basal levels. Instead, the light emission remains constant. This helps to explain why the light-emission maxima for these solvents (acetonitrile, pyridine and acetone) are significantly lower than in DMSO and DMF, as seen in Table 6. Instead of most of the chemiexcited chemiluminophore being produced in the initial seconds, the slower kinetics of the reaction led the production of the chemiluminophore to be more delayed, and so, the light is emitted more steadily over

time. However, the area of CL profile is significantly higher in DMSO/DMF than in acetonitrile/pyridine/acetone (Table 5). This means that the CL reactions in the latter solvents are significantly less efficient (lower Φ_{CL}) and not just slower.

Different values of ΦCL can be explained by changes in either yield of the ground state (S_0) reaction (Φ_R), the singlet chemiexcitation yield (Φ_S) or fluorescence quantum yield of the luminophore (ΦFL), or by a combination of changes thereof. Thus, we started by assessing if Φ_{FL} can be affected by the polarity of the solvent. We have measured the fluorescence of Coelenteramide (the light emitter in the CL reaction of Coelenterazine) in DMF and in acetonitrile, two examples of solvents in which CL was high and low (respectively). We have only used Coelenteramide, as it is the only light emitter to be available commercially. Moreover, the results for the CL reactions of all three imidazopyrazinones were very similar to each other. It should be noted that some authors have indicated that CL states differ from fluorescent states, which could impair our analysis [72,73]. However, subsequent analysis indicated that for Coelenteramide, the CL state is dark state, and so, it must evolve to a bright fluorescent state from which light is emitted [93]. The fluorescence spectrum (Figure 8.C) has a similar maximum in both solvents (~410 nm). Moreover, the fluorescent intensity maximum (in normalized values) are very similar: 0.78 ± 0.04 for DMF and 1.00 ± 0.11 for acetonitrile. The difference between these values is not statistically significant according to an unpaired *t* test (a two-tailed *p* value of 0.1333). Thus, it is not expected that the differences in Φ_{CL} are caused by Φ_F.

The next step was to assess the potential effect of Φ_R in the Φ_{CL} found for different solvents. To this end, we have analyzed the chemiluminescent reaction of Coelenterazine in three solvents: DMF (high CL), acetonitrile (non-negligible but low CL) and diethyl ether (negligible CL). The reaction media after 10 minutes of reaction were analyzed by reverse-phase high performance liquid chromatography coupled to a diode array detector (RP-HPLC-DAD). This analytic technique is very useful to separate, identify components in reaction mixtures. The identification of the peaks as either Coelenterazine or Coelenteramide was made by comparison between the UV spectrum of reaction components and of commercial Coelenterazine and Coelenteramide (Figure 9). The chromatograms obtained in the different solvents are also present in Figure 9.

Our results help to explain the total light output (Table 5 and Table 6). In DMF it was only found a peak attributed to Coelenteramide, which indicates that the ground state reaction is complete (or almost complete). For acetonitrile, the chromatogram showed the presence of both Coelenterazine and Coelenteramide, in a proportion of 0.853 ± 0.014 to 0.147 ± 0.014. This helped to explain why the light output of the CL reaction in acetonitrile is quite lower than in DMF. Namely, the ground state reaction (Φ_R)

is significantly less efficient. In diethyl ether, the situation is even more dramatic as it was only observed the peak attributed to Coelenterazine. Meaning that the Coelenterazine → Coelenteramide conversion does not occur, at least in detectable yields. This explains the negligible light emission in diethyl ether, and by inference, in other solvents (such as toluene and ethyl acetate). In conclusion, we can attribute the significant differences found in the light output in different solvents (and consequently in Φ_{CL}) to different degrees of Φ_R. Having said that, it is necessary to understand what causes these differences in Φ_R.

Φ_R for the CL reaction of imidazopyrazinones is explained by two sequential steps: oxygenation of the imidazopyrazinone core with formation of dioxetanone, and decomposition of the peroxide intermediate with formation of the chemiexcited light emitter. However, the oxygenation step should not be responsible for these major differences due to good solubility of oxygen in various solvents, and to the large excess of oxygen. In fact, the oxygen solubility was found to be higher for solvents such as toluene, acetone and dichloromethane (in which CL was very low or inexistent) than for DMF (in which CL is appreciable) [94].

It is more probable that the differences in Φ_R reside in the thermolysis reaction of dioxetanone. Thus, we have analyzed by RP-HPLC-DAD reaction mixtures in DMF, acetonitrile and diethyl ether in basic pH (0.1 M NaOH). It is known that while neutral dioxetanones present activation barriers at about ~20 kcal mol^{-1}, anionic species decompose with activation energies of about ~10 kcal mol^{-1} [64,65,92,93]. Therefore, increasing the pH should benefit Φ_R by deprotonating the dioxetanone intermediate. In fact, this hypothesis is supported by the experimental results (Figure 10). In diethyl ether, the peak of Coelenterazine decreases from a proportion of ~1 (in acidic pH) to 0.571 ± 0.029, with the corresponding presence of Coelenteramide (0.429 ± 0.029). The increase of the proportion of Coelenteramide is even more significant in acetonitrile, as it increases from 0.147 ± 0.014 to 0.921 ± 0.002. The conversion of Coelenterazine into Coelenteramide is once again complete/nearly complete in DMF.

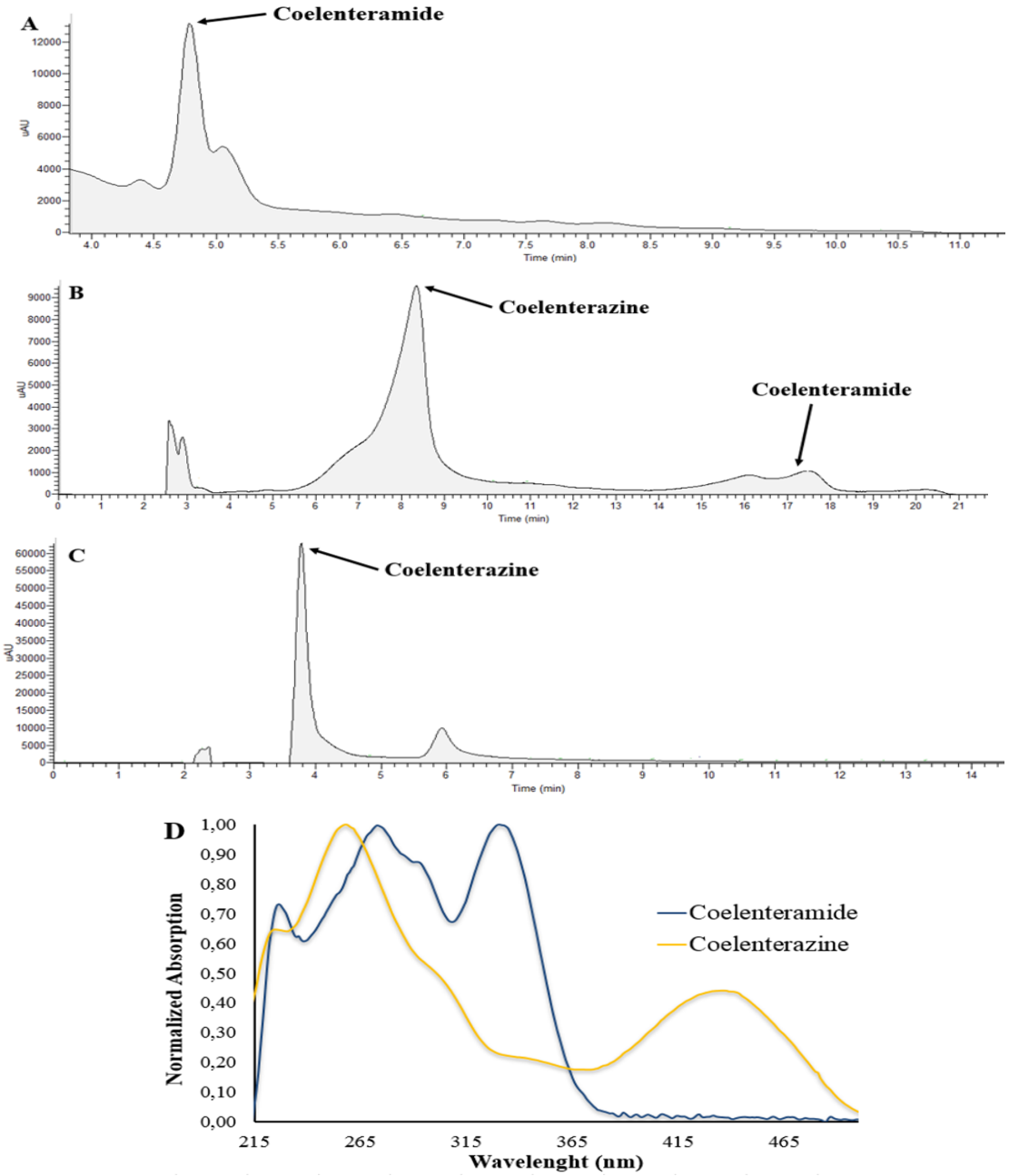


Figure 9- Chromatograms obtained for the reaction mixtures of Coelenterazine CL in DMF (A), acetonitrile (B) and diethyl ether (C), all with addition of acetate buffer pH 5.12 (0.68%). The mobile phase was composed of water (70%) and acetonitrile (30%) for reaction mixtures in acetonitrile and diethyl ether. For reaction mixtures in DMF the percentage of acetonitrile was increased to 40%. The flux was of 0.35 mL per minute.
The reaction mixtures were prepared with 40 µM of Coelenterazine. In Figure 9.D are presented the normalized absorption spectra of commercial Coelenterazine and Coelenteramide (40 µM) in methanol, when analyzed by RP-HPLC-DAD in the conditions referred above.

It was also compared the effect caused by increasing the pH in the CL profile of Coelenterazine in diethyl ether, acetonitrile and DMF. We have found that there is slight difference between the area at acidic and basic pH in DMF (a small increase of 3%), which is not unexpected as there was not any discernible difference in Φ_R as determined by RP-HPLC-DAD. However, increasing the pH from acidic to basic has an extreme effect on the area of the chemiluminescent profile in both diethyl ether (an increase of 60%) and in acetonitrile (an increase of 92%). These results are in line with the increase in Φ_R resulting from increasing the pH of the reaction mixture.

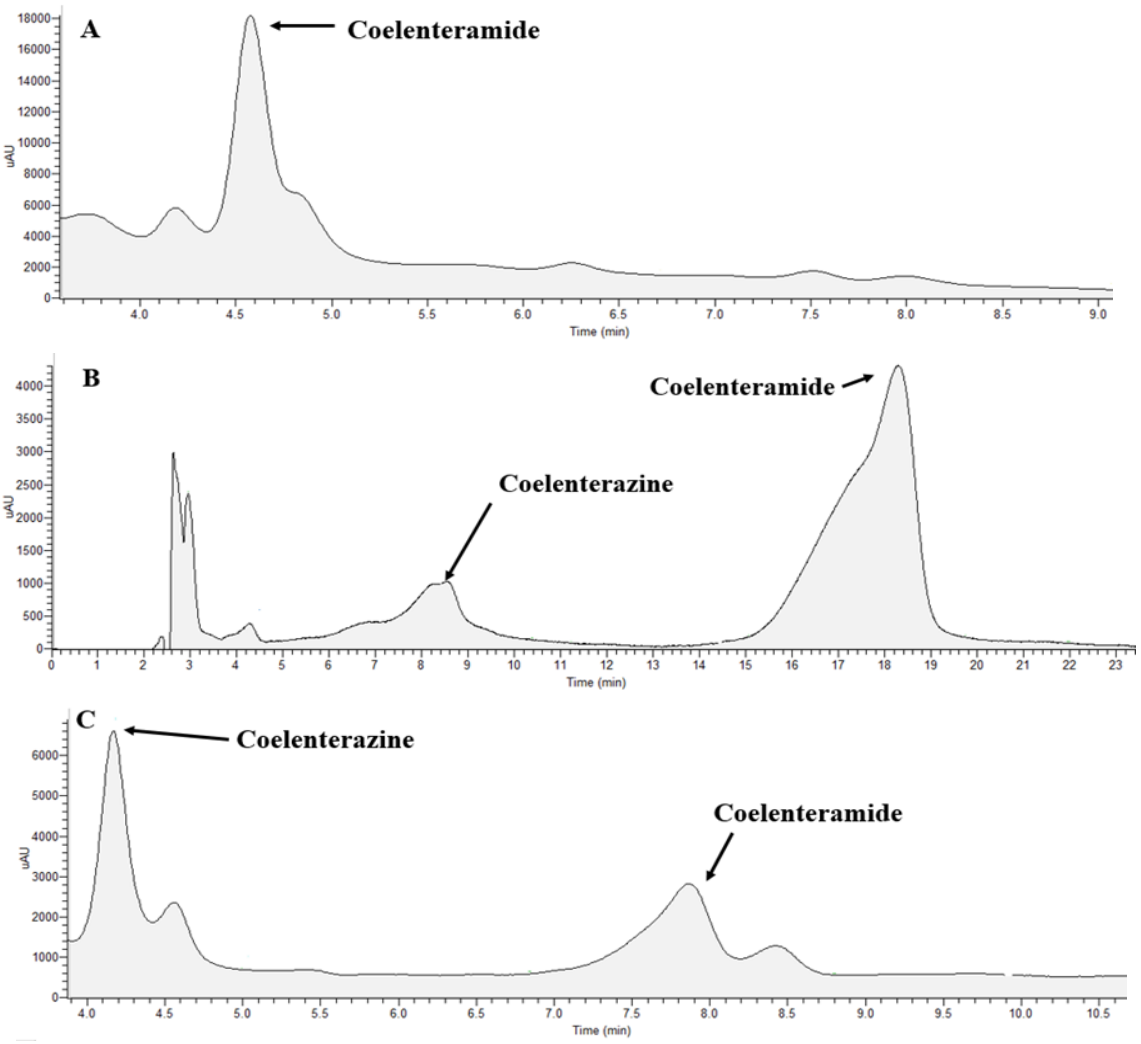


Figure 10- Chromatograms obtained for the reaction mixtures of Coelenterazine CL in DMF (A), acetonitrile (B) and diethyl ether (C), all with addition of NaOH 0.1M. The experimental conditions were the same as the ones indicated in Figure 9.

Thus, our results indicate that the main factor determining Φ_{CL} for imidazopyrazinones in different solvents is the Φ_R. Namely, Φ_R is quite low in most solvents at acidic pH, leading to low/negligible light output, the exception being in DMSO and DMF, in which Φ_R is already quite high due to nearly complete production of Coelenteramide. This appears to be a pH-induced effect, as addition of NaOH increased significantly Φ_R, and subsequently the area of total emitted light. To gain further insight into this matter, we have used a TD-DFT method to characterize the thermolysis reaction of a model imidazopyrazinone dioxetanone [64], in diethyl ether, DMF and acetonitrile. Both the anionic and neutral forms of the dioxetanone were considered. We have used a model dioxetanone already studied by us in a recent study [64]. Namely, one in which R_1 corresponds to an indole group, while R_2 and R_3 correspond to methyl groups (Scheme 9). The results are calculated at the TD UωB97XD/6-31G+(d,p) level of theory using a broken-symmetry technology [64]. The solvent was modelled implicitly with the IEFPCM model.

The potential energy curves for the thermolysis of neutral dioxetanone are presented in Figure 11. These curves are qualitatively identical in all three solvents. The reaction proceeds by O-O bond breaking until generating a biradical transition state (TS). Only after reaching this TS does C-C bond breaking starts. This leads the reaction towards a long and flat biradical region, in which both S_0 and S_1 are degenerated/nearly-degenerated (allowing for chemiexcitation). The energy difference between S_0 and S_1 within the biradical region is not affected very much by the solvent, as it varies between 10.5-11.5 kcal mol^{-1} in DMF/acetonitrile and between 9.6-11.8 kcal mol^{-1} in diethyl ether. The major difference for the thermolysis in different solvents is the S_0 activation barrier. It is of 22.9 kcal mol^{-1} in both DMF and acetonitrile, a value in line with those found experimentally (about ~20 kcal mol^{-1}) [76–78]. However, in nonpolar solvent (diethyl ether), the activation barrier has a significant increase, up to 26.9 kcal mol^{-1}.

These observations are like those obtained for the thermolysis of anionic dioxetanone (Figure 12). The potential curves also led to a biradical TS, due to O-O bond breaking, followed by C-C bond breaking. However, there is no long and flat biradical region in which S_0 and S_1 are degenerated/nearly-degenerated. This is in line with previous computational studies [64,65,92,93]. The S_0-S_1 energy gap is also similar in all solvents: higher than ~17 kcal mol^{-1} in all reaction points except in two points in each reaction, in which the gap is between 14.0 and 16.0 kcal mol^{-1}. Once again, the main difference is related with the S_0 activation barrier: 11.6 kcal mol^{-1} (DMF), 11.7 kcal mol^{-1} (acetonitrile) and 13.3 kcal mol^{-1} (diethyl ether). As in line with both experimental and theoretical studies [13,64,65,67,68,92,93], the main differences are not between solvents but between the chemical forms (neutral or anionic) of dioxetanone. Namely,

the reaction rate should increase with increasing pH (due to lower activation barriers), while the total output should decrease (due to an increase of the S_0-S_1 energy gap, leading to less efficient chemiexcitation). In fact, the theoretical calculations indicate that the main difference for the thermolysis reaction in different solvents should be only related to lower reaction rates for less polar solvents.

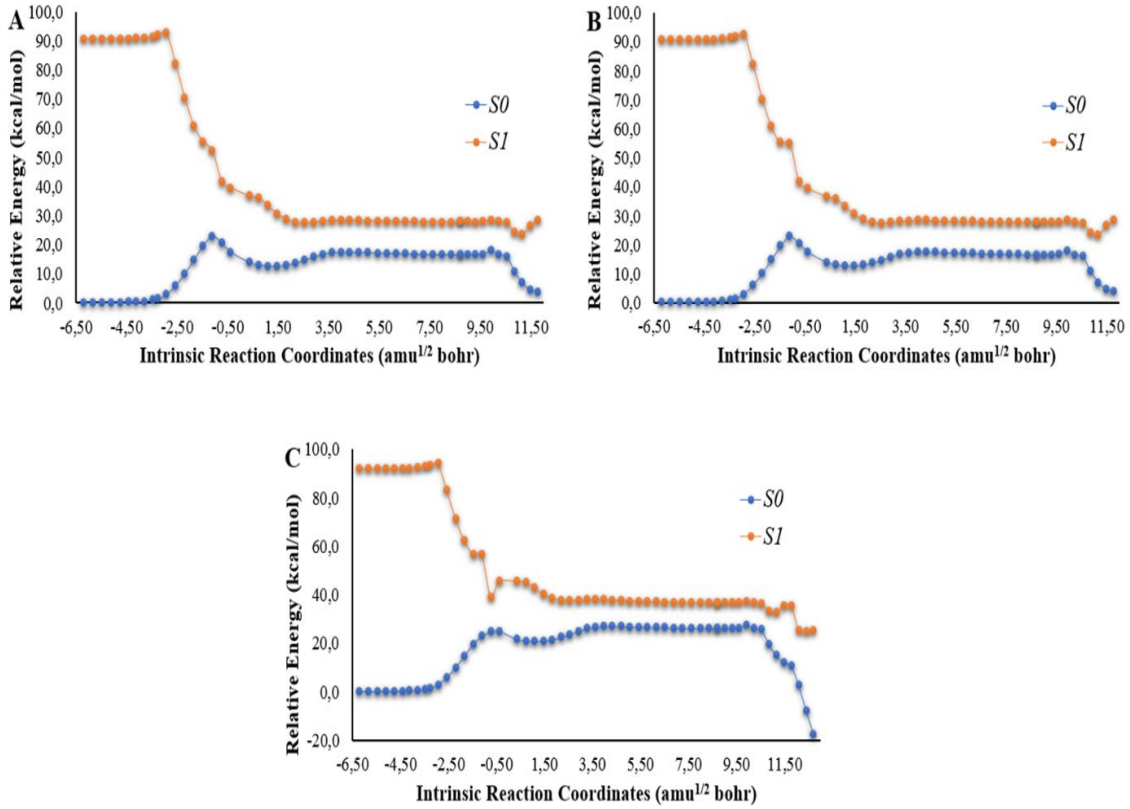


Figure 11- Potential energy curves for S_0 and S_1 states, as a function of intrinsic reaction coordinates, of model neutral dioxetanone (Scheme 9; R_1 = indole, R_2 = R_3 = CH_3). The calculations were made at the TD UωB97XD/6-31+G(d,p) level of theory, in implicit DMF (A), acetonitrile (B) and diethyl ether (C).

However, these results were not able to explain the data obtained in the chromatographic analysis (Figure 9). The lack of Coelenterazine → Coelenteramide conversion in diethyl ether at acidic pH could indeed be explained, at least partially, by the increased S_0 activation barrier for the thermolysis reaction in nonpolar solvents. However, the value of the activation barrier for the thermolysis reaction cannot explain the differences between DMF and acetonitrile at acidic pH. While the theoretical activation barrier is the same in both solvents, the Coelenterazine → Coelenteramide conversion yield is quite different in both solvents (complete/almost complete in DMF

and of about 0.147 in acetonitrile). Thus, these results indicate that the different behavior of Φ_R in the tested solvents is not related to the thermolysis reaction of dioxetanone. Having said that, it should be noted that we have excluded the oxygenation step from being able to explain Φ_R, claiming oxygen has good solubility in various solvents, and to its presence in large excess. However, it is generally considered that the oxygenation step proceeds from ionized Coelenterazine.

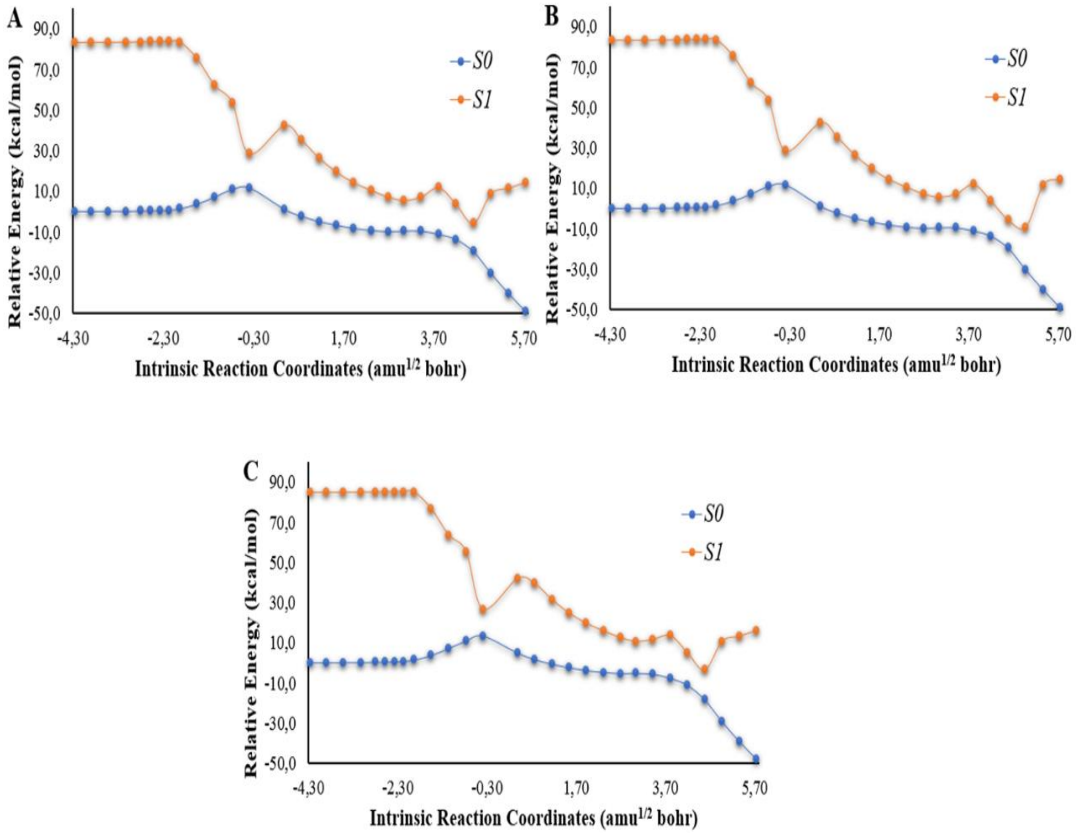
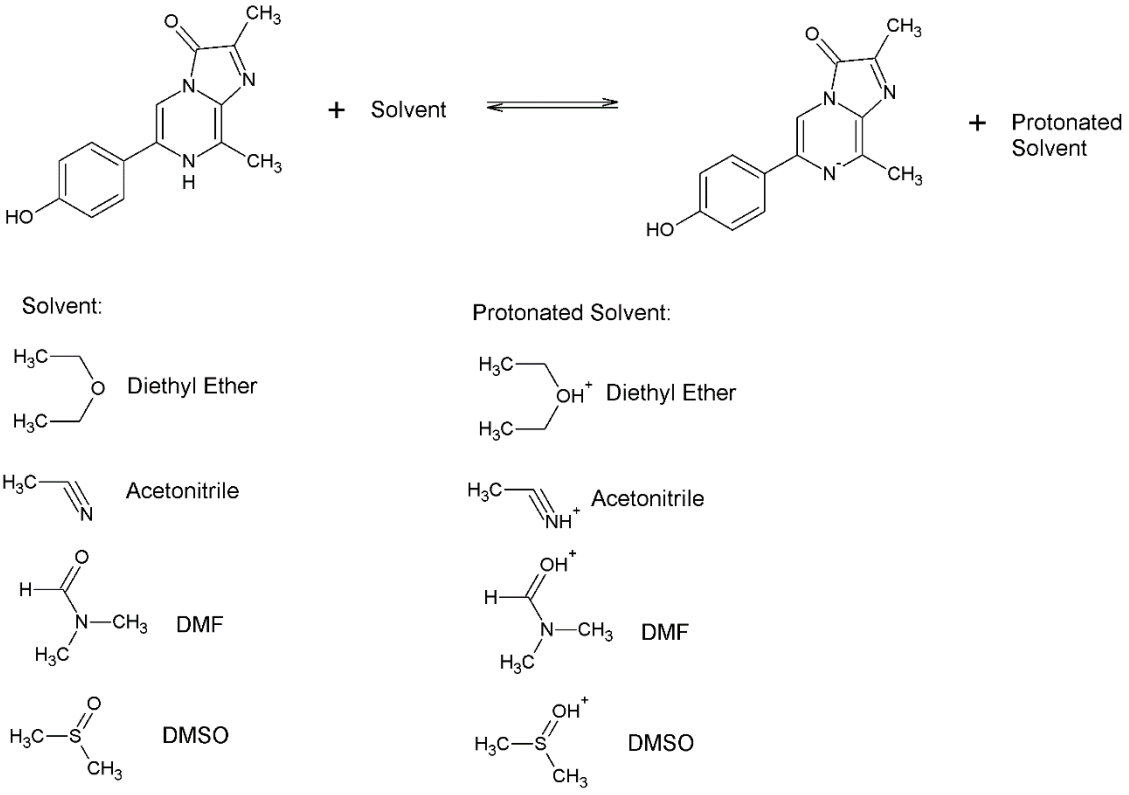


Figure 12- Potential energy curves for S_0 and S_1 states, as a function of intrinsic reaction coordinates, of model anionic dioxetanone (Scheme 9; R_1 = indole, $R_2 = R_3 = CH_3$). The calculations were made at the TD UωB97XD/6-31+G(d,p) level of theory, in implicit DMF (A), acetonitrile (B) and diethyl ether (C).

Thus, it is possible that the differences in Φ_R at acidic pH for different solvents can be related to the ability/inability of the solvent to deprotonate Coelenterazine, and so, trigger the oxygenation step. Thus, we have calculated the relative energies to the deprotonation reaction involving Coelenterazine and solvent molecules (Scheme 10), at the M06-2X+G(d,p) level of theory. The solvent was modelled implicitly with the SMD solvent model. We have found that indeed this reaction is more favorable in DMSO, with DMF being only 0.5 kcal mol^{-1} less favorable. However, the deprotonation reaction is 20.0 and 34.5 kcal mol^{-1} less favorable in acetonitrile and diethyl ether, respectively, than

in DMSO and DMF. Thus, the deprotonation potential of Coelenterazine is higher in DMSO and DMF, solvents in which CL is most intense and Φ_R is quite high, than in acetonitrile and diethyl ether, in which chemiluminescence and Φ_R is quite low/negligible. Thus, we attribute the low/negligible Φ_R in acetonitrile and diethyl ether at acidic pH, to the inability of these solvents to allow for deprotonation of Coelenterazine, and so, preventing the oxygenation step. For their turn, the good results for CL in DMSO and DMF at acidic pH can be explained by deprotonation being allowed in those solvents. This conclusion agrees with the fact that addition of base increases significantly Φ_R in both diethyl ether and acetonitrile, probably by facilitating the deprotonation of Coelenterazine.



Scheme 10- Schematic representation of Coelenterazine and solvent molecules and its respective state of protonation.

It should be noted that there are some results that might contradict previously obtained ones. Namely, we observed here that increasing the pH from acidic (acetate buffer pH 5.12, 0.68%) to basic (NaOH 0.1 M) in DMF led to a 3% increase of the area of the CL profile for Coelenterazine. However, in previous studies, we have found that the same increase in pH in DMSO solutions led to a significant decrease of total light output, for both *Cypridina* luciferin and Coelenterazine [64,92]. To assess this possible

contradiction, we have measured the calculated area (Figure 13) of the CL profile of Coelenterazine, in DMSO, DMF and acetonitrile. Measurements were made at acidic (acetate buffer pH 5.12, 0.68%) and basic pH (addition of NaOH, either 0.1 or 0.3 M).

The light output in DMSO decreases linearity and significantly with increasing pH, reaching a decrease of ~90 % with addition of NaOH 0.3 M. These results are consistent with our previous studies [64,92]. In DMF, the area values are quite similar at acidic and basic (NaOH 0.1 M) pH, but decrease by ~67% with addition of NaOH 0.3 M. For their turn, addition of NaOH 0.1 M to acetonitrile increases the area of emitted light by about ~90%, when comparing with addition of acetate buffer. However, addition of NaOH 0.3 M leads to a significant 44% decrease, in line with the results obtained in DMF. Thus, the results in acetonitrile indicate the occurrence of two pH-related events: the transition from acidic to basic pH, with increase of the light output; further increase of the pH, with a significant decrease of emitted light. We attribute the first event to the deprotonation of Coelenterazine, thus triggering the oxygenation step with higher efficiency. The absence of a similar increase in DMF and DMSO, solvents in which deprotonation appears to be possible at acidic pH, supports this hypothesis. We attribute the second event to the deprotonation of the dioxetanone intermediate as, as we have shown here (Figure 11 and Figure 12) and in previous studies [64,92], neutral dioxetanone allows for a significantly more efficient chemiexcitation than its anionic counterpart. Having said that, these results indicate that Coelenterazine dioxetanone has a similar pK_a in acetonitrile and DMF, as CL is reduced in similar amounts at similar pH conditions (NaOH 0.3 M). Moreover, the pK_a of dioxetanone appears to be smaller in DMSO than in those solvents, as we already have measured a 46% decrease in emitted light with addition of NaOH 0.1 M. Thus, anionic dioxetanone appears to be formed in less basic pH conditions in DMSO than in DMF/acetonitrile, meaning that the pK_a of dioxetanone should decrease with increasing dielectric constant of the solvent. Finally, we have also measured the fluorescence intensity of Coelenteramide in the same conditions (Figure 13), in order to confirm if the pH-induced effect is really due to the deprotonation of dioxetanone and not to quenching of the chemiluminophore. Our experiments confirmed that while some pH-induced quenching occurs, it cannot explain the accentuated pH-induced decrease in CL emission. In DMSO, the fluorescence of Coelenteramide is indeed quenched with increasing pH but just by about ~30%, far from the 90% decrease found for the CL reaction. In acetonitrile, there is not visible any quenching effect for the fluorescence process. It is just in DMF that increasing pH leads to similar quenching for both the fluorescent and CL processes. Thus, this analysis further supports our conclusion that the decrease in CL intensity with increasing pH is due to the deprotonation of the dioxetanone intermediate, leading to less efficient chemiexcitation.

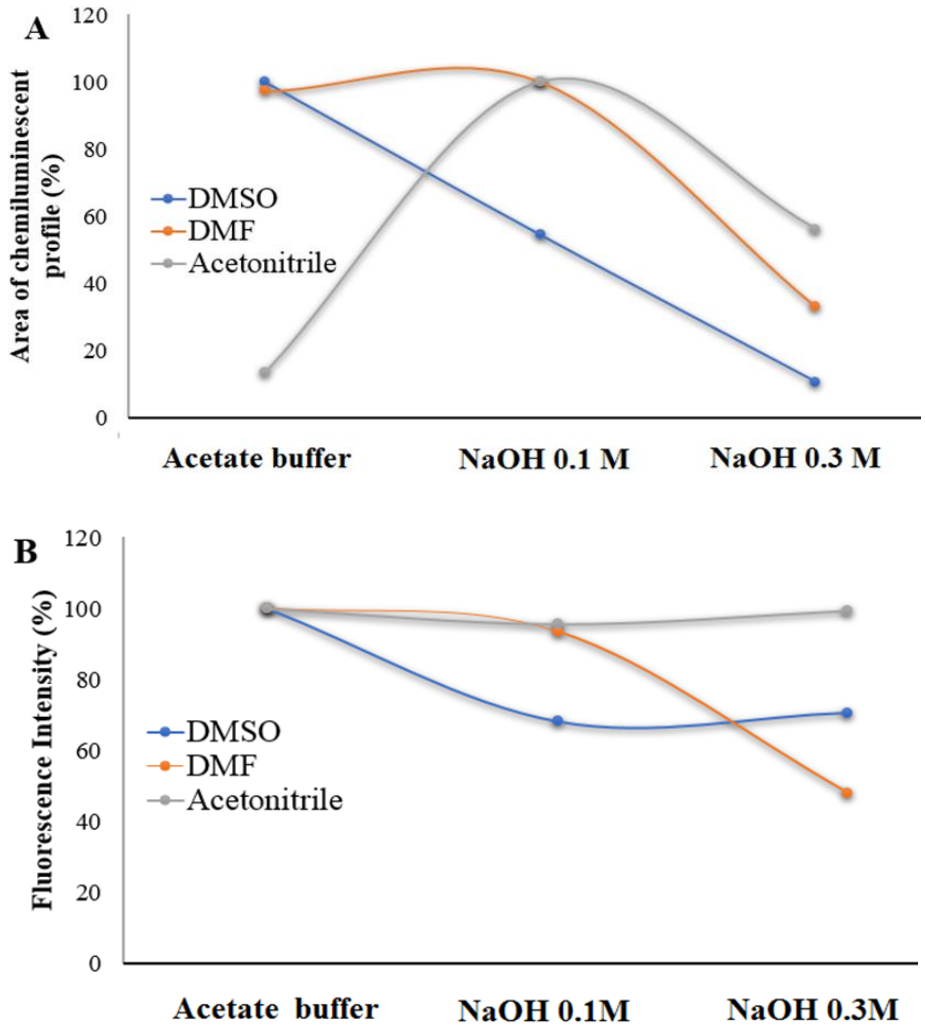


Figure 13- Calculated area of the CL profile (up to 85 seconds) obtained in the chemiluminescent reaction of Coelenterazine (1µM), in either DMF, DMSO and acetonitrile (A). Fluorescence intensity of Coelenteramide (1 µM), in either DMF, DMSO and acetonitrile (B). To the mixtures were added either acetate buffer pH 5.12 (0.68%), NaOH 0.1M or NaOH 0.3 M.

So far, our results have indicated that the yield of emitted light (Φ_{CL}) by the studied imidazopyrazinones in different solvents is controlled mainly by the Φ_R. That is, at acidic pH the imidazopyrazinones are only able to chemiluminesce in solvents (DMSO and DMF) in which deprotonation of the imidazopyrazinone core is possible, thereby allowing for the oxygenation step. Also, at higher pH the total emitted light in different solvents is controlled by the pK_a of the dioxetanone intermediate. Nevertheless, some of our results indicate that Φ_S is nevertheless affected by the polarity of the solvent. At acidic pH, the CL is always higher in DMF for all three imidazopyrazinones than for DMSO in a ~1.8

ratio (Table 5). At basic pH (0.1 NaOH), in which chemiexcitation appears to arise from neutral dioxetanone in both solvents, the CL of Coelenterazine in DMF is higher than in acetonitrile by a ratio of ~6. Despite this, DFT calculations made here and in a previous study [64] indicated that the activation barrier for the thermolysis reaction (22.9 kcal mol^{-1}) is the same in the three solvents. It should be noted that chemiexcitation appears to result from neutral dioxetanone in the conditions compared here for DMSO, DMF and acetonitrile. Also, deprotonation of the imidazopyrazinone core should be equally favorable in DMF and DMSO at acidic pH (due to the high areas of CL, Table 5). Finally, chromatographic and fluorescent analysis shown above indicate that neither Φ_R (Figure 10) nor Φ_{FL} (Figure 8.C) should explain the different total light output of Coelenterazine in DMF and acetonitrile at basic pH (NaOH 0.1 M). It should be noted that DMF, DMSO and acetonitrile can be distinguished by their polarity in the following order [95] : DMF (E_T^N of 0.386) < DMSO (E_T^N of 0.444) < acetonitrile (E_T^N of 0.460). Thus, these results indicate that the chemiexcitation yield of neutral dioxetanone decreases with increasing solvent polarity.

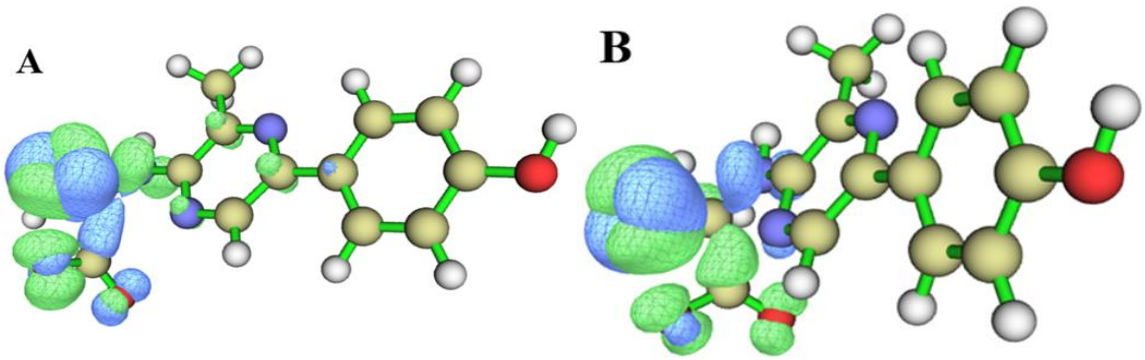


Figure 14- Hole-electron distribution for the $S_0 \rightarrow S_1$ chemiexcitation at the TS structure for the thermolysis reaction of a neutral dioxetanone model (Scheme 10, R_1 = phenol, R_2 = R_3 = CH_3), at the TD UωB97XD/6-31+G(d,p) level of theory in implicit DMF (A) or diethyl ether (B).

Previous work has indicated that efficient chemiexcitation should require only a small reorganization energy for solvation upon transition between states [13,96]. This should be facilitated if the chemiexcitation transition during the thermolysis reaction is accompanied with limited changes of the charge density of the dioxetanone molecule. That is, if transition to *S_1* state is accompanied with limited changes to the molecular dipole moment, the level of rearrangement needed for the surrounding solvent molecules to re-align their dipole molecules with the chemiexcited molecules is smaller. Herein, we

have optimized (at the UωB97XD/6-31G(d,p) level of theory) the TS geometries of neutral dioxetanone in solvents of different polarity (diethyl ether and DMF), and have analyzed the corresponding $S_0 \rightarrow S_1$ transition at the TD UωB97XD/6-31+G(d,p) level of theory. Namely, we have analyzed the hole-electron distribution (Figure 13) and the transition dipole moment (Figure 14) associated with $S_0 \rightarrow S_1$ chemiexcitation. The values were calculated with the Multiwfn program [91], taking into account the wavefunctions obtained with the TD UωB97XD/6-31+G(d,p) calculations. As can be seen from the hole-electron distribution (Figure 14), the $S_0 \rightarrow S_1$ transition is characterized in both solvents by a significant overlap between hole and electron, and by a small distance between the centroids of hole and electron. So, in both solvents chemiexcitation should occur by local excitation (LE), and not by charge-transfer (CT) excitation. As neutral dioxetanones have been found to produce more efficient chemiexcitation (here and in previous studies [45,64,65,92]), especially in DMF, this is another argument against CTIL being a mechanism able to explain efficient chemiexcitation [45,64,65,92], as it would predict a CT transition [69,70]. Analysis of the transition dipole moment (Figure 14) indicates that $S_0 \rightarrow S_1$ transition is not associated with significant changes in the charge density of the dioxetanone moiety in both solvents. However, it also shows that while in diethyl ether the contributions to the transition dipole moment are limited to the dioxetanone moiety, in DMF there are also contributions from the phenol and aminopyrazine groups, indicating that the transition dipole moment is higher in DMF than in diethyl ether. This was confirmed by calculating the transition dipole moment for the $S_0 \rightarrow S_1$ transition in both solvents, which was of 2.65 Debye in diethyl ether and 5.37 Debye in DMF (Figure 15). In conclusion, $S_0 \rightarrow S_1$ transition is associated with decreased reorganization of charge density in solvents of lower polarity, which should facilitate chemiexcitation by requiring a small reorganization energy for solvation [13,96].

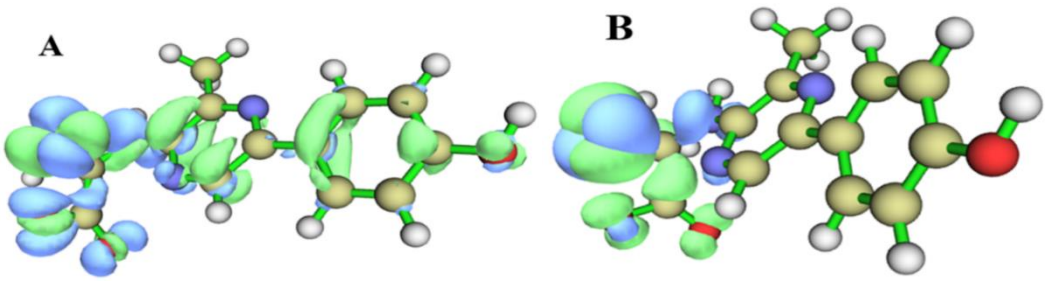


Figure 15- Transition dipole moment for the $S_0 \rightarrow S_1$ chemiexcitation at the TS structure for the thermolysis reaction of a neutral dioxetanone model (Scheme 10, R_1 = phenol, R_2 = R_3 = CH_3), at the TD UωB97XD/6-31+G(d,p) level of theory in implicit DMF (A) or diethyl ether (B).

3.3. Conclusion

It was demonstrated that DMSO and DMF are the only solvents that consistently allow for significant CL at acidic pH, while other solvents (dichloromethane, acetonitrile, acetone, pyridine, toluene, diethyl ether, diglyme and ethyl acetate) allow only for negligible/almost negligible light emission in these conditions. Moreover, HPLC experiments that this can be explained by the S_0 reaction, as the chemiluminophore was only generated in DMF and DMSO in significant amounts, while its concentration in other solvents is negligible. Further analysis attributed this to the inability of most solvents to induce deprotonation of the imidazopyrazinone core, which prevents the oxygenation step of the CL reaction.

This finding was supported by the observation that addition of base led to an increase in total light output, by increasing the amount of produced chemiluminophore. However, further increase of base led to significant inhibition of CL, which cannot be explained by fluorescence quenching of chemiluminophore. This phenomenon was attributed to the deprotonation of the dioxetanone intermediate prior chemiexcitation, as neutral species led to a more efficient chemiexcitation than their anionic counterparts.

Finally, it was also observed that at the same pH, the chemiexcitation efficiency decreases with increasing polarity of the solvent. Based on theoretical calculations, this was explained by reduced changes in charge density upon $S_0 \rightarrow S_1$ chemiexcitation by requiring only a small reorganization energy for solvation upon transition between states.

4. Theoretical study of chemiexcitation mechanism of model dioxetanones from TD-DFT and Multi-Reference Calculations

4.1. Aim

As already talked about, different researchers have tried to explain efficient chemiexcitation in CL and BL reactions by either the CIEEL (ET followed by BET during the thermolysis of organic peroxides) or the CTIL theory (CT followed by BCT during the thermolysis organic peroxides). However, work performed by this group have showed that neither one of these theories can be applied to the light-emitting reactions of imidazopyrazinones, as neither ET/BET not CT/BCT have any clear relationship with efficient chemiexcitation [64,92].

Herein, we have pursued an alternative and general explanation to CIEEL and CTIL for the efficient chemiexcitation of dioxetanone molecules. To this end, the chemiexcitation mechanism of model dioxetanones (Scheme 11) was characterized with a reliable theoretical approach, composed by single-reference DFT and multi-reference CASPT2 calculations and Born-Oppenheimer molecular dynamics (MD).

4.2. Materials and methods

S_0 geometry optimizations for the model dioxetanones (Scheme 11) were performed at the ωB97XD/6-31+G(d,p) level of theory, [62]. The (U) approach was used with a BS technology. IRC calculations were performed [97] The S_1 state was calculated by using the time-dependent (TD) DFT approach, [97] at the TD ωB97XD/6-31+G(d,p) level of theory. S_0 Born-Oppenheimer MD calculations were made at the BS U ωB97XD/6-31+G(d,p) level of theory, [98] starting from the TS structure of $-CH_2CH_3$ and $-CH_2CF_3$ dioxetanones. The temperature was set to 300 K, and second derivatives were calculated at every ten points. 30 trajectories were computed for each molecule. These calculations were made *in vacuo*. All DFT calculations were performed with the Gaussian 09 program package.

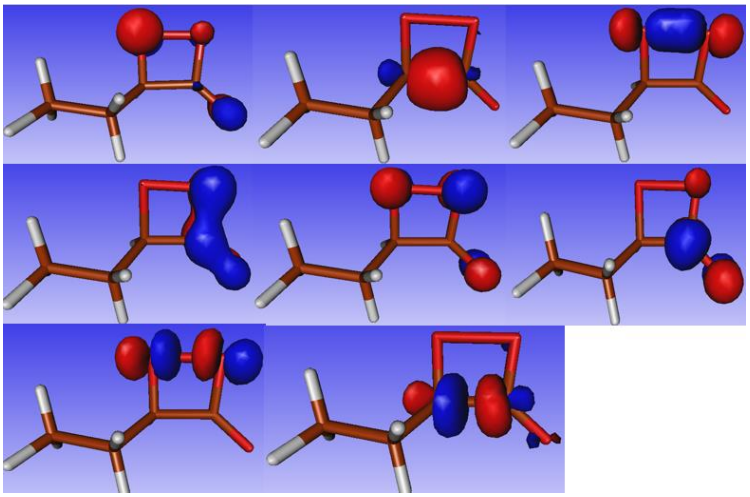


Figure 16- Active orbitals included in the MS-CASPT2 calculations for the thermolysis of -CH_2CH_3 dioxetanone.

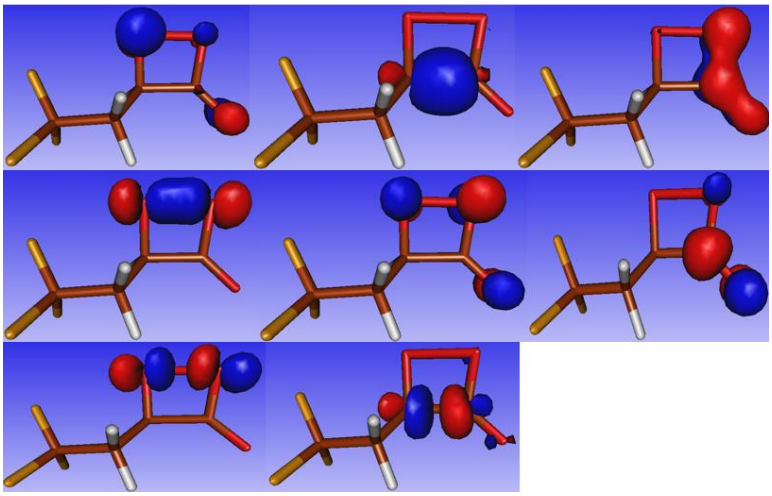
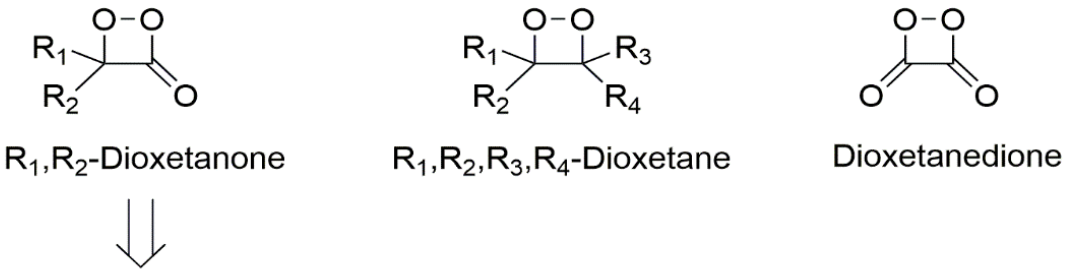


Figure 17- Active orbitals included in the MS-CASPT2 calculations for the thermolysis of -CH_2CF_3 dioxetanone.

Multi-reference calculations were performed on top of ωB97XD/6-31+G(d,p) geometries. The state-average (SA) complete-active-space self-consistent field (CASSCF) method was used to build multiconfigurational wavefunctions, [99] using the relativistic core correlation atomic natural orbital basis set ANO-RCC-VDZ. An active space of 10-in-8 was chosen for the different dioxetanones (as seen in Figure 16 and Figure 17). The multistate (MS) complete-active-space second-order perturbation theory (CASPT2) method was used to compute the dynamical electron correlation [100]. Six roots were considered simultaneously. The multi-reference calculations were performed with the Molcas v8.015-06-18 software [101].



1. R_1=-CH_3 ; R_2=-H
2. R_1=-CH_2CH_3 ; R_2=-H
3. R_1=-OH ; R_2=-H
4. R_1=-CH_2CF_3 ; R_2=-H

Scheme 11- Representation of known cyclic peroxides involved on chemi- and bioluminescence and the model dioxetanone species here studied.

4.3. Results and Discussion

Taking into account the calculation of (S^2) values higher than 0.4 and the analysis of the behavior of both O-O and C-C bonds of the cyclic peroxide, we can conclude that the thermolysis of the four dioxetanones here studies proceeds via a stepwise biradical mechanism. For all structures, the reaction starts by O-O bond breaking, while C-C remains nearly constant. It is only upon the breaking of the peroxide bond that C-C bond stretching occurs. These results are in line with existent in literature [32,36,63–65,80,102].Besides, we have calculated the activation energy for all four reactions, the results can be found on Table 8.

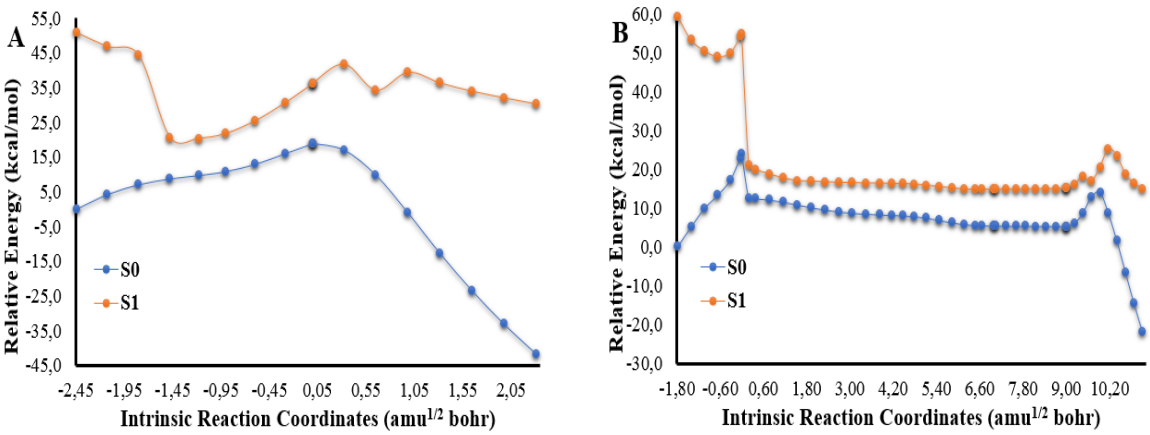
Table 8- Activation energies (Eact, in kcal mol^{-1}) for the thermolysis reaction of four model dioxetanone species (Scheme **11**), at the ωB97XD/6-31+G(d,p).

Species	E_{act}
-CH_3	18.8
-CH_2CH_3	23.9
-OH	23.9
-CH_2CF_3	33.3

Primarily, dioxetanones with -CH_3, -OH and -CH_2CH_3 groups present activation energies in line with those found experimentally [76–78] and [32,36,63–65,80,102] for other dioxetanones (~20 kcal mol^{-1}). On the other hand, the dioxetanone with the -CH_2CF_3 group presents a significantly higher activation energy (33.3 kcal mol^{-1}). Interestingly, it appears not to be a direct correlation between the electron character of

the substituents and the computed activation energy. Strong electron-donating -OH presents a similar or even higher barrier than dioxetanones with alkyl substituents, while the dioxetanone with the strongly electron-withdrawing CF_3 group presents the higher activation barrier.

We have calculated the potential energy curves for the thermolysis of the model dioxetanones (Scheme 11), which are composed of the energy of the S_0 and S_1 states as a function of intrinsic reaction coordinates. We can divide these dioxetanones into two groups, one composed by dioxetanones with -OH and $-CH_2CH_3$ substituents, and the other by the species with $-CH_3$ and $-CH_2CF_3$ groups. As for the first group, these curves indicate that S_0 and S_1 become degenerated/nearly-degenerated in the biradical region, due to O-O bond elongation. In fact, for $-CH_2CH_3$ the S_0-S_1 energy gap is only between 2.9 and 8.8 kcal mol^{-1}, from IRC of -0.36 to 6.11 $amu^{1/2}$ bohr. By its turn, for -OH the energy gap is of 4.0-10.0 kcal mol^{-1}, from IRC of 0.20 to 9.94 $amu^{1/2}$ bohr. Our calculations indicate a less efficient chemiexcitation for the dioxetanones with $-CH_3$ and $-CH_2CF_3$ groups. For the former species, the S_0-S_1 gap is always higher than 10.6 kcal mol^{-1}, while for the latter the gap is higher than 18.0 kcal mol^{-1}. It is not only the values for the S_0-S_1 energy gap that indicates that -OH and $-CH_2CH_3$ induce a more efficient chemiexcitation than $-CH_3$ and $-CH_2CF_3$, but also the length of the PES in which chemiexcitation is possible. For the $-CH_3$ and $-CH_2CF_3$, the reaction is measured only in the range -2.44-2.31 and -5.61-2.33 $amu^{1/2}$ bohr. However, the S_0-S_1 degeneracy region for -OH and $-CH_2CH_3$ is of 9.74 and 6.47 $amu^{1/2}$ bohr, respectively. This indicates that -OH and $-CH_2CH_3$ have a larger biradical region than $-CH_3$ and $-CH_2CF_3$, after O-O bond breaking, which increases the length of the degeneracy region of the former species. As the degeneracy region (which is the one where chemiexcitation is possible) occupies a large portion of the PES, the probability of $S_0 \rightarrow S_1$ transition should increase.



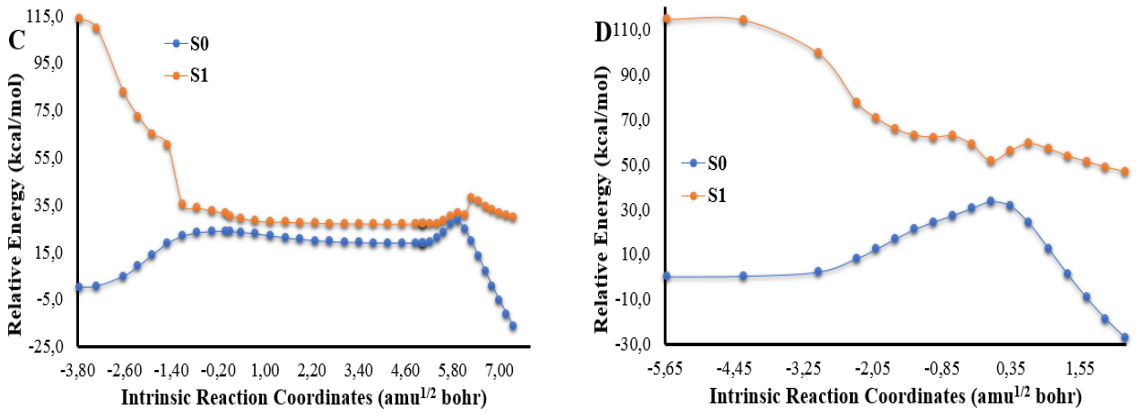


Figure 18- Potential energy curves of S_0 and S_1 states, as a function of intrinsic reaction coordinates, of model dioxetanones (Scheme 11). The curves were calculated at the ωB97XD/6-31+G(d,p) level of theory. Dioxetanone species: $-CH_3$ (A), -OH (B), $-CH_2CH_3$ (C) and $-CH_2CF_3$ (D).

As already said, it is expected that multi-reference calculations predict smaller S_0-S_1 energy gaps than the ones predicted by TD-DFT calculations. To assess the accuracy of this expectation and the quality of the results provided by TD-DFT methods, we have calculated the potential energy curves for the S_0, S_1 and S_2 states of $-CH_2CH_3$ and $-CH_2CF_3$ dioxetanones during their thermolysis reaction, at the MS-CASPT2/ANO-RCC-VDZ level of theory. $-CH_2CH_3$ presented an activation barrier for O-O bond breaking of 22.4 kcal mol^{-1}, only 1.5 kcal mol^{-1} higher than the value obtained with DFT calculations. As expected, the S_0-S_1 energy gap is smaller than the one present in Figure 18, being now between 0.5 and 5.1 kcal mol^{-1} from IRC of 0.38 to 5.93 $amu^{1/2}$ bohr. In the same region of the PES, the S_0-S_2 energy gap is only between 3.7 and 14.1 kcal mol^{-1}, which indicates the possibility for $S_0 \rightarrow S_2$ chemiexcitation. More importantly, the MS-CASPT2 results support the ones obtained at the TD-DFT level and indicate that $-CH_2CH_3$ should present a more efficient chemiexcitation than $-CH_2CF_3$. For this latter species, the S_0-S_1 and S_0-S_2 energy gaps are always higher than 27.5 and 34.8 kcal mol^1, which are too high to allow for chemiexcitation. The main difference between MS-CASPT2 and DFT calculations is the activation barrier (26.4 *vs.* 33.3 kcal mol^{-1}). The value obtained by MS-CASPT2 calculation is more in line with the activation barriers presented by other species. Nevertheless, all the qualitative conclusions obtained by DFT methods are supported by the multi-reference calculations.

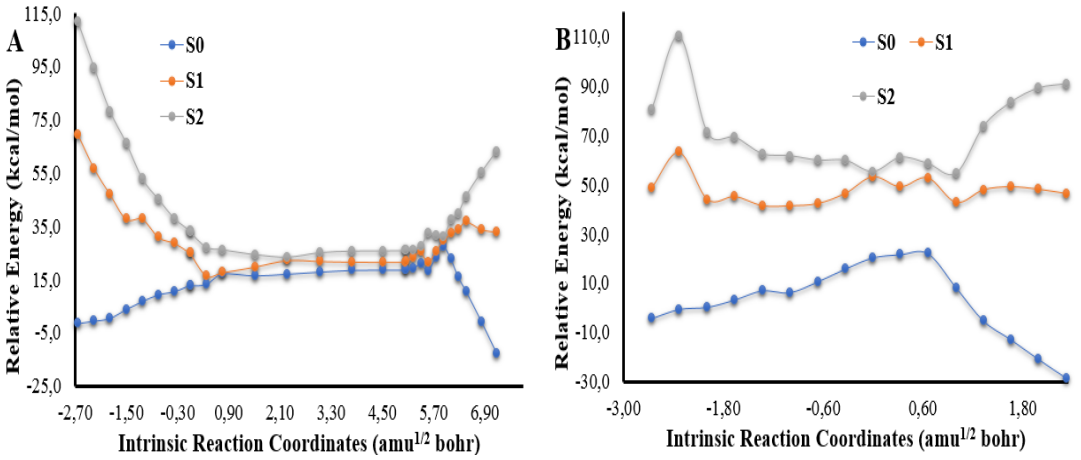


Figure 19- Potential energy curves of the S_0, S_1 and S_2 states as a function of intrinsic reaction coordinates of model dioxetanones (Scheme 11). The calculations were made at the MS-CASPT2/ANO-RCC-VDZ, on top of geometries obtained in ωB97XD/6-31+G(d,p) optimizations. Dioxetanones species: $-CH_2CH_3$ (A) and $-CH_2CF_3$ (B).

The main difference between the potential energy curves of -OH/$-CH_2CH_3$ and $-CH_3$/$-CH_2CF_3$ is an increase in energy of the S_0 state at the end of the biradical region for the former (Figure 18). These correspond to saddle points associated with C-C bond breaking. The increases are of 9.3 kcal mol^{-1} and 8.7 kcal mol^{-1} for $-CH_2CH_3$ and -OH, respectively. These increases were also present in the DFT calculations of other dioxetanones, [65,93], thus this is not a new finding. For example, an increase of 3.7 kcal mol^{-1} was found for a model of Coelenterazine dioxetanone [93]. The MS-CASPT2 calculations also determined a similar increase of 9.7 kcal mol^{-1} (Figure 19). The presence of these saddle points may affect positively the S_1 chemiexcitation yield as this barrier may force the reacting molecules to spend more time in a region where S_0 and S_1 are nearly-degenerated [65,93]. Nevertheless, these barriers are still significantly smaller than the ones associated with O-O bond breaking, which is the rate-limiting step of the thermolysis reaction.

Having provided evidence for the -OH and $-CH_2CH_3$ species presenting higher S_1 chemiexcitation yields than $-CH_3$ and $-CH_2CF_3$, it is essential to determine what is the mechanism behind the chemiexcitation. As already referred, while CIEEL and CTIL mechanisms have been used to explain efficient chemiexcitation, recent evidence has indicated that they fail in doing so [64]. In previous studies, [64] we have tentatively explained this by hypothesizing that some dioxetanones have access to the region of S_0-S_1 degeneracy due to attractive electrostatic interaction between the keto and CO_2 moieties, which will delay C-C bond scission and increase the length of the biradical

region. To determine if this explanation can be applied to these models dioxetanones, we have measured the CT between the CO_2 and keto moieties as a function of intrinsic reaction coordinates for all four species (Figure 20).

The general picture for all species is the same, with CO_2 having negative charge while the keto moiety presenting positive charge during the reaction. Moreover, while the charge separation between moieties tend to decrease from the reactant to the TS, it increases during the biradical region. The major difference between molecules is the degree of charge separation, with the maximum charge separation being of 0.258e for -CH_3, 0.400e for -OH, 0.388e for -CH_2CH_3 and 0.172e for -CH_2CF_3. Thus, the charge separation between moieties is significantly higher for molecules that can access the region of S_0-S_1 degeneracy, which supports the hypothesis that access to this region is given by attractive electrostatic interactions that extend the length of the biradical region by delaying C-C bond scission.

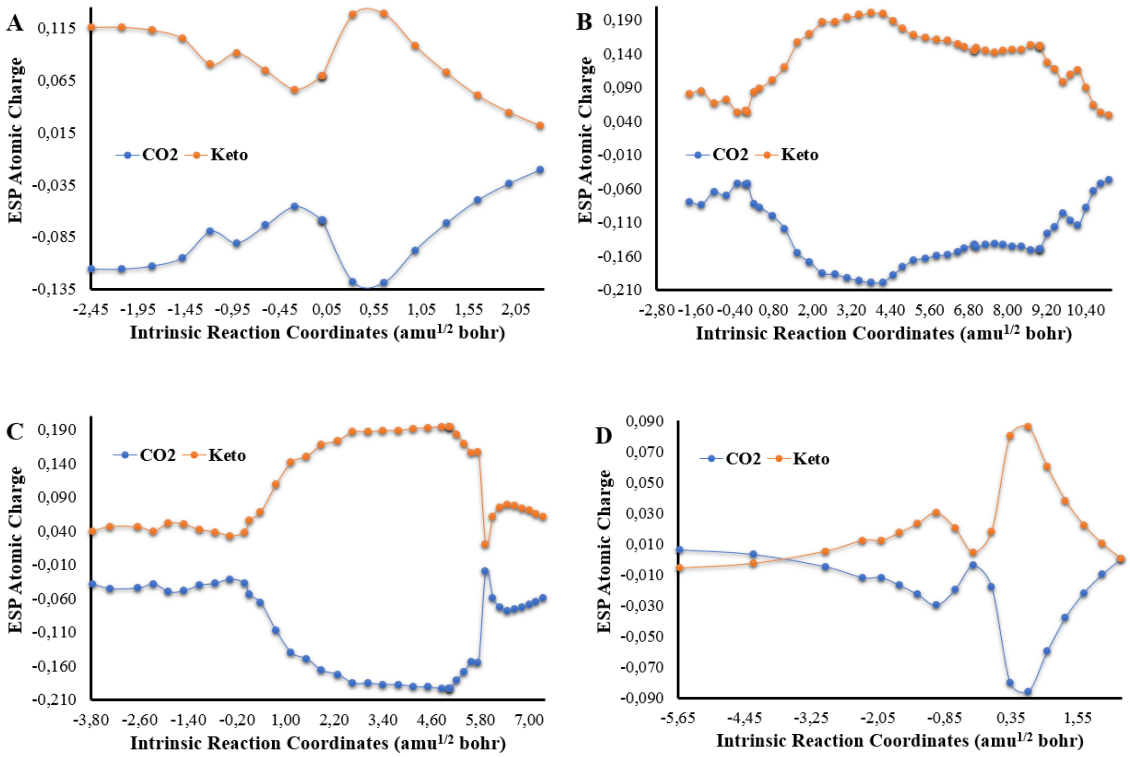


Figure 20- ESP atomic charges, as a function of intrinsic reaction coordinates, of model dioxetanones. The charge densities were calculated at the ωB97XD/6-31+G(d,p) level of theory. Dioxetanone species: -CH_3 (A), -OH (B), -CH_2CH_3 (C) and -CH_2CF_3 (D).

We have used the activation strain model, [103] also known as distortion/interaction model, [104] developed by Bickelaupt and Houk [105] to determine if the interaction energy is indeed affected during the thermolysis in ways in which it can

be correlated with chemiexcitation. In this approach, the potential energy surface $\Delta E(\zeta)$ is decomposed into two main contributions along the reaction coordinate ζ: the reaction strain ($\Delta E(\zeta)_{strain}$) is associated with the structural distortion that the reactants undergo during the reaction, while $\Delta E(\zeta)_{int}$ corresponds to the interaction energy between these increasingly distorted reactants. $\Delta E(\zeta)_{strain}$ is determined by the rigidity of the reactants, resulting from the strength of bonds that must break or the flexibility of bond angles that get deformed. $\Delta E(\zeta)_{int}$ is related to the bonding capabilities and mutual interaction between the increasingly deformed reactants along the reaction coordinate. As dioxetanone's thermolysis is a unimolecular reaction, the analysis will not be between reactants but between the keto and CO_2 moieties.

The values of $\Delta E(\zeta)$, $\Delta\Delta E(\zeta)_{strain}$ and $\Delta\Delta E(\zeta)_{int}$ are plotted as function of intrinsic reaction coordinates for all species (Figure 21). The four species can be divided into two groups (-OH/-CH_2CH_3 and -CH_3/-CH_2CF_3), which are consistent with the potential efficiency of chemiexcitation. For -CH_3/-CH_2CF_3, $\Delta\Delta E(\zeta)_{strain}$ is increasingly negative, while $\Delta\Delta E(\zeta)_{int}$ is increasingly positive.

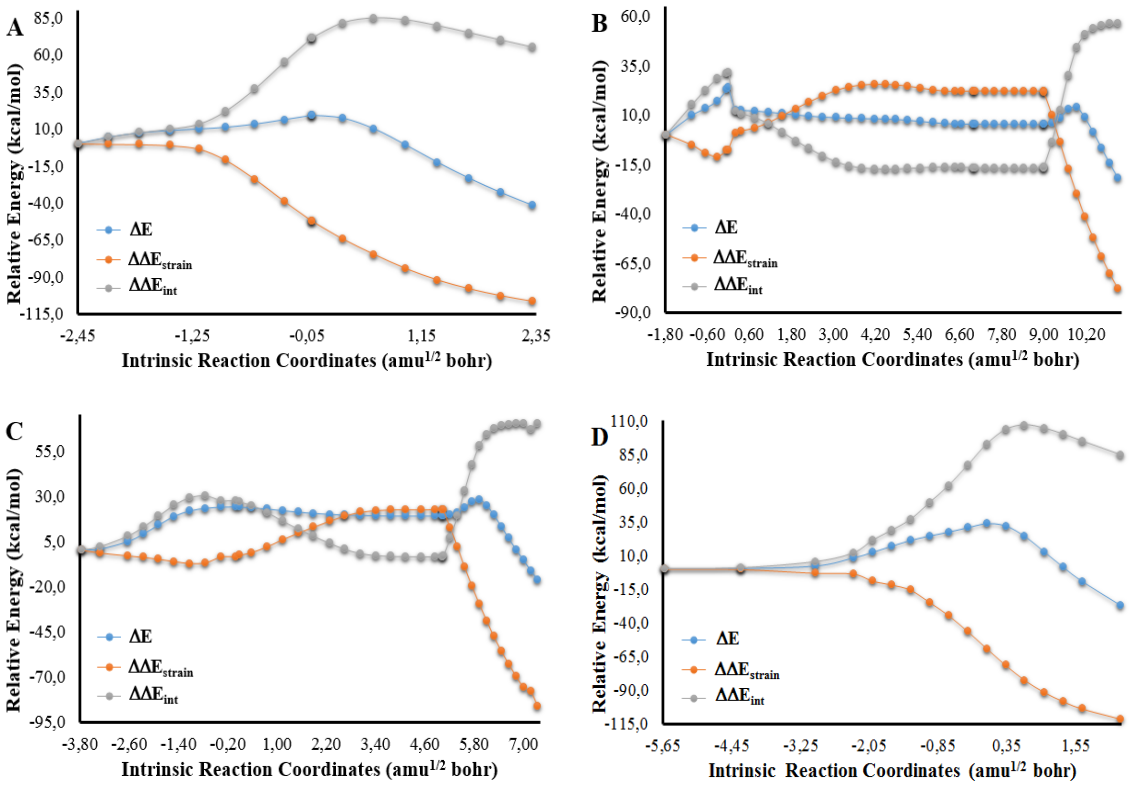


Figure 21- E(ζ), ΔΔE(ζ)strain and ΔΔE(ζ)int values plotted as a function of intrinsic reaction coordinates, during the thermolysis of model dioxetanones (Scheme 11). They were calculated at the ωB97XD/6-31+G(d,p) level of theory. Dioxetanone species: -CH_3 (A), -OH (B), -CH_2CH_3 (C) and -CH_2CF_3 (D).

First, this means that the thermolysis reaction reduces the strain of the peroxide ring. Secondly, the interaction between keto and CO_2 fragments become increasingly unfavorable during thermolysis. This is consistent with our hypothesis that the reduced length of the biradical region during the thermolysis of these species is related to reduced electrostatic interactions.[64] The use of the activation strain model also indicates that the $\Delta E(\zeta)$ between the reactant and the TS (associated with O-O bond breaking) is determined mainly by $\Delta\Delta E(\zeta)_{int}$, as the interaction between fragments become increasingly unfavorable. After the TS, $\Delta E(\zeta)$ is controlled by $\Delta\Delta E(\zeta)_{strain}$, as the rupture of the peroxide ring significantly reduces the strain of the system, which explains the exothermicity of the system.

The thermolysis reaction of -OH and $-CH_2CH_3$ can be divided into distinct phases, in terms of the activation strain model. The initial phase (from the reactant to the TS) is identical to $-CH_3$ and $-CH_2CF_3$, with $\Delta\Delta E(\zeta)_{int}$ being increasingly positive and $\Delta\Delta E(\zeta)_{strain}$ negative. The main difference occurs after the TS during the biradical region. In this region, the interaction between fragments become increasingly favorable, until the C-C bond scission. This supports our hypothesis that attractive interactions extend the biradical region, and so, give access to a region of S_0-S_1 degeneracy. In fact, the length of the biradical region of -OH is higher than for $-CH_2CH_3$, and $\Delta\Delta E(\zeta)_{int}$ is more negative in the biradical region for the former (between -3.1 and -17.5 kcal mol^{-1}) than for the latter (-1.9 and -3.6 kcal mol^{-1}).

Besides $\Delta\Delta E(\zeta)_{int}$, $\Delta\Delta E(\zeta)_{strain}$ presents an opposite behavior in the biradical region and becomes positive. In the case of $-CH_3$ and $-CH_2CF_3$ both the keto and CO_2 fragments have negative $\Delta E(\zeta)_{strain}$, which explains the negative $\Delta\Delta E(\zeta)_{strain}$ during the entirety of the reaction. For the contrary, for -OH and $-CH_2CH_3$ only keto has negative $\Delta E(\zeta)_{strain}$, while CO_2 presents positive values of $\Delta E(\zeta)_{strain}$, which explains why $\Delta\Delta E(\zeta)_{strain}$ is positive on the biradical region (Figure 21). Thus, it is the CO_2 moiety that increases the strain in the thermolysis of -OH and $-CH_2CH_3$ dioxetanones. The main difference between key geometrical parameters (O-O and C-C bond lengths) of -OH/$-CH_2CH_3$ and $-CH_3$/$-CH_2CF_3$ is that for the latter O-O bond stretching is more significant until the TS, after which this increase is more moderate. C-C bond scission starts at the TS. For the former, due to increased interaction between moieties, O-O bond stretching remains significant after the TS, and C-C bond scission only starts much after the TS. The significant increase of O-O bond length without the possibility of C-C bond scission for -OH/$-CH_2CH_3$, leads to an approximation of the two oxygen heteroatoms of the CO_2 moiety. This can be seen by following the O-C-O angle of the CO_2 moiety as a function of intrinsic reaction coordinates (Figure 22), which reaches values as low as ~112º. This should lead to repulsion between these heteroatoms. For the contrary, the O-C-O angle only reaches

values as low as ~124º for -CH_3/-CH_2CF_3, indicated oxygen-oxygen repulsion should have a more limited impact.

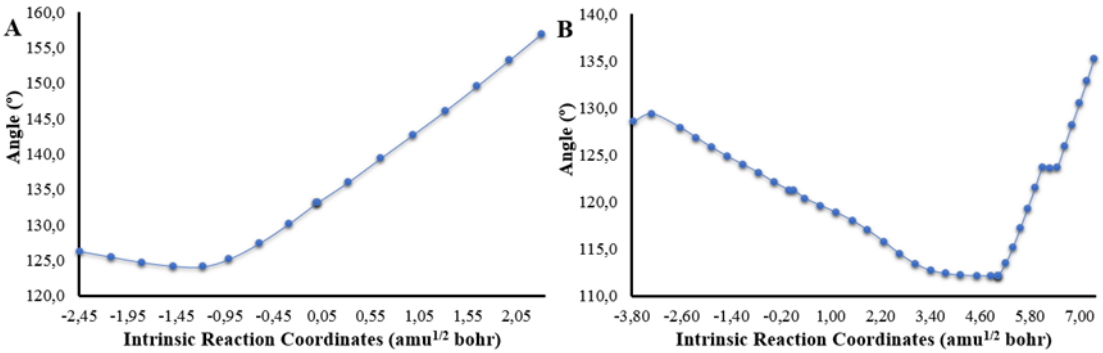


Figure 22- Variation of the O-C-O angle (in Å), as a function of intrinsic reaction coordinates, of the CO_2 moieties of model dioxetanones during their thermolysis reactions. Dioxetanone species: -CH_3 (A) and -CH_2CH_3 (B).

If the hypothesis that the increased interaction between moieties is the one responsible for extending the biradical region and delaying the rupture of the peroxide ring, that should be noticeable on the dissociation kinetics. That is, the time that takes to go from the TS to the point where the C-C bond of the peroxide is fully ruptured. Therefore, we have performed S_0 Born-Oppenheimer MD (BOMD) calculations starting from the TS to a structure with a broken C-C bond (cutoff of 1.8 Å), at the ωB97XD/6-31+G(d,p) level of theory. No other states than S_0 were considered.

BOMD calculations were performed for -CH_2CH_3 and -CH_2CF_3 dioxetanones, as they are representative of systems with potentially efficient/inefficient chemiexcitation (respectively). We have obtained a dissociation time of 3.56 ± 0.35 fs for -CH_2CF_3 dioxetanone. This rapid dissociation is in line with its unfavorable interaction energy between moieties, as determined by the activation strain model. By its turn, the dissociation time for -CH_2CH_3 is four times higher (14.20 ± 0.62 fs) than for -CH_2CF_3 dioxetanone. Thus, BOMD simulations support the notion that the increased interaction between keto and CO_2 moieties significantly delays the rupture of the peroxide bond and extends the biradical region.

4.4. Conclusion

It was provided an alternative mechanism to CIEEL and CTIL for explaining the efficient chemiexcitation of dioxetanones, which is not based on ET and/or CT steps and charge annihilation. Instead, it is based on the degree of interaction between the keto and CO_2 moieties of dioxetanone. If favorable, the detachment of CO_2 to produce the

light emitter is delayed, and the reacting molecules have access to a zone of S_0-S_1 degeneracy within the biradical region of the PES, which favors chemiexcitation. If the interaction is repulsive, the detachment of CO_2 is too quick for the reacting molecules to have access to the zone of degeneracy, which decreases the efficiency of chemiexcitation.

5. Synthesis and evaluation of self-illuminating photosensitizers

5.1. Aim

Herein, we have tried to develop and synthesize novel Coelenterazines that act both as a self-activation molecule as a photosensitizer, without the need of any energy transfer steps (except to O_2 to generate singlet oxygen). To this end, six new Coelenterazine derivatives were synthesized, and were characterized spectroscopically in terms of CL and ability to produce singlet oxygen. Proof-of-concept was provided by performing *in vitro* toxicity assays in tumor cell lines.

It should be noted that this part of the work is confidential, as it is undergoing a patenting process (Patent PPP59213, Pending), which resulted from this work. Thus, the structures of these molecules are not presented here, and they are referred to as Compounds 1-6.

5.2. Materials and methods

5.2.1. Synthesis Methodology

As these new compounds are confidential, the synthesis methodology cannot be described in detail. Nevertheless, it can be said that the synthesis followed the general scheme for Coelenterazine and derivatives. Namely, the synthesis reaction is initiated by a palladium-catalyzed Suzuki coupling involving an appropriated precursor (such as 2-amino-3,5-dibromopyrazine) and the desired arylboronic acid. The resulting intermediate is used in another palladium-catalyzed Suzuki coupling reaction involving a target arylboronic acid. The final step is a condensation reaction, in which the product o of the second step of the reaction reacts wither with appropriated diethoxy derivatives or methylglyoxal and analogues.

5.2.2. Kinetic chemiluminescent assay

Compounds 3,4 and 5 were dissolved in methanol. Kinetic chemiluminescent assays were performed in a homemade luminometer using a Hamamatsu HC135-01 photomultiplier tube, at ambient temperature. To prepare the light reactions was used a solution of DMSO. To this solvent was added either acetate buffer pH 5.12 (0.68%). The injection of the DMSO solution reaction into a tube containing the compounds initiated the reaction. The final solution of compounds had a concentration of 10 µM. To integrate and record the light, it was used 0.1 s intervals.

5.2.3. Measurement of chemiluminescence and fluorescence spectra

A Horiba Jovin Yvon Fluoromax 4 spectrofluorometer was used to measure the chemiluminescence spectra for Compounds 3, 4 and 5. The integration time was of 0.1s and for the emission monochromators were used slit widths of 29 nm. Quartz cells were used. The spectra were obtained in solutions with a final volume of 500 μL, being the Compounds concentration of 10 μM.

5.2.4. Fluorescent assay for detection of singlet oxygen

The detection of the singlet oxygen generation was made by photobleaching of 9,10-anthracenediyl-bis(methylene)dimalonic acid (ABDA). [106–109]. ABDA reacts with $^1O_2$ to form an endoperoxide and the decrease in amount of ABDA can be measured by measuring the fluorescence intensity when excited at 380 nm [109]. A Horiba Jovin Yvon Fluoromax 4 spectrofluorometer was used to measure the fluorescence spectra. The integration time was of 0.1s. The slit width used was 5 nm. ABDA (50 μM) was added to a solution of DMSO at neutral pH, with addiction of phosphate buffer pH 7,4 (0,075M), to which were added increasing concentrations of the synthetized compounds (5, 10, 20 and 50 μM).

5.2.5. *In vitro* assays for the cellular viability

Cytotoxicity of compounds was assessed through the 3-(4,5-Dimethylthiazol-2-yl)-2,5-diphenyltetrazolium bromide (MTT) and lactate dehydrogenase (LDH) assay [110–112]. The MTT test was performed after an incubation of both 24h and 48h. LDH was determined spectrophotometrically by estimating the release of LDH into media. Total cellular LDH was determined after lysing cells; the amount of LDH released into media at any given time during the incubation was expressed as the percentage of total LDH. It was tested increasing concentrations of the synthetized compounds (1, 10, 20, 50 and 100 μM). The assays were performed with HepG2 cell lines, which consist on liver hepatocellular carcinoma cells.

5.3. Results and discussion

5.3.1. Chemiluminescence and fluorescence of Compounds 3, 4 and 5 in DMSO

The CL of Compounds 3, 4 and 5 was recorded in a homemade luminometer. The CL profile were obtained, between times of 0 and 85 s presented in Figure 23. We

have calculated the area of the CL profile, between the same time [92]. These values are presented in Figure 23. The area values can be considered as a measure of total light output, and so, an indicative for chemiluminescence quantum yield (Φ_{CL}).

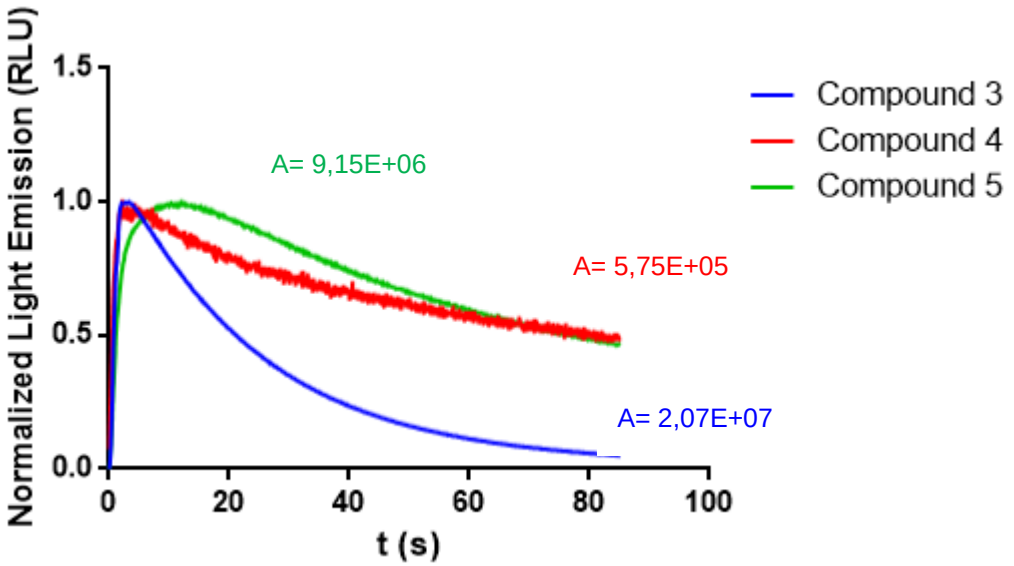


Figure 23- CL profile (light emission as a function of time) for Compounds 3, 4 and 5 and respective area of chemiluminescence profile.

In all compounds, the reaction starts on an initial burst of light, which is responsible for most of emitted light. After the initial maximum, there is a decay toward lower values. However, only the CL of Compound 3 reaches basal levels in the recorded period, while the decay for the other Compounds is less steep. Also, the area of CL profile is higher in Compounds 3 and 5 than in Compound 4. This means that the CL reaction in the latter compound are significantly less efficient (lower value of ΦCL). It should be noted that CL emission results from the radiative decay from the chemiexcited S_1 state to the S_0 state. Thus, we can say that the higher the CL emission the higher the number of molecules chemiexcited to their S1 state. As the use of these derivatives as PS would entail the chemiexcitation of molecules to their T_1 state (instead of their S_1 state), one would expect the Compounds with lower CL (lower S_1 molecules) to be the ones with higher probability to behave better as PS. Namely, Compounds 4 and 5 appear to have a higher potential for acting as PSs than Compounds 3.

The fluorescence spectrum (Figure 24) has a similar maximum in Compounds 4 and 5 (~440 nm) and in Compound 3 the maximum is ~430. Besides, we have obtained the CL spectra for Compounds 3 and 5 (Figure 25). As seen in Figure 25, the spectra are similar, with emission maximum at ~475 nm.

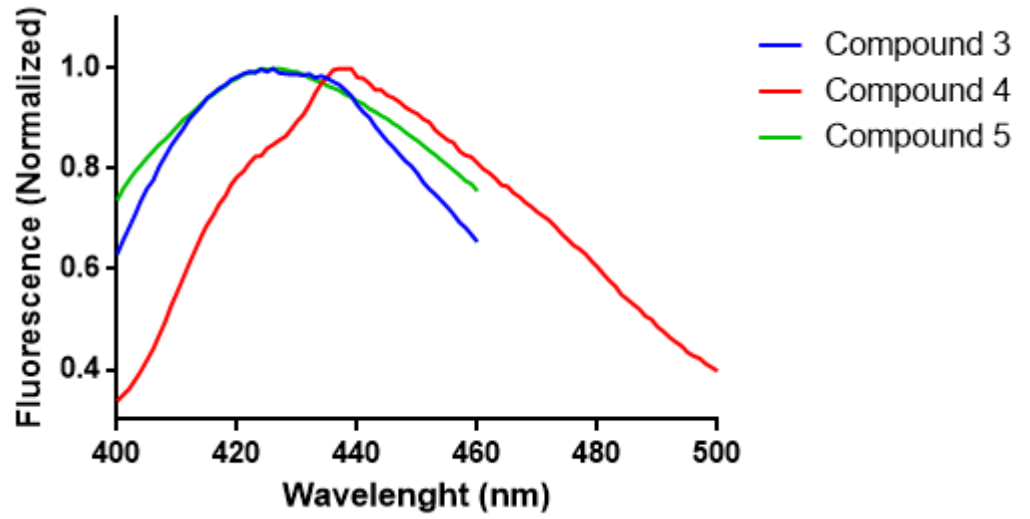


Figure 24- Fluorescence spectra (normalized) for light emitter species of the Compounds 3, 4 and 4.

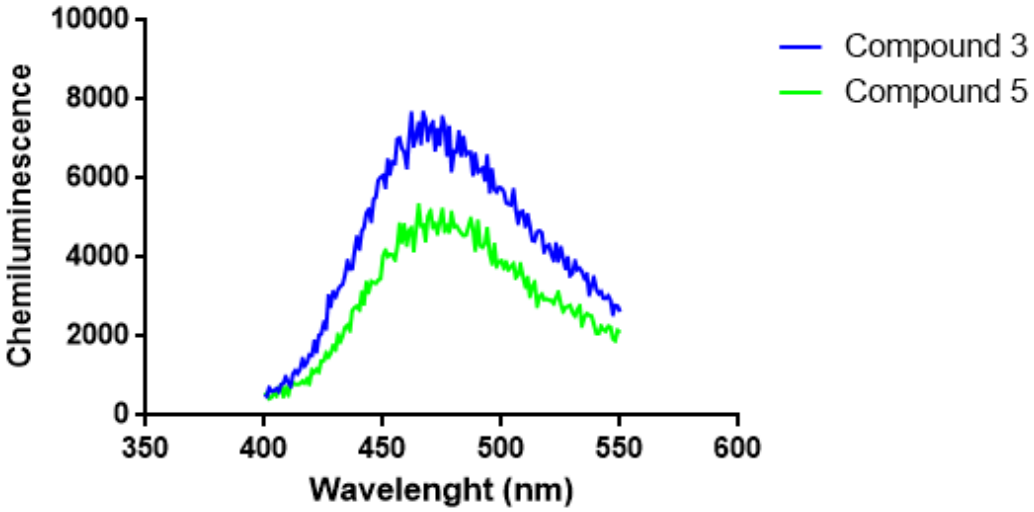


Figure 25- CL spectra of the light-emitting reaction of Compounds 3 and 5.

5.3.2. Fluorescent assay for detection of singlet oxygen

The ability to produce ROS (namely, singlet oxygen) was monitored by observing the fluorescence quenching of ABDA in the presence of the difference Compounds. ABDA is a known fluorescence probe for singlet oxygen. [106–109]. ABDA (50 µM) was added to a solution of DMSO at neutral pH, with addiction of phosphate buffer pH 7,4 (0,075M), to which were added increasing concentrations of the Compounds (5, 10, 20 and 50 µM). The results can be found in Figure 26.

.

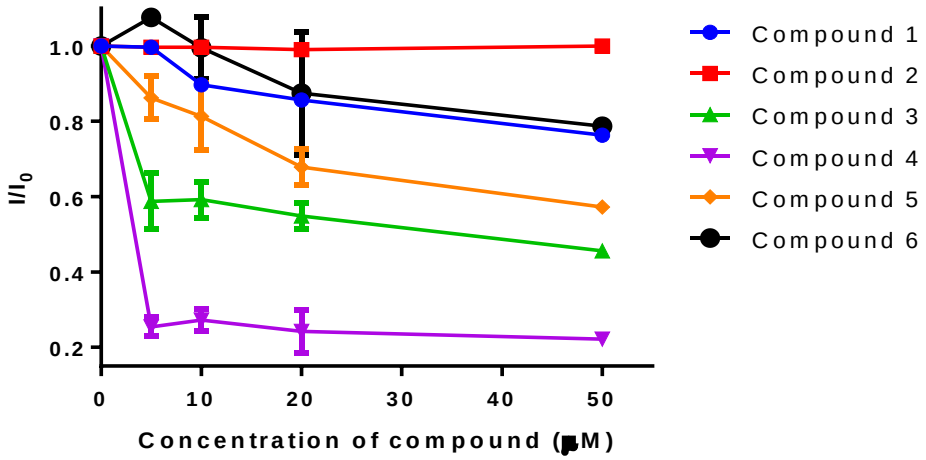


Figure 26- Analysis of the fluorescence of an oxygen singlet probe (ABDA), with increasing concentrations of the studied compounds. Values were obtained at neutral (phosphate buffer pH 7.4).

By analyzing the results, we can see that, with exception of compound 2, all compounds are able to produce singlet oxygen, as quenching of the fluorescence produced by ABDA is detected. The effect is more pronounced at higher concentration of the compounds (50 µM). At this concentration, the quenching observed was of 24% for Compound 1, 0% for Compound 2, 49% for Compound 3, 78% for Compound 4, 43% for Compound 5, and 21% for Compound 6. These results allow us to conclude that the synthesized compounds (except Compound 2) can produce singlet oxygen.

Two things should be noticed. First is that the highest ABDA quenching for Compound 5 is in line with its lower CL area. This indicates that the attempt of exchanging chemiexcited S_1 states for T_1 ones. The second thing is that Compound 3 were able to induce a significant ABDA quenching, while still present a relevant CL area. Thus, it can be concluded that the chemiexcitation yield of Compound 3 should be quite high, as it produced enough S_1 and T_1 states to generate both light and singlet oxygen in relevant amounts.

5.3.3. *In vitro* toxicity assays

Having accessed the ability of compounds to produce singlet oxygen, we have studied the effect of compounds 1-5 on cell viability. This was made by increasing the concentrations of the synthetized compounds (1, 10, 20, 50 and 100 µM), in two time periods: 24h and 48. Percent viability was obtained by comparing with control cell viability, considered as 100%. Data represented in Figure 27, characterize the mean ±

SD of measurements of three independent experiments, as the result of one-way ANOVA factorial analysis.

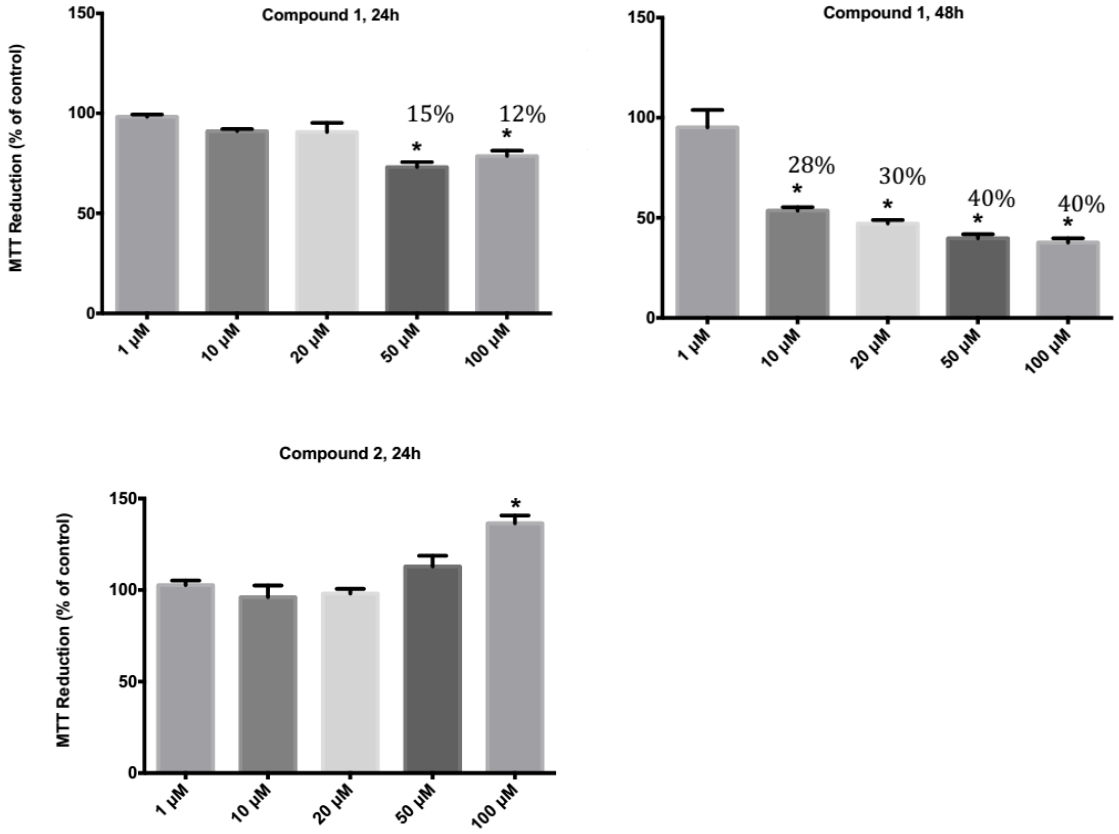


Figure 27- Percent viability measured by MTT reduction assays for Compounds 1 (24 and 48h) and 2 (24H), at increasing concentrations. The percentage values above some bars refer to toxicity measured with the LDH assay, when statistically significative. Percent viability was obtained by comparing with control cell viability, considered as 100%. Data represents the mean ± SD of measurements of three independent experiments. Results of the one-way ANOVA factorial analysis.

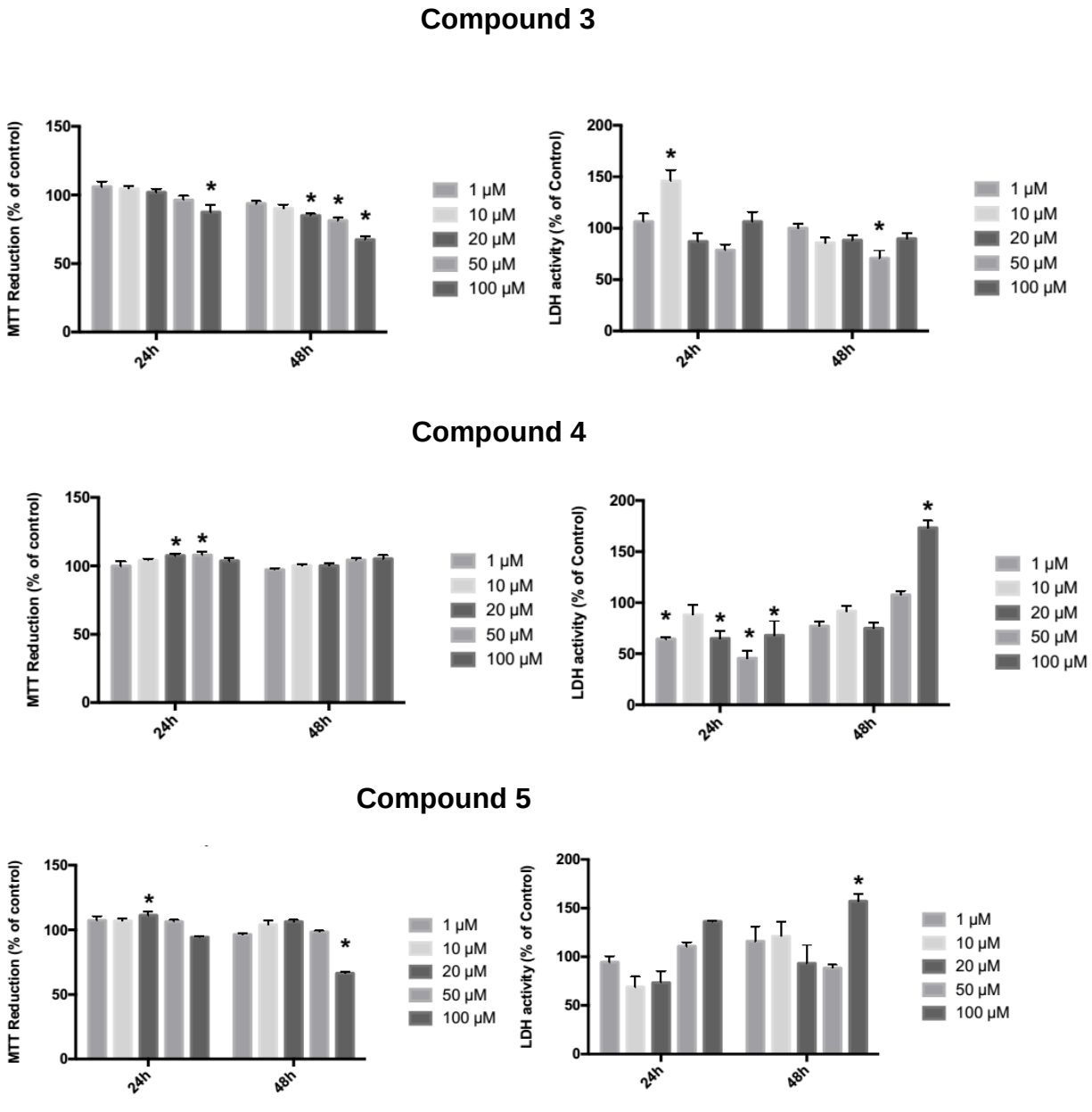


Figure 28- Percent of cytotoxicity measured by MTT assay (bars) and percentage of total LDH of compounds 3-5 (24 and 48h), at increasing concentrations of both compounds. Percent viability was obtained by comparing with control cell viability, considered as 100%. Data represent the mean ± SD of measurements of three independent experiments. Results of the one-way ANOVA factorial analysis.

The data shown in Figure 27 reveal no toxicity of Compound 1 at 24h exposure for the concentrations 1, 10 and 20µM, while the concentrations 50 and 100µM showed a small degree (15% and 12%, respectively) of toxicity. However, at 48h exposure, Compound 1 causes a significant degree of toxicity: between 28% to 40% in the LDH assay. To the contrary, Compound 2 did not present any toxicity at 24h. These results

support the use of singlet oxygen-producing CL Coelenterazines as PS. Namely, while Compound 1 was able to produce singlet oxygen and cytotoxicity, Compound 2 was able of neither. This support the assumption that cytotoxicity generated by Compound 1 can indeed be attributed to the production of singlet oxygen.

Analysis of Compounds 3-5 (Figure 28) also showed evidence for cytotoxicity, but only at higher concentrations and higher time of exposure. For instance, Compound 3 induced at concentration 20-100 μM a reduced MTT reduction ability. Nevertheless, the LDH assay did not show evidence for cytotoxicity. Similar results were obtained for Compound 5, which induced a reduced MTT reduction ability when present in a concentration of 100 μM. Interestingly, in this case the results obtained in the MTT assay are associated with a toxicity of 57%, which was obtained by measuring the LDH activity. The most unexpected result was that of compound 4. While it induced by far the highest degree of ABDA quenching (indicative of the production of singlet oxygen), it did not induce any cytotoxicity. In fact, the LDH assay at 24h indicates that this molecule can even be cytoprotective. The exception to this is the LDH assay at 48h with a concentration of 100 μM. However, this result is somewhat strange, given the cytoprotective nature at 24h and the absence of deleterious effects recorded in the MTT assay. Thus, further experiments should be made before stating that Compound 4 is cytotoxic at 48h with a concentration of 100 μM.

In conclusion, the present in vitro assays showed that some of the synthesized Compounds are capable of cytotoxicity toward tumor cells in the absence of light. However, the results are not fully in line with the production of singlet oxygen as recorded in the laboratory with the use of the fluorescent probe ABDA. More specifically, Compound 4 present the higher generation of singlet oxygen but appears cytoprotective. Also, while Compound 5 presented higher values of toxicity (57%) when compared with Compound 1 (40%), which is in line with their ability to produce singlet oxygen, the cytotoxicity of Compound 5 was only seen at the higher time and concentration. For the contrary, Compound 1 induced cytotoxicity at both 24h and 48h and in a wide range of concentrations. Thus, it is possible that the delivery, internalization and/or metabolism of the cell is affecting the production of singlet oxygen by these compounds, and so, the toxicity generated by each compound.

5.4. Conclusions

Novel Coelenterazine derivatives were synthesized and characterized for CL and ability to produce ROS in the absence of light. Five of six synthesized compounds were able to produce singlet oxygen in the absence of light. Thus, supporting the development

of self-activating PS based on Coelenterazine. Further proof-of-concept was provided by *in vitro* toxicity assays, which demonstrated that some of the new PSs were able to induce relevant cytotoxicity toward tumor cells.

Taking this into account, we were able to develop novel photosensitizers that can be self-excited via a CL reaction, without the need for either photoexcitation or energy transfer steps.

6. Conclusions and future work

Various conclusions can be obtained from this Master thesis, which its author thinks that can be used for improving the properties of CL and BL systems, with specially emphasis for those based on imidazopyrazinones. More importantly, this work demonstrated the use of Coelenterazine as the basis for new self-activated PSs for use in PDT, towards the treatment of tumors irrespective of their size and localization in the body.

6.1. Conclusions from the study of the chemiexcitation of Coelenterazine and Cypridina luciferin

The first conclusion is that the CL of both Coelenterazine and *Cypridina* luciferin is pH-dependent: the reaction rate increases with increasing pH, while the total light output has an opposite behavior. Further studies attributed these differences to changes of the neutral-anionic equilibria of the dioxetanone intermediate. More specifically, neutral dioxetanone undergoes thermolysis with a higher activation energy than the anion. However, the thermolysis of the neutral species provides a pathway for a more efficient chemiexcitation, which explains why the total light output decreases with increasing pH.

It was also found that this higher chemiexcitation efficiency results from neutral dioxetanone having access (during its thermolysis) to a region of the PES where S_0 and S_1 are degenerated. To the contrary, anionic dioxetanone does not have access to this region. The access to this region was explained by attractive electrostatic interactions between the CO_2 and oxyluciferin moieties, which allow for the reacting molecules to spend time in the region of degeneracy. On the contrary, repulsive electrostatic interactions between the moieties of anionic dioxetanones lead to a quicker CO_2 detachment and prevent access to the region of degeneracy.

6.2. Conclusions from the comparison of the chemiluminescence of Coelenterazine, Coelenterazine-e and Cypridina luciferin

The present work demonstrated that DMSO and DMF are the only solvents that allow for significant CL at acidic pH, while other solvents allow only for negligible light emission. Further analysis attributed this to the inability of most solvents to induce deprotonation of the imidazopyrazinone core, which prevents the oxygenation step of the CL reaction.

Finally, it was also observed that at the same pH, the chemiexcitation efficiency decreases with increasing polarity of the solvent. Based on theoretical calculations, this

was explained by reduced changes in charge density upon $S_0 \rightarrow S_1$ chemiexcitation by requiring only a small reorganization energy for solvation upon transition between states.

6.3. Conclusions from the characterization of the chemiexcitation mechanism for model dioxetanones

By performing detailed computational calculations, it was possible to develop a new mechanism for the efficient chemiexcitation of dioxetanones, which is an alternative to known theories such as CIEEL and CTIL. Namely, this new mechanism is not based on ET and/or CT steps and subsequent charge annihilation. Instead, the proposed mechanism is based on the degree of interaction between the keto and CO_2 moieties of dioxetanone. If favorable, the detachment of CO_2 to produce the light emitter is delayed, and the reacting molecules have access to a zone of S_0-S_1 degeneracy within the biradical region of the PES, which favors chemiexcitation. If the interaction is repulsive, the detachment of CO_2 is too quick for the reacting molecules to have access to the zone of degeneracy, which decreases the efficiency of chemiexcitation.

6.4. Conclusions from the synthesis of self-illuminating photosensitizers

We have developed for the first new photosensitizers for PDT that are both: capable of self-activation in the absence of light due to a CL reaction; capable of the production of ROS by itself, without the need for energy transfer steps between a luminophore and a photosensitizer. Proof-of concept was provided initially by measuring the production of singlet oxygen with a spectroscopic approach involving a fluorescent probe. Further confirmation was obtained by performing *in vitro* toxicity assays.

In conclusion we were able to develop novel photosensitizers that can be self-activated, without the need for either photoexcitation or energy transfer steps. This opens the door for using PDT for treating tumors irrespective of their size and localization in the body.

6.5. Future work

While the present work has reasonably characterized the chemiexcitation mechanism of imidazopyrazinone-based molecules, further work should be made to ensure that the mechanism proposed here can be applied to other systems in which dioxetanones are present (such as the known system of the fireflies). The same can be said for CL reactions involving other types of cyclic peroxides, such as dioxetanes and dioxetanedione.

Nevertheless, most of the possible future work is related to the development of Coelenterazine-based photosensitizers for PDT. While the present work provided proof-

of-concept for self-activating photosensitizers, the characterization of these molecules is still not completed. For example, it is still necessary to determine the yield of the CL reaction, and to identify all reaction intermediates and products. It also remains to study in more detail the interaction of the new Coelenterazine derivatives with superoxide anion. Finally, extensive work remains to assess the delivery and internalization pathways for these compounds, and to obtain more information regarding their cellular metabolism. Determination of their potential toxicity toward other *in vitro* cell lines, and well as *in vivo*, is also essential.

7. References

[1] Laptev, R., Nisnevitch, M., Siboni, G., Malik, Z., and Firer, M.A. (2006) Intracellular chemiluminescence activates targeted photodynamic destruction of leukaemic cells. *British Journal of Cancer*. 95 (2), 189–196.

[2] Mroz, P., Yaroslavsky, A., Kharkwal, G.B., and Hamblin, M.R. (2011) Cell death pathways in photodynamic therapy of cancer. *Cancers*. 3 (2), 2516–2539.

[3] Josefsen, L.B. and Boyle, R.W. (2008) Photodynamic therapy and the development of metal-based photosensitisers. *Metal-Based Drugs*. 2008.

[4] Lovell, J.F., Liu, T.W.B., Chen, J., and Zheng, G. (2010) Activable photosensitizers for imaging and therapy. *Chemical Reviews*. 110 (5), 2839–2857.

[5] Bancirova, M. and Lasovský, J. (2011) The photodynamic effect: The comparison of chemiexcitation by luminol and phthalhydrazide. *Luminescence*. 26 (6), 410–415.

[6] Theodossiou, T., Hothersall, J.S., Woods, E. a, Chemiluminescence, I., Cells, N.I.H., Okkenhaug, K., et al. (2003) Firefly Luciferin-activated Rose Bengal : Firefly Luciferin-activated Rose Bengal : In Vitro Photodynamic Therapy by. *Cancer Research*. 63 (8), 1818–1821.

[7] Da Silva, L.P. and Esteves Da Silva, J.C.G. (2011) Computational studies of the luciferase light-emitting product: Oxyluciferin. *Journal of Chemical Theory and Computation*. 7 (4), 809–817.

[8] Navizet, I., Liu, Y.J., Ferré, N., Roca-Sanjuán, D., and Lindh, R. (2011) The chemistry of bioluminescence: An analysis of chemical functionalities. *ChemPhysChem*. 12 (17), 3065–3076.

[9] Pinto, L. and Esteves, J.C.G. (2012) Firefly Chemiluminescence and Bioluminescence : Efficient Generation of Excited States. 1–7.

[10] Kitada, N., Saitoh, T., Ikeda, Y., Iwano, S., Obata, R., Niwa, H., et al. (2018) Toward bioluminescence in the near-infrared region: Tuning the emission wavelength of firefly luciferin analogues by allyl substitution. *Tetrahedron Letters*.

[11] Pinto Da Silva, L., Simkovitch, R., Huppert, D., and Esteves Da Silva, J.C.G. (2013) Theoretical photodynamic study of the photoprotolytic cycle of firefly oxyluciferin. *ChemPhysChem*. 14 (12), 2711–2716.

[12] Pinto Da Silva, L. and Esteves Da Silva, J.C.G. (2015) Chemiexcitation induced proton transfer: Enolate oxyluciferin as the firefly bioluminophore. *Journal of Physical Chemistry B*. 119 (6), 2140–2184.

[13] Ishii, Y., Hayashi, C., Suzuki, Y., and Hirano, T. (2014) Chemiluminescent 2,6-diphenylimidazo[1,2-a]pyrazin-3(7H)-ones: a new entry to Cypridina luciferin

analogues. *Photochem. Photobiol. Sci.* 13 (2), 182–189.

[14] Tomabechi, Y., Hosoya, T., Ehara, H., Sekine, S.I., Shirouzu, M., and Inouye, S. (2016) Crystal structure of nanoKAZ: The mutated 19 kDa component of Oplophorus luciferase catalyzing the bioluminescent reaction with coelenterazine. *Biochemical and Biophysical Research Communications*. 470 (1), 88–93.

[15] Wu, J.Y., Chen, Y.P., and Su, C.S. (2015) Density and viscosity of ionic liquid binary mixtures of 1-n-butyl-3-methylimidazolium tetrafluoroborate with acetonitrile, N,N-dimethylacetamide, methanol, and N-methyl-2-pyrrolidone. *Journal of Solution Chemistry*. 44 (3–4), 395–412.

[16] Roda, A. and Guardigli, M. (2012) Analytical chemiluminescence and bioluminescence: Latest achievements and new horizons. *Analytical and Bioanalytical Chemistry*. 402 (1), 69–76.

[17] Vasquez, E.S., Feugang, J.M., Willard, S.T., Ryan, P.L., and Walters, K.B. (2016) Bioluminescent magnetic nanoparticles as potential imaging agents for mammalian spermatozoa. *Journal of Nanobiotechnology*. 14 (1), 1–9.

[18] Bronsart, L.L., Stokes, C., and Contag, C.H. (2015) Multimodality Imaging of Cancer Superoxide Anion Using the Small Molecule Coelenterazine.

[19] Kaskova, Z.M., Tsarkova, A.S., and Yampolsky, I. V (2016) Chem Soc Rev chemical analysis , biology and medicine. *Chemical Society Reviews*. 45 6048–6077.

[20] Shimomura, O. and Johnson, F.H. (1970) Mechanisms in the Quantum Yield of Cypridina Bioluminescence. *Photochemistry and Photobiology*. 12 (4), 291–295.

[21] da Silva, L.P. and Esteves da Silva, J.C.G. (2011) Kinetics of inhibition of firefly luciferase by dehydroluciferyl-coenzyme A, dehydroluciferin and l-luciferin. *Photochemical & Photobiological Sciences*. 10 (6), 1039.

[22] Kaskova, Z.M., Tsarkova, A.S., and Yampolsky, I. V. (2016) 1001 Lights: Luciferins, Luciferases, Their Mechanisms of Action and Applications in Chemical Analysis, Biology and Medicine. *Chem. Soc. Rev.* 45 (21), 6048–6077.

[23] Luker, K.E. and Luker, G.D. (2010) Bioluminescence imaging of reporter mice for studies of infection and inflammation. *Antiviral Research*. 86 (1), 93–100.

[24] Mccapra, F. (1990) AND. 51 21–28.

[25] Ku, H.C. and Tu, C.H. (1998) Density and viscosity of binary mixtures of propan-2-ol, 1-chlorobutane, and acetonitrile. *Journal of Chemical and Engineering Data*. 43 (3), 465–468.

[26] Augusto, F.A., De Souza, G.A., De Souza, S.P., Khalid, M., and Baader, W.J. (2013) Efficiency of electron transfer initiated chemiluminescence. *Photochemistry and Photobiology*. 89 (6), 1299–1317.

[27] Augusto, F.A., Antonio Francé s-Monerris, ab, Ignacio Fdez Galvá, bc, Roca-Sanjuá, D., Bastos, E.L., Baader, W.J., et al. (2017) Mechanism of activated chemiluminescence of cyclic peroxides: 1,2-dioxetanes and 1,2-dioxetanones. *Phys. Chem. Chem. Phys. Phys. Chem. Chem. Phys*. 19 (19), 3955–3962.

[28] Koo, J. young and Schuster, G.B. (1978) Chemiluminescence of Diphenoyl Peroxide. Chemically Initiated Electron Exchange Luminescence. A New General Mechanism for Chemical Production of Electronically Excited States. *Journal of the American Chemical Society*. 100 (14), 4496–4503.

[29] Koo, J. young and Schuster, G.B. (1977) Chemically Initiated Electron Exchange Luminescence. A New Chemiluminescent Reaction Path for Organic Peroxides. *Journal of the American Chemical Society*. 99 (18), 6107–6109.

[30] Catalani, L.H. and Wilson, T. (1989) Electron Transfer and Chemiluminescence. Two Inefficient Systems: 1,4-Dimethoxy-9,10-diphenylanthracene Peroxide and Diphenoyl Peroxide. *Journal of the American Chemical Society*. 111 (7), 2633–2639.

[31] Fernando, H., Oliveira, D., Marcelo, A., Felipe, A., L, L.F.M., Erick, L., et al. (2012) Singlet Quantum Yields in the Catalyzed Decomposition of 1 , 2-Dioxetanones. 2 2012.

[32] Yue, L., Liu, Y., and Fang, W. (2012) Mechanistic Insight into the Chemiluminescent Decomposition of Fire fl y Dioxetanone.

[33] Isobe, H., Takano, Y., Okumura, M., Kuramitsu, S., and Yamaguchi, K. (2005) Mechanistic insights in charge-transfer-induced luminescence of 1,2-dioxetanones with a substituent of low oxidation potential. *Journal of the American Chemical Society*. 127 (24), 8667–8679.

[34] Da Silva, L.P. and Da Silva, J.C.G.E. (2013) Interstate crossing-induced chemiexcitation as the reason for the chemiluminescence of dioxetanones. *ChemPhysChem*. 14 (5), 1071–1079.

[35] Pinto da Silva, L., Magalhaes, C.M., and Esteves da Silva, J.C.G. (2016) Interstate Crossing-Induced Chemiexcitation Mechanism as the Basis for Imidazopyrazinone Bioluminescence. *ChemistrySelect*. 1 (12), 3343–3356.

[36] Ding, B.W., Naumov, P., and Liu, Y.J. (2015) Mechanistic insight into marine bioluminescence: Photochemistry of the chemiexcited cypridina (sea firefly) lumophore. *Journal of Chemical Theory and Computation*. 11 (2), 591–599.

[37] Merenyi, G., Lind, J., and Eriksen, T.E. (1990) Lu m i no1 C h e m il u m inescence : Chemistry , Excitation , Emitter. 5 53–56.

[38] Gaikwad, A., Silva, M., and Pérez-Bendito, D. (1995) Selective stopped-flow determination of manganese with luminol in the absence of hydrogen peroxide.

Analytica Chimica Acta. 302 (2–3), 275–282.

[39] Rose, A.L. and Waite, T.D. (2001) Chemiluminescence of luminol in the presence of iron(II) and oxygen: Oxidation mechanism and implications for its analytical use. *Analytical Chemistry*. 73 (24), 5909–5920.

[40] Magalhães, C.M., Esteves, C.G., and Pinto, L. (2016) Chemiluminescence and Bioluminescence as an Excitation Source in the Photodynamic Therapy of Cancer : A Critical Review. 2286–2294.

[41] Pinto Da Silva, L. and Esteves Da Silva, J.C.G. (2012) TD-DFT/molecular mechanics study of the photinus pyralis bioluminescence system. *Journal of Physical Chemistry B*. 116 (6), 2008–2013.

[42] Pinto Da Silva, L. and Esteves Da Silva, J.C.G. (2014) Quantum/molecular mechanics study of firefly bioluminescence on luciferase oxidative conformation. *Chemical Physics Letters*. 608 45–49.

[43] Leitão, J.M.M. and Esteves da Silva, J.C.G. (2010) Firefly luciferase inhibition. *Journal of Photochemistry and Photobiology B: Biology*. 101 (1), 1–8.

[44] Ribeiro, C. and Esteves da Silva, J.C.G. (2008) Kinetics of inhibition of firefly luciferase by oxyluciferin and dehydroluciferyl-adenylate. *Photochemical & Photobiological Sciences*. 7 (9), 1085.

[45] Min, C.G., Pinto da Silva, L., Esteves da Silva, J.C.G., Yang, X.K., Huang, S.J., Ren, A.M., Zhu, Y.Q. (2017) Computational Investigation of the Fluorescent and Chemiluminescent States Equilibrium Constants for Coelenteramide. *ChemPhysChem*. 18 1–29.

[46] Takahashi, H., Nishina, A., Fukumoto, R.H., Kimura, H., Koketsu, M., and Ishihara, H. (2005) Selenocarbamates are effective superoxide anion scavengers in vitro. *European Journal of Pharmaceutical Sciences*. 24 (4), 291–295.

[47] Teranishi, K. (2007) Luminescence of. 35 82–111.

[48] Schipper, M.L., Patel, M.R., and Gambhir, S.S. (2006) Evaluation of firefly luciferase bioluminescence mediated photodynamic toxicity in cancer cells. *Molecular Imaging and Biology*. 8 (4), 218–225.

[49] Hsu, C.Y., Chen, C.W., Yu, H.P., Lin, Y.F., and Lai, P.S. (2013) Bioluminescence resonance energy transfer using luciferase-immobilized quantum dots for self-illuminated photodynamic therapy. *Biomaterials*. 34 (4), 1204–1212.

[50] Kim YR, Kim S, Choi JW, Choi SY, Lee SH, Kim H, Hahn SK, Koh GY, Y.S. (2015) Bioluminescence-Activated Deep-Tissue Photodynamic Therapy of Cancer. *Theranostics*. 8 (5), 805–817.

[51] Yuan, H., Chong, H., Wang, B., Zhu, C., Liu, L., Yang, Q., et al. (2012) System for Anticancer and Antifungal Activities Chemical Molecule-Induced Light-

Activated System for Anti- cancer and Antifungal Activities. 8–11.

[52] Zhang, Y., Pang, L., Ma, C., Tu, Q., Zhang, R., Saeed, E., et al. (2014) Small molecule-initiated light-activated semiconducting polymer dots: An integrated nanoplatform for targeted photodynamic therapy and imaging of cancer cells. *Analytical Chemistry*. 86 (6), 3092–3099.

[53] Fan, W., Huang, P., and Chen, X. (2016) Overcoming the Achilles' heel of photodynamic therapy. *Chem. Soc. Rev.* 45 (23), 6488–6519.

[54] Cui, S., Yin, D., Chen, Y., Di, Y., Chen, H., Ma, Y., et al. (2013) In Vivo Targeted Deep- Tissue Photodynamic Therapy Based on Near- Infrared Light Triggered Upconversion Nanoconstruct--Supporting Information. *ACS Nano*. 7 (1), 676–688.

[55] Liu, J., Liu, K., Feng, L., Liu, Z., and Xu, L. (2016) Biomaterials Science chemotherapy , photodynamic therapy and oxide for the model system †. 15–17.

[56] Wang, C., Tao, H., Cheng, L., and Liu, Z. (2011) Near-infrared light induced in vivo photodynamic therapy of cancer based on upconversion nanoparticles. *Biomaterials*. 32 (26), 6145–6154.

[57] Xing, H., Zheng, X., Ren, Q., Bu, W., Ge, W., Xiao, Q., et al. (2013) Computed tomography imaging-guided radiotherapy by targeting upconversion nanocubes with significant imaging and radiosensitization enhancements. *Scientific Reports*. 3 9–11.

[58] Chen, H., Wang, G.D., Chuang, Y.J., Zhen, Z., Chen, X., Biddinger, P., et al. (2015) Nanoscintillator-Mediated X-ray Inducible Photodynamic Therapy for in Vivo Cancer Treatment. *Nano Letters*. 15 (4), 2249–2256.

[59] Kervinen, M., Jukka, P., Finel, M., and Hassinen, I.E. (2004) Lucigenin and coelenterazine as superoxide probes in mitochondrial and bacterial membranes. 324 45–51.

[60] Figueira, T.R., Barros, M.H., Camargo, A.A., Castilho, R.F., Ferreira, J.C.B., Kowaltowski, A.J., et al. (2013) Mitochondria as a Source of Reactive Oxygen and Nitrogen Species: From Molecular Mechanisms to Human Health. *Antioxidants & Redox Signaling*. 18 (16), 2029–2074.

[61] Pelicano, H., Carney, D., and Huang, P. (2004) ROS stress in cancer cells and therapeutic implications. *Drug Resistance Updates*. 7 (2), 97–110.

[62] Chai, J. and Head-gordon, M. (2008) Long-range corrected hybrid density functionals with damped atom – atom dispersion corrections w. 6615–6620.

[63] Ding, B.W. and Liu, Y.J. (2017) Bioluminescence of firefly squid via mechanism of single electron-transfer oxygenation and charge-transfer-induced luminescence. *Journal of the American Chemical Society*. 139 (3), 1106–1119.

[64] Pinto Da Silva, L., Pereira, R.F.J., Magalhães, C.M., and Esteves Da Silva, J.C.G. (2017) Mechanistic Insight into Cypridina Bioluminescence with a Combined Experimental and Theoretical Chemiluminescent Approach. *Journal of Physical Chemistry B*. 121 (33), 7862–7871.

[65] Pinto da Silva, L., Magalhães, C.M., Crista, D.M.A., and Esteves da Silva, J.C.G. (2017) Theoretical modulation of singlet/triplet chemiexcitation of chemiluminescent imidazopyrazinone dioxetanone via C_8 -substitution. *Photochemical & Photobiological Sciences*. 16 (6), 897–907.

[66] Scalmani, G. and Frisch, M.J. (2010) Continuous surface charge polarizable continuum models of solvation. I. General formalism. *Journal of Chemical Physics*. 132 (11),.

[67] Hirano, T. (2008) Firefly luminescence: A historical perspective and recent developments. *Photochemical & Photobiological Sciences*. 7 (2), 146.

[68] Takahashi, Y., Kondo, H., Maki, S., Niwa, H., Ikeda, H., and Hirano, T. (2006) Chemiluminescence of 6-aryl-2-methylimidazo[1,2-a]pyrazin-3(7H)-ones in DMSO/TMG and in diglyme/acetate buffer: support for the chemiexcitation process to generate the singlet-excited state of neutral oxyluciferin in a high quantum yield in the Cypridina . *Tetrahedron Letters*. 47 (34), 6057–6061.

[69] Goto, T. and Fukatsu, H. (1969) Cypridina bioluminescence VII. chemiluminescence in micelle solutions - a model system for cypridina bioluminescence. *Tetrahedron Letters*. 10 (49), 4299–4302.

[70] Usami, K. and Isobe, M. (1996) Low-temperature Photooxygenation of Coelenterate Luciferin Analog Synthesis and Proof of 1,2-Dioxetanone as Luminescence Intermediate. 52 (37), 12061–12090.

[71] Kondo, H., Igarashi, T., Maki, S., Niwa, H., Ikeda, H., and Hirano, T. (2005) Substituent effects on the kinetics for the chemiluminescence reaction of 6-arylimidazo[1,2-a]pyrazin-3(7H)-ones (Cypridina luciferin analogues): Support for the single electron transfer (SET)-oxygenation mechanism with triplet molecular oxygen. *Tetrahedron Letters*. 46 (45), 7701–7704.

[72] Chen, S.F., Navizet, I., Roca-Sanjuán, D., Lindh, R., Liu, Y.J., and Ferré, N. (2012) Chemiluminescence of coelenterazine and fluorescence of coelenteramide: A systematic theoretical study. *Journal of Chemical Theory and Computation*. 8 (8), 2796–2807.

[73] Roca-Sanjuán, D., Delcey, M.G., Navizet, I., Ferré, N., Liu, Y.J., and Lindh, R. (2011) Chemiluminescence and fluorescence states of a small model for coelenteramide and Cypridina oxyluciferin: A CASSCF/CASPT2 study. *Journal of Chemical Theory and Computation*. 7 (12), 4060–4069.

[74] Guido, C.A., Jacquemin, D., Adamo, C., and Mennucci, B. (2015) Electronic Excitations in Solution: The Interplay between State Specific Approaches and a Time-Dependent Density Functional Theory Description. *Journal of Chemical Theory and Computation*. 11 (12), 5782–5790.

[75] Naumov, P., Wu, C., Liu, Y.-J., and Ohmiya, Y. (2012) Spectrochemistry and artificial color modulation of Cypridina luminescence: indirect evidence for chemiexcitation of a neutral dioxetanone and emission from a neutral amide. *Photochemical & Photobiological Sciences*. 11 (7), 1151.

[76] Nery, A.L.P., Röpke, S., Catalani, L.H., and Baader, W.J. (1999) Fluoride-triggered decomposition of m-sililoxyphenyl-substituted dioxetanes by an intramolecular electron transfer (CIEEL) mechanism. *Tetrahedron Letters*. 40 (13), 2443–2446.

[77] Matsumoto, M., Ito, Y., Murakami, M., and Watanabe, N. (2002) Synthesis of 5-tert-butyl-1-(3-tert-butyldimethylsiloxy)phenyl-4,4-dimethyl-2,6,7-trioxabicyclo[3.2.0]heptanes and their fluoride-induced chemiluminescent decomposition: Effect of a phenolic electron donor on the CIEEL decay rate in aprotic polar solvent. *Luminescence*. 17 (5), 305–312.

[78] Tanimura, M., Watanabe, N., Ijuin, H.K., and Matsumoto, M. (2011) Intramolecular Charge-Transfer-Induced Decomposition Promoted by an Aprotic Polar Solvent for Bicyclic Dioxetanes Bearing a 4-(Benzothiazol-2-yl)-3-hydroxyphenyl Moiety. *Journal of Organic Chemistry*. 76 (3), 902–908.

[79] Liu, F., Liu, Y., De Vico, L., and Lindh, R. (2009) Theoretical study of the chemiluminescent decomposition of dioxetanone. *Journal of the American Chemical Society*. 131 (17), 6181–6188.

[80] Farahani, P., Lundberg, M., Lindh, R., and Roca-Sanjuán, D. (2015) Theoretical study of the dark photochemistry of 1,3-butadiene via the chemiexcitation of Dewar dioxetane. *Phys. Chem. Chem. Phys.* 17 (28), 18653–18664.

[81] Pinto, L., Pereira, R.F.J., Magalhães, C.M., and Esteves, J.C.G. (n.d.) Mechanistic Insight into Cypridina Bioluminescence with a Com- bined Experimental and Theoretical Chemiluminescent Approach. 15–19.

[82] Wu, C., Nakamura, H., Murai, A., and Shimomura, O. (2001) Chemi- and bioluminescence of coelenterazine analogues with a conjugated group at the C-8 position. 42 2997–3000.

[83] Saito, R., Hirano, T., Maki, S., and Niwa, H. (2014) Synthesis and chemiluminescent properties of 6,8-diaryl-2-methylimidazo[1, 2-a]pyrazin-3(7H)-ones: Systematic investigation of substituent effect at para-position of phenyl group at 8-position. *Journal of Photochemistry and Photobiology A: Chemistry*.

293 12–25.

[84] Lourenço, J.M., Esteves, J.C.G., and Pinto, L. (2018) Combined experimental and theoretical study of Coelenterazine chemiluminescence in aqueous solution. *Journal of Luminescence*. 194 (October 2017), 139–145.

[85] Toya, Y.; Nakatsuka, S.; Goto, T. (1985) Structure of Cypridina Biluciferyl, a Dimer of Cypridina Luciferyl Radical Having Bioluminescent Activity. *Tetrahedron Lett*. 26 (2), 239–242.

[86] Eremeeva, E. V., Markova, S. V., Westphal, A.H., Visser, A.J.W.G., Berkel, W.J.H. va., and Vysotski, E.S. (2009) The intrinsic fluorescence of apo-obelin and apo-aequorin and use of its quenching to characterize coelenterazine binding. *FEBS Letters*. 583 (12), 1939–1944.

[87] Shimomura, O. and Teranishi, K. (2000) Light-emitters involved in the luminescence of coelenterazine. *Luminescence : The Journal of Biological and Chemical Luminescence*. 15 (1), 51–8.

[88] Crozier, A., Lean, M.E.J., McDonald, M.S., and Black, C. (1997) Quantitative Analysis of the Flavonoid Content of Commercial Tomatoes, Onions, Lettuce, and Celery. *Journal of Agricultural and Food Chemistry*. 45 (3), 590–595.

[89] Zhao, Y. and Truhlar, D.G. (2008) The M06 suite of density functionals for main group thermochemistry, thermochemical kinetics, noncovalent interactions, excited states, and transition elements: Two new functionals and systematic testing of four M06-class functionals and 12 other function. *Theoretical Chemistry Accounts*. 120 (1–3), 215–241.

[90] Marenich, A. V., Cramer, C.J., and Truhlar, D.G. (2009) Universal solvation model based on solute electron density and on a continuum model of the solvent defined by the bulk dielectric constant and atomic surface tensions. *Journal of Physical Chemistry B*. 113 (18), 6378–6396.

[91] Lu, T. and Chen, F. (2012) Multiwfn: A multifunctional wavefunction analyzer. *Journal of Computational Chemistry*. 33 (5), 580–592.

[92] Magalhães, C.M., Esteves da Silva, J.C.G., and Pinto da Silva, L. (2018) Study of coelenterazine luminescence: Electrostatic interactions as the controlling factor for efficient chemiexcitation. *Journal of Luminescence*. 199 (January), 339–347.

[93] Min, C.G., Ferreira, P.J.O., and Pinto da Silva, L. (2017) Theoretically obtained insight into the mechanism and dioxetanone species responsible for the singlet chemiexcitation of Coelenterazine. *Journal of Photochemistry and Photobiology B: Biology*. 174 18–26.

[94] Nakamura, M., Suzuki, T., Ishizaka, N., Sato, J.I., and Inouye, S. (2014) Identification of 3-enol sulfate of Cypridina luciferin, Cypridina luciferyl sulfate, in

the sea-firefly Cypridina (Vargula) hilgendorfii. *Tetrahedron*. 70 (12), 2161–2168.

[95] Reichardt, C. (1994) Solvatochromic Dyes as Solvent Polarity Indicators. *Chemical Reviews*. 94 (8), 2319–2358.

[96] Kavarnos, G.J. and Turro, N.J. (2002) Photosensitization by reversible electron transfer : theories , experimental evidence , and examples Photosensitization by Reversible Electron Transfer : Theories , Experimental Evidence , and Examples. *Chemical Reviews*. 86 (May), 401–449.

[97] Hratchian, H.P. and Schlegel, H.B. (2005) Using Hessian Updating To Increase the Efficiency of a. *Journal of Chemical Theory and Computation*. 1 (1), 61–69.

[98] Li, X., Millam, J.M., and Schlegel, H.B. (2000) Ab initio molecular dynamics studies of the photodissociation of formaldehyde, H2CO→H2+CO: Direct classical trajectory calculations by MP2 and density functional theory. *Journal of Chemical Physics*. 113 (22), 10062–10067.

[99] Roos, B.O. (1980) The complete active space SCF method in a fock-matrix-based super-CI formulation. *International Journal of Quantum Chemistry*. 18 (14 S), 175–189.

[100] Andersson, K., Malmqvist, P.Å., Roos, B.O., Sadlej, A.J., and Wolinski, K. (1990) Second-order perturbation theory with a CASSCF reference function. *Journal of Physical Chemistry*. 94 (14), 5483–5488.

[101] Aquilante, F., Autschbach, J., Carlson, R.K., Chibotaru, L.F., Delcey, M.G., De Vico, L., et al. (2016) Molcas 8: New capabilities for multiconfigurational quantum chemical calculations across the periodic table. *Journal of Computational Chemistry*. 37 (5), 506–541.

[102] Magalhães, C., Esteves, J.C.G., Pinto, L., Magalhães, C.M., and Esteves, J.C.G. (2016) Theoretical Optimization of the Electron Transfer Theoretical optimization of the electron transfer involving chemiluminescent coelenterazine. (February),.

[103] Wolters, L.P. and Bickelhaupt, F.M. (2015) The activation strain model and molecular orbital theory. *Wiley Interdisciplinary Reviews: Computational Molecular Science*. 5 (4), 324–343.

[104] Ess, D.H. and Houk, K.N. (2007) Distortion / Interaction Energy Control of 1 , 3-Dipolar Cycloaddition Reactivity. 10646–10647.

[105] Bickelhaupt, F.M. and Houk, K.N. (2017) Analyzing Reaction Rates with the Distortion/Interaction-Activation Strain Model. *Angewandte Chemie - International Edition*. 56 (34), 10070–10086.

[106] Pearton, S. (2010) Editorial: Doped nanostructures. *Nanoscale*. 2 (7), 1057.

[107] Zhao, B., Yin, J.J., Bilski, P.J., Chignell, C.F., Roberts, J.E., and He, Y.Y. (2009) Enhanced photodynamic efficacy towards melanoma cells by encapsulation of

Pc4 in silica nanoparticles. *Toxicology and Applied Pharmacology*. 241 (2), 163–172.

[108] Wojtoniszak, M., Rogińska, D., Machaliński, B., Drozdzik, M., and Mijowska, E. (2013) Graphene oxide functionalized with methylene blue and its performance in singlet oxygen generation. *Materials Research Bulletin*. 48 (7), 2636–2639.

[109] Qian, H.S., Guo, H.C., Ho, P.C.L., Mahendran, R., and Zhang, Y. (2009) Mesoporous-silica-coated up-conversion fluorescent nanoparticles for photodynamic therapy. *Small*. 5 (20), 2285–2290.

[110] Abe, K. and Matsuki, N. (2000) Measurement of cellular 3-(4,5-dimethylthiazol-2-yl)-2,5-diphenyltetrazolium bromide (MTT) reduction activity and lactate dehydrogenase release using MTT. *Neuroscience Research*. 38 (4), 325–329.

[111] Fotakis, G. and Timbrell, J.A. (2006) In vitro cytotoxicity assays: Comparison of LDH, neutral red, MTT and protein assay in hepatoma cell lines following exposure to cadmium chloride. *Toxicology Letters*. 160 (2), 171–177.

[112] Holder, A.L., Goth-Goldstein, R., Lucas, D., and Koshland, C.P. (2012) Particle-induced artifacts in the MTT and LDH viability assays. *Chemical Research in Toxicology*. 25 (9), 1885–1892.